INVESTIGATION OF SHELL MICROSTRUCTURE OF MICROBUBBLES FOR DIAGNOSTIC ULTRASOUND

A Thesis Submitted to
the Graduate School of Engineering and Sciences of
İzmir Institute of Technology
in Partial Fulfillment of the Requirements for the Degree of

MASTER OF SCIENCE

in Chemical Engineering

by
Derya KÖSE

July, 2013
İZMİR

We approve the thesis of **Derya KÖSE**

Examining Committee Members:

_____

Assist. Prof. Dr. Sevgi KILIÇ ÖZDEMİR
Department of Chemical Engineering, İzmir Institute of Technology

_____

Prof. Dr. Volga BULMUŞ
Department of Chemical Engineering, İzmir Institute of Technology

_____

Prof. Dr. Hürriyet POLAT
Department of Chemistry, İzmir Institute of Technology

11 July 2013

_____

Assist. Prof. Dr. Sevgi KILIÇ ÖZDEMİR
Supervisor, Department of Chemical Engineering, İzmir Institute of Technology

_____

Prof. Dr. Fehime Seher ÖZKAN
Head of the Department of
Chemical Engineering

_____

Prof. Dr. R. Tuğrul SENGER
Dean of the Graduate School of
Engineering and Sciences

ACKNOWLEDGEMENTS

I would like to express my deepest appreciation to all those who provided me the possibility to complete this report. A special gratitude I give to my supervisor, Assist. Prof. Dr. Sevgi Kılıç Özdemir, whose contribution in stimulating suggestions and encouragement, helped me to coordinate my study.

Furthermore I would also like to acknowledge with much appreciation the crucial role of designing shear stress experiments to Assoc. Prof. Dr. Ekrem Özdemir. I'm also greatfull to Assist. Prof. Dr. Hadi M. Zareie who gave the permission to use all required equipment and the necessary materials to complete the SPR experiments. I would like to express my special thanks of gratitude to Uğur Kayran for spending his time for my study and his frienship.

My thanks and appreciations also go to my friends from the Department of Chemical Engineering. I want to thank Sezen Duygu Alıcı, Aysu Sağdiç, Şeniz Bölükçü, Ceren Süngüç, Damla Taykoz, Emre Demirkaya, Melis Olçum, Eda Ülkeryıldız, Görkem Toprak for their warm friendship and support.

Last but not least, i would like to thank my family. I would have not finished this project without the support of my family who has always been there for me whenever I need them, the encouragement they give to keep me going and their love to empower me that never fails all the time. Finally, i want to dedicate my thesis to my little angel, Duru Bayraktar.

ABSTRACT

INVESTIGATION OF SHELL MICROSTRUCTURE OF MICROBUBBLES FOR DIAGNOSTIC ULTRASOUND

In this study we reported the effect of shear stress, protein adhesion, temperature, secondary interactions and gas core on microbubble stability which are the main reasons of microbubble dissolution in body. Air filled DSPC/PEG40St microbubbles were examined under shear stress. Increasing PEG40St molar ratio increased the resistivity microbubbles against shear stress. To investigate effect of emulsifier type, microbubbles were produced by mixing DSPC with DSPE-PEG1000, DSPE-PEG2000 and PEG40St at 5:5 molar ratio and PEG40St microbubbles were more stable since it provide better curvature to microbubble shell due to its shape. Shear stress experiments were also performed at different temperatures. With increasing temperature microbubbles became less stable since van der Waals interactions between shell components decreased. When microbubbles were filled with perfluorocarbon, since its solubility is lower and more hydrophobic than air, the stability of microbubbles against shear stress increased.

Protein adhesion to microbubble shell was investigated by Langmuir Blodgett (LB) and Surface Plasmon Resonance techniques. Both techniques showed that, as the PEG40St molar ratio and packing density increased, protein adhesion decreased.

Secondary interactions between shell components were examined via LB technique and visualized via Brewster Angle Microscopy. As third component to DSPC/PEG40St mixture, StGly, $StNH_2$, DSPS, DSTAP was added and ternary mixtures were generally miscible. Since StGly and $StNH_2$ has single tail, they cannot provide curvature in bubble surface. DSPS and DSTAP mixtures may be recommended drug delivery.

ÖZET

TANISAL ULTRASONDA KULLANILAN MİKROKÖPÜKÇÜKLERİN KABUK MİKRO YAPISININ ARAŞTIRILMASI

Bu çalışmada mikroköpükçüklerin vücut içersinde disolüsyonunun temel nedenleri olan kayma gerilimi, protein yapışması, sıcaklık, mikroköpükçük içersindeki gazın mikroköpükçük stabilitesine etkisi incelenmiştir. Kayma gerilimi deneyleri değişik kompozisyonlarda hazırlanan DSPC/PEG40St hava mikroköpükçüklerinin fizyolojik kayma gerilimleri altında sirküle edilmesi ile yapılmış olup PEG40St yüzdesi arttıkça mikroköpükçüklerin kayma gerilimine karşı daha dirençli olduğu görüşmüştür. Emülsifiyer çeşidinin etkisini incelemek için DSPC'yi DSPE-PEG1000, DSPE-PEG2000 and PEG40St ile 5:5 molar oranında karıştırarak mikroköpükçükler hazırlanmıştır ve PEG40St ile hazırlanan mikroköpükçüklerin daha stabil olduğu görülmüştür. Kayma geriliminin farklı sıcaklıklarda etkisini görmek için DSPC/PEG40St 5:5 mikroköpükçükleri 4^{o}C, 25^{o}C ve 38^{o}C'de incelenmiştir. Artan sıcaklıkla birlikte van der Waals etkileşimlerinin zayıflaması nedeniyle mikroköpükçüklerin stabilitesi düşmüştür. Mikroköpükçükler hava yerine perflorokarbon gazı ile doldurulduğunda, perflorokarbon gazı daha hidrofobik ve daha düşük çözünürlüklü olduğu için mikroköpükçüklerin stabilitesini arttırmıştır.

Mikroköpükçük kabuk yapısına protein yapışması Langmuir Blodgett (LB) ve Surface Plasmon Resonance (SPR) teknikleri ile incelenmiştir. Her iki teknik de PEG40St molar oranı ve yoğunluğu arttıkça protein yapışmasının azaldığını göstermiştir.

Bu çalışmanın bir başka amacı mikroköpükçük kabuk yapısındaki komponentler arasındaki ikincil etkileşimlerini etkisini incelemekti. DSPC/PEG40St formülasyonuna üçüncü komponent olarak StGly, $StNH_2$, DSPS, DSTAP eklendi ve oluşturulan monotabakaların faz davranışları LB yöntemi ile incelendi ve Brewster Açı Mikroskobu ile gözlemlendi. Elde edilen sonuçlar, DSPS ve DSTAP ilaç taşınımı için üretilen mikroköpükçüklerin yapısına katılmak için önerilebilir.

TABLE OF CONTENTS

LIST OF FIGURES

Figure **Page**

LIST OF TABLES

Table **Page**

CHAPTER 1

INTRODUCTION

Ultrasound is one of the widespread crossectional imaging modality used all over the world (Liang & Blomley, 2003). Sound waves with frequencies greater than 20,000 hertz cannot be detected by human ear are defined as ultrasound (Coatney, 2001). In diagnostic ultrasound imaging generally frequencies between 2 and 15 MHz are used. Sound waves at these frequencies are transmitted with the help of a small probe. The acoustic impedance of a particular tissue is calculated by the product of the transmission velocity of sound and the tissue density. When two tissues with different densities are located next to each other, an acoustic impedance mismatch is formed and as a result of this mismatch sound waves are reflected. Large difference in tissue densities leads to greater mismatch, so that more sound waves are reflected and returned to the transducer (Coatney, 2001). Due to these properties ultrasound imaging is the best imaging technique for soft tissue imaging. On the other hand, since the acoustic impedance difference between red blood cells and plasma is low, ultrasonic blood echoes are two orders of magnitude smaller than tissue echoes and this result in artifacts in imaging small blood vessels and receptors in these vessels (Kwan & Borden, 2010). In order to increase the image quality, contrast agents are needed that highly reflect the sound waves. Enhancement of the reflection of sound waves results in increase in the amount of sound waves returning to the transducer and signal to noise ratio.

Ultrasound contrast agents can be defined as biocolloids made of biocompatible materials. There are many types of biocolloids used as ultrasound contrast agents such as gas-liquid emulsions (microbubbles), liquid-liquid emulsions (nanodrops), liposomes and some other particles (Kwan & Borden, 2010). The intrinsic properties of the biocolloid determine the degree of the acoustic backscatter. Acoustic backscatter is enhanced with the density difference between the surrounding tissue and biocolloid (Kwan & Borden, 2010). Since submicron (nanoparticle) ultrasound contrast agents are not compressible and cannot oscillate strongly with the passing acoustic wave, they are less echogenic than microbubbles.

Microbubbles are gas filled micron (1-10 μm) sized spheres suspended in aqueous phase and used for diagnostic contrast enhanced ultrasound imaging (Geers et al., 2011). The ideal microbubble contrast agents should be inert, intravenously injectable, stable during cardiac and pulmonary passage, durable within the blood pool with a well-specified tissue distribution, provide a period of effect equivalent to that of the imaging examination (Quaia, 2005). To develop an ideal microbubble, mainly two parameters were considered. These are encapsulating materials and filling gas. Microbubbles are generally filled with air or a hydrophobic gas and the gas core encapsulated with a thin shell to enhance stability.

The microbubble shell may consist of a protein (albumin), lipid, surfactant, or biocompatible polymer (Hernot & Klibanov, 2008). However, protein shelled microbubbles cannot circulate in the blood stream freely since they adhere to tissues. Polymeric shells are not resistive against to gas diffusion since they form a rigid shell and sonic cracks occur during imaging. Lipid shelled microbubbles are flexible and can circulate in body unobstructed. Lipid-coated microbubbles generally include a secondary species, such as polyethylene glycol stearate (PEG-stearate), as an emulsifier that promotes rapid microbubble production (M. Borden, 2009). Emulsifier inhibits the bubble coalescence by forming a brush layer on the microbubble surface and immune response (Mark A Borden et al., 2006). In literature, it was reported that brush is formed by long PEGs like PEG2000, PEG5000 and short PEG chains like PEG40St cannot form brush to stabilize microbubbles (Kwan & Borden, 2010). However, in another literature study El-Khouri et al. reported that PEG40St has a large crossectional area that is sufficient to induce the morphological transitions (El-Khouri et al., 2011).

Since lipid microbubbles are non-rigid and new class of spherical particles, there is not many well established method available to determine shell properties. Since formation of microbubbles is based on the intermolecular interactions between the shell components, Langmuir Blodgett (LB) technique sets the best lay out to study the interaction between the components in 2D scale and relate the results to shell characteristics. From LB technique surface pressure of the mixed film as a function of mean molecular area data is obtained. By using surface pressure and mean molecular area data, information about the phase behavior of shell components and flexibility of the mixed film can be obtained.

Today, there are number of commercial microbubbles used as ultrasound contrast agents. Definity$^{(R)}$ is one of the lipid coated commercial microbubbles In a

literature study performed with Definity, results showed that showed that one bolus injection provides only 3 min imaging (Williams et al., 2011). On the other hand, required time for ultrasound imaging is between 10 min and 45 min. Main factors affecting microbubble dissolution in the body mainly results from shear stress in blood vessels, protein adhesion and temperature. In this study, it was aimed to investigate protein adhesion to microbubble shell and effect of shear stress ,temperature on microbubble stability. Protein adhesion was tested with LB and SPR techniques. Shear stress experiments were performed by circulating microbubbles in tube. Another goal of the study was to examine the effect of secondary interactions on microbubble shell stability. Effect of secondary forces on microbubble shell stability was investigated by using Langmuir Blodgett technique and phase behavior of monolayers was visualized with Brewster Angle Microscopy. For this purpose, as a third component to DSPC and PEG40St mixture, 1-steoyl-rac-glycerol (StGly), Stearylamine ($StNH_2$), 1,2-distearoyl-sn-glycero-3-(phospho-l-serine) (DSPS), or 1,2-stearoyl-3-trimethylammonium-propane (DSTAP) was added to the microbubble formulation. Among third components, StGly have ability to make hydrogen bonding, DSPS is anionic and as well as capable of hyrogen bonding, $StNH_2$ and DSTAP are cationic and able to make electrostatic interaction.

CHAPTER 2

LITERATURE SURVEY

2.1. Type of Microbubbles

Nowadays, microbubbles have acquired attention of medical community owing to their great potential as ultrasound contrast agents, drug and gene delivery vehicles (Bekeredjian, Grayburn, & Shohet, 2005; Mark A Borden, Pu, Runner, & Longo, 2004; Mayer & Grayburn, 2001). Microbubbles are gas filled spheres of 1-10 μm in diameter coated by surfactants or an encapsulating elastic shell (Forsberg, Shi, & Goldberg, 2000).

In the earlier stages of microbubble development, naked air filled microbubbles were produced. However, due to high solubility of air in blood and lung filtration, microbubbles were observed to dissolve in seconds (Dijkmans et al., 2004). Since naked microbubbles have very short life time, they are not useful for imaging and drug delivery applications. It was proposed that microbubble stability is achieved by coating it with a thin shell. This thin shell may consist of polymer, surfactant and lipid (M.A. Borden & Longo, 2002). Among these, lipids are often preferred because they have smilar properties to cell membranes. Phospholipids are amphiphilic molecules which have and hydrophilic head group and a hydrophobic tail. Using amphiphilic materials as shell component beneficial since they self-assemble into monolayer and thereby they provide control of shell surface texture. Moreover, using amphiphilic materials also enhance the flexibility (Dicker, Mleczko, Schmitz, & Wrenn, 2010).

Coating material of the microbubble determines the properties of the microbubble.

2.2. Polymer Coated Microbubbles

The microbubbles coated with a thick shell consisting of cross-linked or entangled polymeric species are called polymer coated microbubbles. Use of polymeric shells is advantageous since they are stable and provide good surface for adsorption or transport the drug (El-Sherif & Wheatley, 2003).

Wheatly et al. formed polymeric microbubble by using the ionotropic gelation of alginate. On the other hand, produced microbubbles were too large for intravenous administration (Wheatley, Schrope, & Shen, 1990). In another literature study, by using biodegradable copolymers poly(D,L-lactide-co-glycolide) (PLGA) small sized microbubbles were produced. On the other hand, their lifetime was found to be short (Cui et al., 2005).

Bloch et al. reported that, polymeric shelled microbubbles show different behavior compared to lipid coated microbubbles. At low ultrasound intensity, stiff polymer coated microbubbles were found to be not oscillating and sonic cracks were observed (Bloch, Wan, Dayton, & Ferrara, 2004).

2.3. Protein Coated Microbubbles

Microbubbles were coated with an adsorbed layer of saccharide or protein in 1980's. Albunex® is the first commercial protein coated, air filled microbubble which is approved by FDA. On the other hand, due to high solubility in blood and thin shell structure, Albunex® microbubbles were found to be unstable against gas diffusion (Hernot & Klibanov, 2008). Optison is another FDA approved albumin coated microbubble. Optison® is filled with perfluoropropane while Albunex® is filled with air (Mark A Borden, Dayton, Zhao, & Ferrara, 2004). Dayton et al. compared the echogenity of Albunex® and Optison® and found that Optison microbubbles were found to produce a "first echo" with greater harmonic content than Albunex. They observed that albumin coated microbubbles become more echogenic during shell break down (Dayton, Morgan, Klibanov, Brandenburger, & Ferrara, 1999).

In previous literature studies protein coated microbubbles were functionalized to carry ligand and genes, and they reported that microbubbles specifically bounded to endothelial cells (Korpanty, Grayburn, Shohet, & Brekken, 2005).

2.4. Surfactant Coated Microbubbles

In order to stabilize microbubbles, surfactants are used as coating material due to their excellent flexibility. On the other hand, only some of the surfactant microbubbles were found to be stable only for some surfactant's mixtures at only a few certain molar ratios (Singhal, Moser, & Wheatley, 1993). Singhal et al. studied the effect of molar ratio by mixing Tween 80 and Span 60 surfactants. Their results showed that in Span 60/Tween 80 mixtures highest microbubble yield was obtained in the 0.6-0.75 composition range (Singhal et al., 1993). However obtained microbubbles were not stable. In another literature study, Whang et al. reported that mixtures of while mixtures of Tween 80 and Span 80 cannot form stable microbubbles, Tween 40 and Span 40 can produce stable microbubbles (Wang, Moser, & Wheatley, 1996). They attributed their result from the low surface activity of Span 80 and high steric effect due to ethylene group in the hydrocarbon chain (Singhal et al., 1993; Wang et al., 1996).

In another literature study, Dressaire et al. formed stable microbubbles from sucrose stearate by a blending process in 75%wt glucose syrup (Dressaire, Bee, Bell, Lips, & Stone, 2008). Although these microbubbles were stable in suspension for over a year, they were not resistant against to dilution (Dressaire et al., 2008).

2.5. Lipid Coated Microbubbles

Today, lipid coated microbubbles are mostly preferred as ultrasound contrast agent and they are under development for drug gene delivery vehicles (Kwan & Borden, 2012b).

Lipid stabilizes the microbubble and improves its in vivo life by imparting a barrier between the gas and aqueous medium to reduce thrombogenic effects (Ferrara, Borden, & Zhang, 2009). Since phospholipids mimic the cell membranes and are biocompatible, they are mostly favored as shell component. There is variety of lipids having hydrophilic head groups and hydrophobic tail groups and the prospect of multicomponent mixtures suggest an immense parameter space over which to manipulate the shell composition. For instance, lipids having different saturation degree, charged head group and steric stabilizers like poly(ethylene glycol) (PEG) can be used. Unger et al. developed a phospholipid coated microbubble called Definity and it is

approved by US FDA. The lipid coating in Definity is consist of three different phospholipids Dipalmitoylphosphatidylcholine (DPPC), Dipalmitoylphosphatidic acid (DPPA), and dipalmitolyphosphatidylethanolamine– PEG5000 (DPPE–PEG5000) (Unger et al., 2004). Chosen all phospholipids are a-saturated and 16 carbon in length. Using phospholipid having long acyl chains increases the microbubble's shelf life and in vivo life.

Microbubbles are not only used as ultrasound contrast agents but also proposed as drug or gene delivery vehicles. Drugs can be conjugated to microbubble shell with the help of a charge dependent non covalent bonding (Dijkmans et al., 2004). Microbubble shell composition can be easily manipulated by adding a charged lipids to the emulsion mixture preparation. The positively charged groups of some synthetic lipids like DSTAP make electrostatic interactions possible between the lipids and plasmid DNA, which have an overall negative charge. Borden et al. made a cationic microbubble by mixing cationic phospholipid DSTAP with DSPC and PEG40St and used it for DNA adsorption. First they optimized the charged lipid composition since inclusion of a charged lipid to the microbubble shell could disturb the lipid packing. They showed that, the microbubbles were stable up to 40% DSTAP composition and according to the obtained results, DSTAP increased the DNA adsorption (Mark A Borden, Caskey, Little, Gillies, & Ferrara, 2007).

2.6. Langmuir Blodgett Monolayers

Molecular ordered thin organic films, alternating in thickness from about a few nanometers (a monolayer) to hundred nanometers, reveal a substantial technological potential.

Effect of oily films on a water surface was first reported by Benjamin Franklin in 1774. In 1891, method of manipulation of oily films at the air-water interface with movable barriers was described by Agnes Pockels. After that, Raleigh reported that, the film prepared by Pockel was a monolayer (Roberts, 1990) . In order to understand behavior of monolayer at air – water interface, Langmuir developed the theoretical and experimental concept in 1917 (Ulman, 1995). The first studies on multiple depositions of long aliphatic carboxylic acids onto a solid substrate were performed by Katherine Blodgett in 1929 and this technique called Langmuir Blodgett technique. The initial

investigations were mainly related to the interfacial phenomena, however currently the interest is shifted to functional LB films with prospective applications such as thin film optics, sensors and transducers, protective layers, patternable materials, models for biological membranes.

Characteristic of a monolayer may be elucidated with obtaining surface pressure – mean molecular area isotherm by LB technique at air-water interface. Langmuir balance is a standard method for measuring surface pressure (π) of the monolayer.

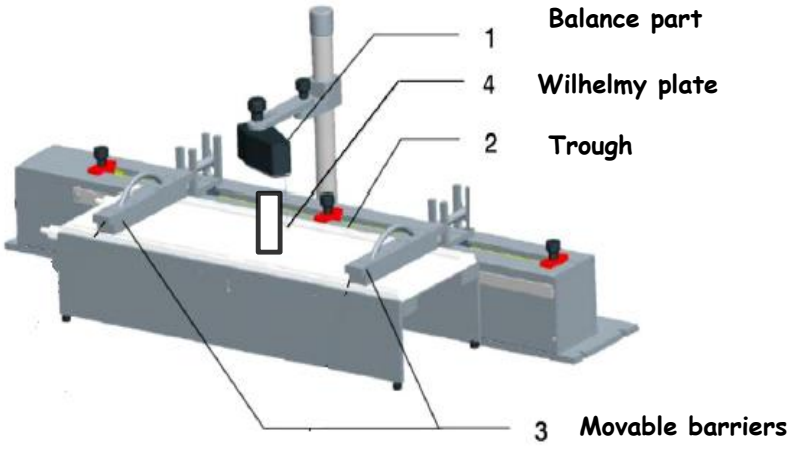

Figure 2.1. Langmuir Blodgett through

As seen in Figure 2.1 LB instrument consist of a wilhelmy plate attached to a transducer, a teflon through and two movable barriers. The movable barriers move simultaneously to compress or expand the interface in the interior. The wilhelmy balance measures the surface tension, σ, of the interface by determining the force on the wilhelmy plate (Fuller, 2003). Surface pressure is calculated with equation 2.1 where σ_0 (mN/m) is surface tension of subphase in the absence of the monolayer, σ (mN/m) is surface tension in the presence of the monolayer (Moghaddam, Ali, et al., 2011).

$$\pi = \sigma_0 - \sigma \tag{2.1}$$

Typical surface pressure - mean molecular area isotherm of a monolayer obtained during compression is seen is in Figure 2.2. Before compression of the spread sample, due to large mean molecular area molecules are apart from each other and a

gaseous monolayer (G) is formed. With the compression of barriers, area per molecules decreases and surface pressure starts to increase because of the repulsive interaction between molecules. In this case, monolayer reaches to liquid condense (LC) phase. With the further reduction of the mean molecular area, surface pressure increases very rapidly and this phase of the monolayer is analogous to solid phase (S). Solid phase of the monolayer is very incompressible and further compression of a solid monolayer result in collapse of the monolayer.

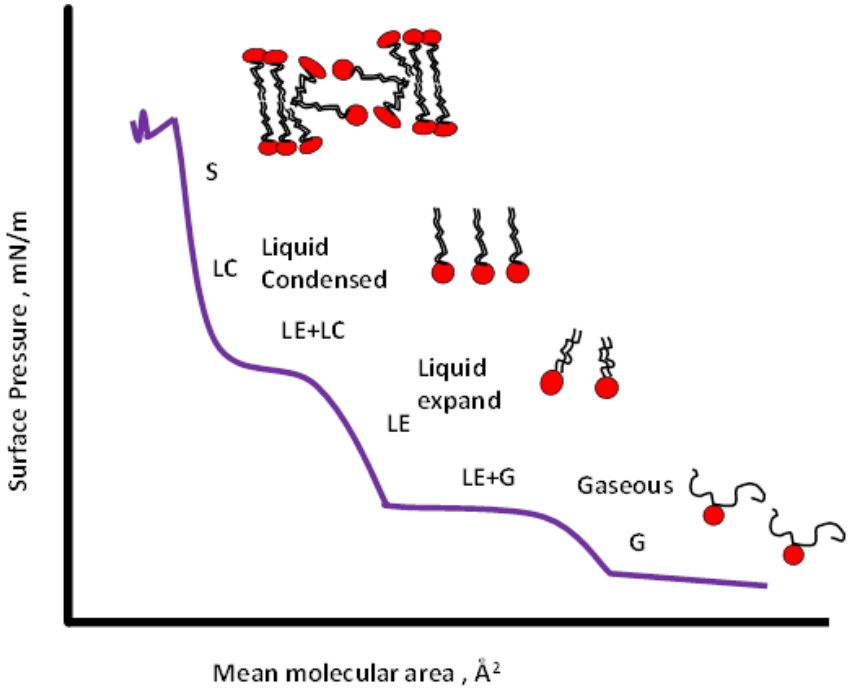

Figure 2.2. Typical surface pressure – mean molecular area isotherm

2.7. Visualizing Monolayer Morphology with Brewster Angle Microscopy

The Langmuir monolayers have various phases which can be visualized with Brewster Angle Microscopy (BAM). Phase behavior and morphology of monolayers can be visualized via BAM. Principle of Brewster angle is represented in Figure 2.3. The existence of a Brewster angle requires p-polarized light. The reflectivity coefficient r_p becomes zero at the Brewster angle and thus no light is reflected there. A monolayer at the air-water interface reflects light $r_p = 10^{-6}$ which is enough for creating image. BAM is superior to fluorescence microscopy, since it does not require any label which

could have an undesired effect on the systems. With fluorescent probe it is problematic to determine the end of the phase transition upon compression, since the probe is enriched in the fluid phase (Hoenig & Moebius, 1991). The direct observation of monolayers in the absence of any probe by light reflection prevents such complications. The laser diode used for the reflectivity measurements was substituted by a He-Ne laser for BAM.

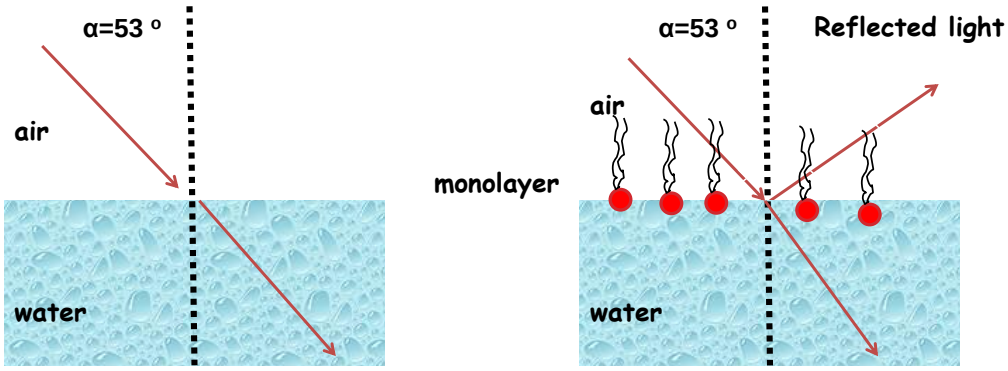

Figure 2.3. Illustration of Brewster angle principle

2.8. Protein Adsorption and PEGylation of Microbubble Surface

Poly(ethylene glycol) (PEG) is used widely to improve the biocompatibility of foreign materials for in vivo and in vitro applications since it is non- immunogenic and non-antigenic (Harris, 1992). PEG is generally used as coating for microbubbles and other vesicles(Xu, Holland, & Marchant, 2001). Another important parameter makes PEG preferable is its resistance to protein adhesion (Heuberger, Drobek, & Spencer, 2005). Ethylene oxide (EO) surface grafts are employed to diminish protein adsorption to the biomedical polymers' surface. Common models of grafted poly(ethylene oxide) films attribute its protein resistance to two main reasons. These are steric or osmotic repulsion between proteins and the PEG chains and the assumption that the EO segments completely repel proteins (N. Efremova, Sheth, & Leckband, 2001).

PEG attached on surfaces can have different conformations depending on the interaction with the surface, grafting density and interaction with the solvent (Zhao & Brittain, 2000). The PEG chain can be chemically bonded to the substrate or may be physically adsorbed on the surface. At low PEG concentrations pancake conformation is

observed which is not effective for preventing protein adsorption. When PEG starts to form a depletion layer, a coiled formation in a mushroom conformation occurs. If the distance between the chains is shorter than the radius of gyration, chains are not allowed to occupy the mushroom conformation any longer; they are crowded and stretched away from the surface forming a brush conformation (D. Lasic, 1997).

Based on theory and physicochemical experiments, with the increasing polymer density, protein repulsion increases. On the other hand, Lasic et al. stated that, biological stability as measured by liposome circulation time in blood exhibits a saturation/ maximum profile around the mushroom to brush transition (D. D. Lasic, 1994).

Protein adsorption to monolayers is commonly investigated using QCM and SPR. As an alternative to these methods, use of LB technique presents same advantageous since physiological environments can be easily obtained by tuning the system parameters as pH, temperature and ionic strength etc. Besides, LB technique is an inexpensive method requires no special substrate.

2.8.1. Protein Adsorption via Surface Plasmon Resonance

Surface plasmon resonance (SPR) is an optical technique used for measuring the refractive index of very thin layers of material adsorbed on a metal surface (Pattnaik, 2005). When a fraction of the light energy incident at a sharply defined angle interact with the delocalized electrons in the metal film (plasmon), the reflected light intensity is reduced. The SPR technique is based on the fact that, at appropriate conditions, photons can excite the surface plasmons on a metallic film. In that way, photons transformed into a surface plasmon and it depends on the adsorbate's refractive index (Markey, 1999).

In this study, SPR is used as complementary method to LB technique to investigate the protein adsorption to the microbubble monolayer.

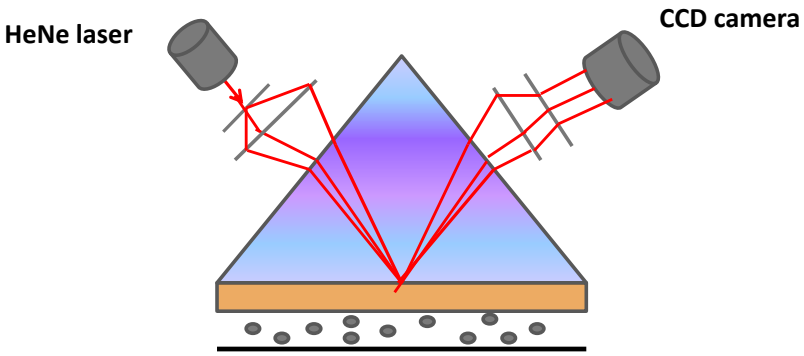

Figure 2.4.Geometrical setup of SPR

In many literature studies, protein resistance of PEG grafted monolayers and lipopolymers were examined by using SPR (Harder, Grunze, Dahint, Whitesides, & Laibinis, 1998). Efremova et al. investigate the protein adsorption to uncharged lipid bilayers displaying poly(ethylene glycol) chains by using SPR (N. V. Efremova, Bondurant, O'Brie, & Leckband, 2000). They examined the DSPE and DSPE PEG-lipid mixtures. They coated the SPR substrates with Langmuir Blodgett technique. Results showed that, as the PEG molar ratio increased, protein adsorption decreased due to extended conformation of PEG. They also supported their results with force – distance measurements (Efremova, Bondurant et al. 2000). Uchida et al. studied effect of PEG molecular weight on nonspecific protein adsorption. They studied with PEGs having 2000 and 5000 and their mixtures. They reported that, all PEG types prevented nonspecific protein adhesion. However, mixed PEG chain-tethered surface constructed showed an almost complete nonfouling character. They also reported that, even shorter PEG layer to increase the PEG surface density played a substantial role in reducing nonspecific adsorption (Uchida, Otsuka, Kaneko, Kataoka, & Nagasaki, 2005)

CHAPTER 3

MATERIALS AND METHODS

3.1. Materials

In this study, 1,2-distearoyl-sn-glycero-3-phosphocholine 99% (DSPC), Stearylamine 99% ($StNH_2$), 1-steoyl-rac-glycerol (StGly) 99%, DSPE-PEG1000 99%, DSPE-PEG2000 99%, Polyethylene glycol 40 stearate 99% (PEG40St), 1-Octanethiol (98%) and polystyrene latex particles (with 3μm diameter) were purchased from Sigma Aldrich and 1,2-distearoyl-sn-glycero-3-(phospho-l-serine) 99% (DSPS), 1,2-stearoyl-3-trimethylammonium-propane 99% (DSTAP) were purchased from Avanti Polar Lipids. Bovine serum albumin (BSA) was purchased from Merck. The solvents chloroform and methanol with 99.99% purity were obtained from Sigma Aldrich and Merck respectively and used without further purification. Chemical structures of used components are given in Table 3.1.

Table 3.1. Chemical structures of used components

Component	Chemical Structure
DSPC (zwitterionic)	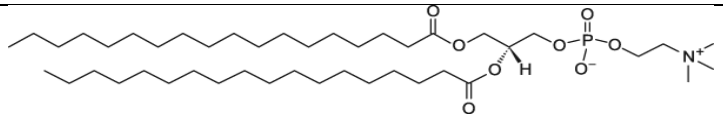
PEG40St (nonionic)	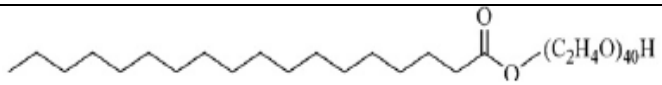
DSPE-PEG1000 (nonionic)	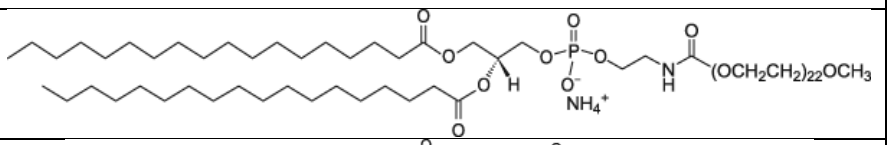
DSPE-PEG2000 (nonionic)	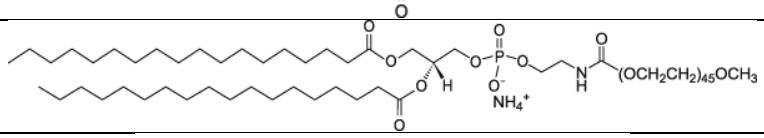
StGly (nonionic)	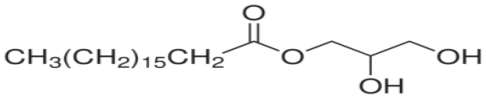
$StNH_2$ (Cationic)	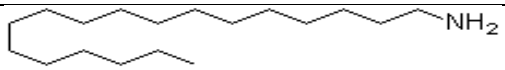
DSPS (anionic)	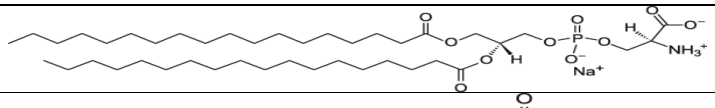
DSTAP (cationic)	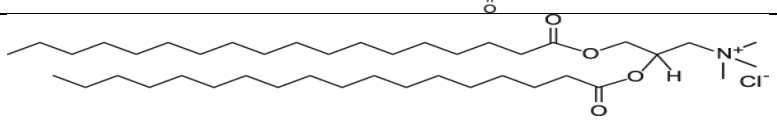

3.2. Methods

3.2.1. Microbubble Preparation

Mixture of lipid and emulsifier weighed at predetermined molar ratios was dissolved in chloroform. Chloroform was evaporated via N_2 stream and incubated under vacuum environment at 25 ^{o}C overnight. 4 ml of PBS (pH 7.2) and propylene glycol (PG) mixture at volume ratio of 4:1 was added to the resulting dry lipid-emulsifier film and hydrated for two hours at main phase transition temperature of phospholipid (55°C). Mixture was sonicated at air solution interface with probe type sonicator (S-4000 MISONICS) at 50 AMP. 5 ml of PBS was added to resulting mixture and the solution was allocated to 2ml tubes and centrifuged at 2000 rpm for 4 min. After centrifugation, infranatant part was removed and the cake was re-suspended in PBS. Same procedure

was applied until obtaining a non-turbid infranatant solution. To the cake, PBS:PG (4:1) mixture was added up to 1 ml line in the tube and microbubble solutions were combined into a syringe and allocated in tubes at equal volumes. Obtained microbubble suspension stored at 4 ^{o}C overnight before the analysis. However, there was PFC at the head space during sonication and storage.

In order to determine initial concentration and size distribution of microbubbles, optical microscopy images of microbubbles were taken by using a counting chamber (Thoma Glass) and binocular optic microscope (OLYMPUS) attached to a digital camera (TUCSEN). Thereafter, optical microscopy images were processed by a software (NIH, ImageJ).

3.2.2. Shear Stress Experiments

Experimental set up used for shear stress experiments is illustrated in Figure 3.1. To examine the effect of shear stress on microbubbles, at a known concentration of 0.05 ml microbubble was injected to a pipe with 1.5 mm diameter filled with PBS (pH 7.2) by a 16 gauge (1.29 mm) syringe. Microbubbles were circulated with a peristaltic pump (Longer pump BT100L). Different shear stress conditions were provided by changing the flow rate while diameter of pipe kept constant. Used flow rates are revealed in Table 3.2. Constant temperature was provided by using a water bath during the experiment. After circulating the microbubble under shear stress at defined time, microbubbles were collected into tubes and change in the concentration and size distribution was determined via optical microscopy.

Table 3.2 Flow rates used in shear stress experiments

Shear Stress (Pa)	**Q(ml/min)**
0.028	0.56
0.11	2.19
0.28	5.57
0.42	8.35

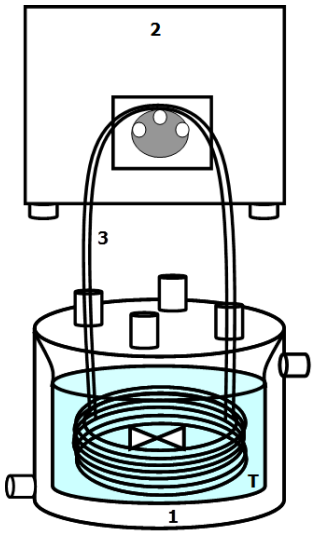

Figure 3.1.Experimental setup for shear stress: (1) jacketed reactor, (2) peristaltic pump, (3) pipe

In order to check if reproducible results can be obtained, polystyrene latex particles were used since their size and number are not affected by the effect of shear. Shear stress experiments were performed at the same conditions with microbubbles and not considerable change was observed in the concentration of the polystyrene latex particles as seen in Figure 3.2. This control experiment showed that, system is appropriate for testing effect of shear stress on microbubbles.

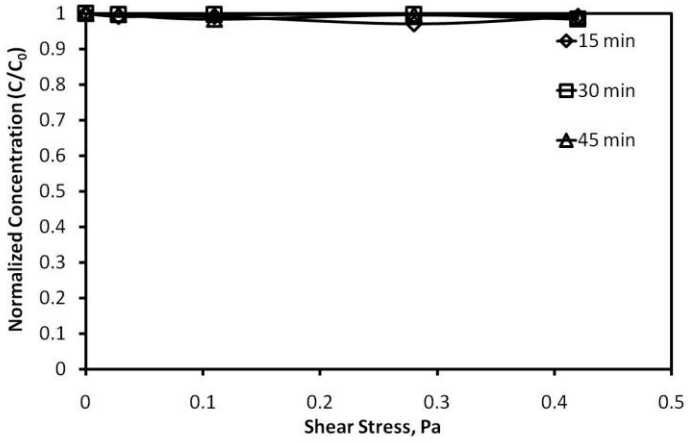

Figure 3.2. Shear stress setup control experiment with polystyrene latex particles

3.2.3. Protein Adsorption Experiments

Protein adsorption experiments were carried out by using Langmuir-Blodgett and surface plasmon resonance technique.

Langmuir Blodgett Technique

Mixtures of DSPC/PEG40St at molar ratio of 5:5, 7:3 and 9:1 were prepared with the same method explained in Langmuir Blodgett experiments. Mixtures spread on the air water interface. Monolayers compressed up to a predetermined surface pressure (30 mN/m and 40mN/m) and BSA solution was injected with an L shaped needle as represented in Figure 3.3. Total BSA concentration in the through was 50 nM. Change in the surface pressure was measured after BSA injection was monitored for 1 hour. Same procedure repeated without injecting protein in order to calculate change the difference in surface pressure. Experiments were performed at 20 ^{o}C and 38 ^{o}C to investigate effect of temperature.

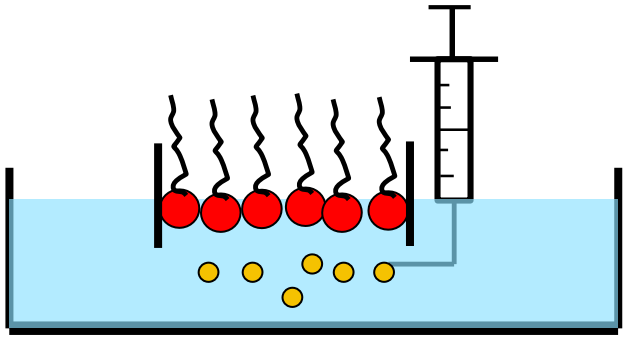

Figure 3.3. Protein injection protocol in LB experiments

Surface Plasmon Resonance

For SPR experiments, gold coated substrates were used. In order to make surface of substrate hydrophobic, self-assembly technique was applied. To achieve a good self-assembled surface, substrate surface must be very clean. For this purpose, first gold substrate was rinsed with acetone and sonicated in acetone for 5 min. After sonication, it was dried with nitrogen. Then 3:1 (H_2SO_4:H_2O_2) piranha solution was dropped to the gold coated surface of the substrate. After waiting for 2 minutes, substrate was rinsed with ultrapure water. If the water was flowing as thin film from the surface of the substrate, it was accepted as clean. If not, substrate was dried and same procedure repeat until obtaining a clean substrate. By dissolving 1-octanethiol in ethanol 1mM solution was prepared and filled into small containers. The clean substrate was immersed into the container and container backfilled with argon gas in order to minimize oxygen exposure and container was sealed with cap and parafilm. Substrates were kept immersed in thiol solution for 24 h.

The resulting hydrophobic substrate was coated by using dipping technique in LB trough. First, self-assembled substrate was taken out the container, rinsed with ethanol and dried with N_2. Clean substrate attached to the LB dipper and as happened in LB experiments, sample spread on the air-water interface. After equilibration of monolayer for 20 min, constant rate compression was applied until reaching the target surface pressure and again waited for 20 min for monolayer equilibration. After that, substrate dipped into the monolayer vertically and monolayer deposited to substrate. Substrates were coated at 30 mN/m and 40 mN/m surface pressures. Experiments were performed at 20 ^{o}C and 38 ^{o}C constant temperatures.

Protein adhesion to monolayer coated substrates was examined via SPR (Nanodev). After reaching the equilibrium, ultrapure water was pumped onto surface for 5 min at 100 μl/min flow rate and then 1mg/ml BSA solution was sent for 30 min at 30 μl/min flow rate. Then surface was washed with ultrapure water for 10 min. This procedure was repeated for 2 times and shift of angle with respect to time was measured. Experiments were performed at the same temperature at which coating was done in LB trough.

Amount of BSA adhesion to surfaces was calculated with the method described by Jung et al. (Jung, Campbell, Chinowsky, Mar, & Yee, 1998). Equations are as follows:

$$Rmax = m(n_a - n_s) \tag{3.1}$$

$$d = \frac{ld}{2}\left(\frac{R}{Rmax}\right) \tag{3.2}$$

$$N = \frac{\rho}{M_w} * N_a \tag{3.3}$$

$$\theta = dxN \tag{3.4}$$

$$C_{BSA} = \frac{\theta}{N_a} * M_w \tag{3.5}$$

Where;

d (nm): adsorbed layer thickness

ld (nm): decay length of evanescent wave (roughly ld= λ*37% ± 13)

λ (nm): wavelength of laser (705 nm)

m = sensitivity factor (2.7)

n_a = adsorbed layer refractive index (1.575)

n_s = bulk layer refractive index (1.33)

R= refractive index unit (RIU) change (read off the SPR sensogram)

R_{max}= Maximum change in RIU

ρ=density of BSA solution (1mg/ml)

N_a= Avagadro's number

M_w= molecular weight of BSA

θ= number of molecules per cm^2

C_{BSA}= ng BSA per cm^2

Typical SPR sensogram is represented in Figure 3.4. R value gathered from the graph as seen in Figure 3.4. Refractive index (RI) value of BSA was taken as 1.575 (Arwin, 1986) and RI of ultrapure water was taken as 1.33 (Hell, Reiner, Cremer, & Stelzer, 1993).

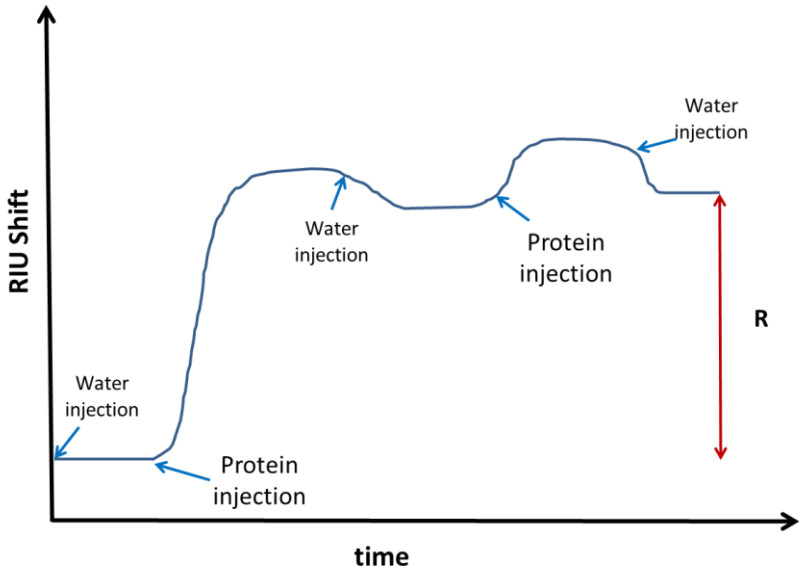

Figure 3.4. Typical SPR sensogram

3.2.4. Langmuir Blodgett Experiments

In order to prepare spreading solutions of pure phospholipids, their binary and ternary mixtures with PEG40St, respective components were weighed and dissolved with appropriate solvent. DSPS containing mixtures dissolved in chloroform-methanol

mixture at 8:2 volume ratio while other mixtures dissolved in chloroform. To obtain homogeneous solutions, after solvent addition samples hold in sonic bath.

In the ternary mixtures, as a third component to DSPC/PEG40St mixture, DSPS, DSTAP, StGly and $StNH_2$ added. Molar ratios of the prepared mixtures were 0:5:5, 4:5:1, 2:5:3 for DSPC/PEG40St/DSPS and DSPC/PEG40St/DSTAP mixtures while 7:2:1, 5:2:3, 6:2:2 and 4:2:4 for DSPC/PEG40St/$StNH_2$.

Characterization of the Samples

Surface pressure versus mean molecular area isotherms of the prepared solutions were obtained by using Langmuir minitrough (KSV Instruments Ltd., Helsinki, Finland). The Teflon trough was equipped with two barriers placed on the through symmetrically and a Wilhelmy plate for the surface pressure measurements. Wilhelmy plate was made from filter paper. Trough was filled with ultrapure water (Millipore SAS 67120 Molsheim,France) with 18.2 MΩ.cm specific resistance. Before spreading the solution, surface pressure of the water was measured which must be maximum 0.2 mN/m if the water has no impurities. In order to deposit desired amount of solution onto water, micro syringe (Hamilton) was used. After spreading the solution, solvent was allowed to evaporate for about 20 minute before monolayer compression. Surface pressure-area (Π-A) isotherms of the mixed monolayers were obtained by symmetric compression of barriers at a rate of 5 mm/min. The temperature of the through was kept constant by using a water bath circulator (Wise Circu) at 20 ^{o}C. For each spreading solutions, experiments were repeated at least three times to make sure repeatability and reproducibility of the measurements.

Phase behavior and morphology of the pure and mixture monolayers were investigated by Brewster Angle Microscopy (KSV Optrel BAM300) atthached to Langmuir Blodgett trough. The Brewster Angle Microscope (BAM) consists of a CCD camera, two polarizers and a 10mW He-Ne laser. According to the Brewster Angle principle, when a p-polarized light is sent to the air-water interface, no reflection occurs from the surface at the incident angle. Therefore, the angle was adjusted to 53^{o} which is incident angle for air-water interface. Then respective solutions were spreaded onto water and reflected light created the image of the sample. To observe the effect of surface pressure on monolayer phase behavior, BAM images were taken at different surface pressures.

Data Analysis for Langmuir Blodgett Experiments

To investigate information on the miscibility and the interactions between the molecules in the mixed films, additivity rule was used. According to the additivity rule, if the components of the mixture are immiscible or ideally miscible, mean molecular area of the mixture is a linear function of composition (Gaines, 1966). Ideal mean molecular area of the mixtures calculated for binary and ternary mixtures as seen equation 3.6. A_1, A_2 and A_3 represent the mean molecular areas of the respective components in their pure Π-A isotherms at a given surface pressure (π) and x_1, x_2 and x_3 are molar fractions of the components in the mixtures.

$$A^{ideal} = x_1A_1 + x_2A_2 + x_3A_3 + \cdots \tag{3.6}$$

Deviation from the ideality was calculated by subtracting the ideal mean molecular area from the measured mean molecular (A_{123}) area at a given surface pressure.

$$A_{ex} = A_{123} - A_{ideal} = A_{123} - (x_1A_1 + x_2A_2 + x_3A_3) \tag{3.7}$$

Molecular interactions among the mixed film components were evaluated by calculating the excess gibbs free energy of mixing based on the equation 3.8 where N is the avagadro number (Chou & Chu, 2003).

$$\Delta G_{exc} = N \int_{\pi_1}^{\pi_2} (A_{123} - (x_1A_1 + x_2A_2 + x_3A_3)\, d\pi \tag{3.8}$$

To investigate the fluidity of monolayers, compression modulus was calculated from the Π-A isotherm data points according to the equation 3.9 (Wydro & Witkowska, 2009).

$$C_s^{-1} = -A\left(\frac{d\pi}{dA}\right) \tag{3.9}$$

CHAPTER 4

RESULTS AND DISCUSSIONS

4.1. Effect of Shear Stress on Microbubble Stability

Microbubble size distribution and concentration are important parameters since microbubbles are used for diagnostic and treatment purposes (Kaya, Gregory V, & Dayton, 2009). When microbubbles are used for contrast enhancement in ultrasound imaging, increase in the image quality is directly related to microbubble size and concentration (Barrack & Stride, 2009). In the same way, when microbubbles are used for drug delivery, the dosage of the drug injected to the patient depends on the microbubble concentration. In this case, the change in the microbubble size distribution and concentration needed to be known.

In previous literature studies, effect of injection rate and needle size on microbubble stability (Kaya et al., 2009; Talu, Powell, Longo, & Dayton, 2008) were investigated. However, circulation time, temperature and composition effect on microbubble stability have not been examined so far. In this part of the study, a a system designed to elucidate effect of composition, circulation time and temperature.

4.1.1. Effect of Emulsifier Content on Microbubble Stability

Before testing microbubbles under shear stress, one of our research group member performed the static stability experiments with DSPC/PEG40St microbubbles by changing the emulsifier content. As seen in Figure 4.1, increasing PEG40St molar ratio prolonged the life of microbubbles up to 50%. However, starting from 60% PEG40St molar ratio, increasing PEG40St molar ratio started to decrease microbubble stability (Sağdiç, 2013). Based on these results, DSPC/PEG40St microbubbles at 5:5, 6:4, 7:3, 8:2 and 9:1 molar ratios were tested under physiological shear stress conditions which are 0.028, 0.11, 0.28 and 0.42 Pa (Wiese, Barthel, & Dimitroff, 2009) at 25 ^{o}C. Experiments were performed for 15 and 30 min circulation times. In a literature study

performed with rats, the microbubble dosage to get image was determined as 10^9/ml (Burns & Wilson, 2006). Therefore, initial concentration of microbubbles was adjusted as 10^9/ml. After circulation of microbubbles under predetermined shear stresses, change in the size distributions and concentration of microbubbles were determined.

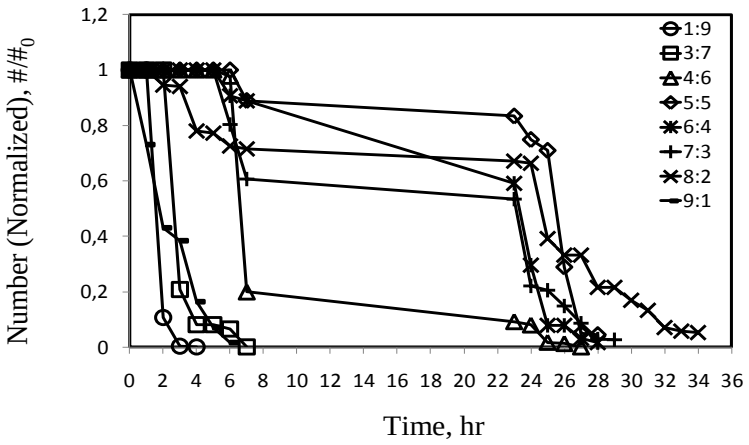

Figure 4.1. Static stability of DSPC/PEG40St microbubbles

DSPC/PEG40St 9:1 microbubble size distribution did not changed significantly after 15 min circulation under. 0.028, 0,11 and 0.28 Pa as seen in Figure 4.2. However, its concentration decreased with the effect of shear stress rapidly. Because of this reason, the experiment for 30 min circulation could not performed for 9:1 microbubbles.

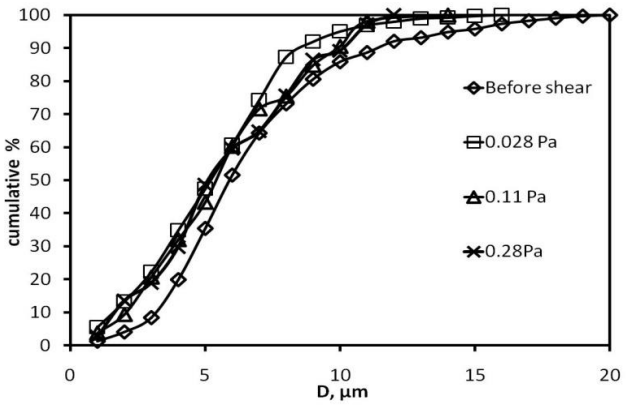

Figure 4.2. Size distribution of DSPC/PEG40St 9:1 microbubbles after circulation under shear stress 15 min at T=25 ^oC

DSPC/PEG40St 8:2 microbubbles also became when they exposed to shear stress for 15 min circulation. On the other hand, increase in exerted shear stress did not change the size distribution significantly as seen in Figure 4.3 (a). After 30 min circulation, microbubble size distribution change did not exhibit a trend with shear stress as shown in Figure 4.3 (b). Similar to 6:4 microbubbles, after exposing to 0.42 Pa shear stress, due to bubble coalescence microbubbles become larger than the microbubbles even exposed to no shear stress.

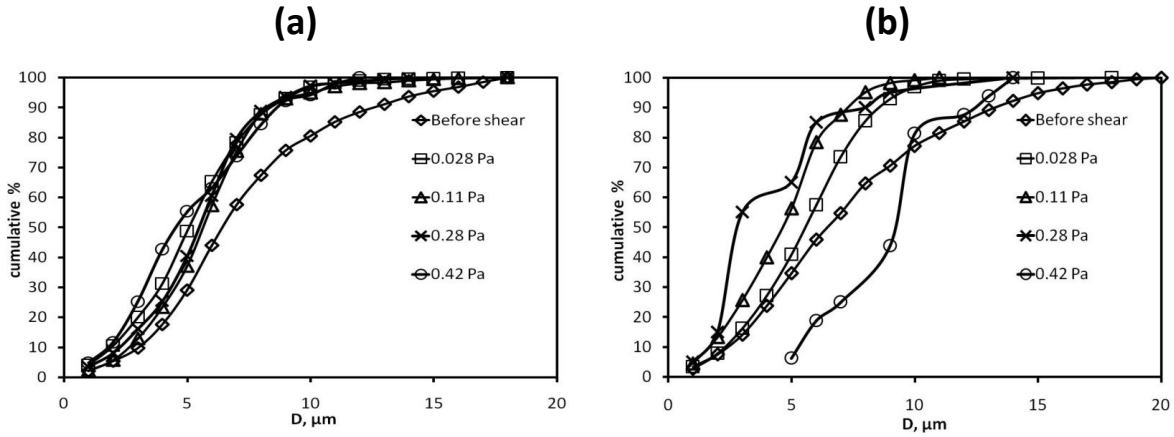

Figure 4.3. Size distribution of DSPC/PEG40St 8:2 microbubbles after circulation under shear stress for circulation time of (a) 15 min and (b) 30 min at T=25 ^{o}C

DSPC/PEG40St 7:3 microbubbles exhibited more stable behavior compared to the other compositions. After 15 min circulation under shear stress, minor changes occurred in size distribution of microbubbles as seen in Figure 4.4 (a). Increasing circulation time shifted microbubble sizes to smaller diameters with increasing shear stress.

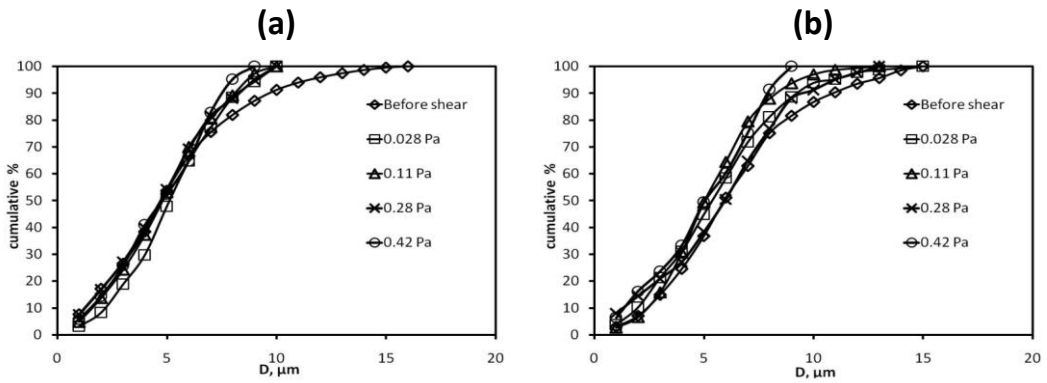

Figure 4.4. Size distribution of DSPC/PEG40St 7:3 microbubbles after circulation under shear stress for circulation time (a) 15 min and (b) 30 min at T=25 ^{o}C

As illustrated in Figure 4.5, similar trend was observed for DSPC/PEG40St 6:4 microbubbles with 5:5 microbubbles. Size of microbubbles shifted to smaller diameter after exposing to 0.028, 0.11 and 0.28 Pa. However, when 0.42 Pa shear stress was exerted to microbubbles, size distribution again shifted larger diameter. Increase in the size of microbubbles may result from bubble coalescence due to high shear stress.

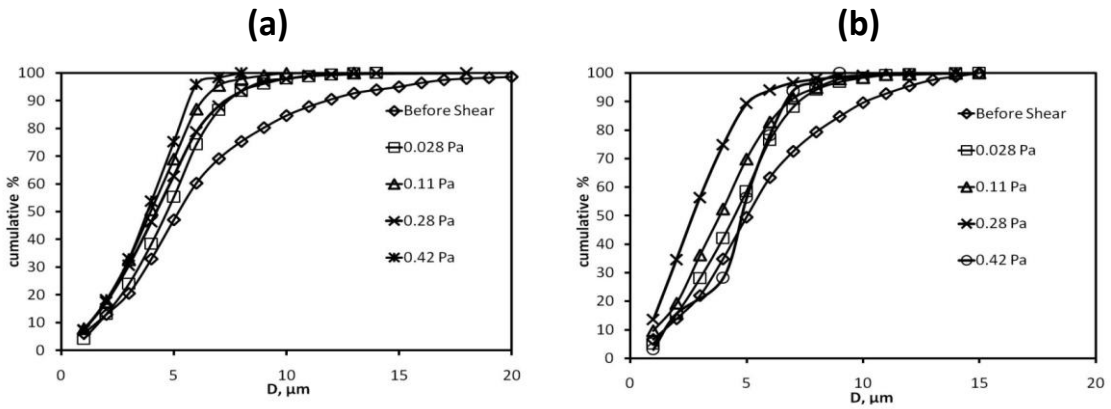

Figure 4.5. Size distribution of DSPC/PEG40St 6:4 microbubbles after circulation under shear stress for circulation time (a) 15 min and (b) 30 min at T=25 ^{o}C

In Figure 4.6, size distributions of DSPC/PEG40St 5:5 microbubbles' before and after subjecting shear stresses are shown for circulation time of 15 min and 30 min. As illustrated in Figure 4.6 (a), circulation of microbubbles under shear stress for 15 min resulted in reduce in the size of microbubbles. After microbubbles were exposed to 0.028 Pa shear stress, decrease in the size of microbubbles was prominent. After

circulation under 0.11 Pa shear stress, microbubbles got smaller compared to microbubble size distribution at 0.028 Pa. However further increase in shear stress did not change microbubble size distribution considerably, exhibiting similar behavior at 0.28 and 0.42 Pa shear stresses. Increasing circulation time also affected the microbubble size distribution. As shown in the Figure 4.6 (b), 5:5 microbubbles did not show a trend with shear stress when circulation time prolonged to 30 min. But, microbubbles in general were found to be getting smaller compared to initial conditions after circulating in each shear stress.

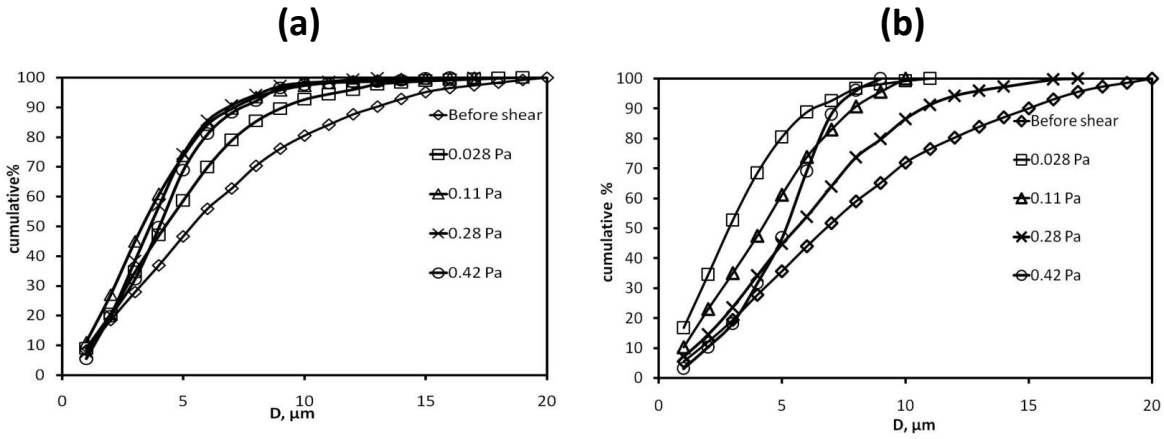

Figure 4.6. Size distribution of DSPC/PEG40St 5:5 microbubbles after circulation under shear stress for circulation time (a) 15 min and (b) 30 min at T=25 ^{o}C

In Figure 4.7 change in concentrations of microbubbles for 15 and 30 min circulation times are illustrated. Under same shear stress, microbubble concentration decreased more rapidly with the increasing circulation time. DSPC/PEG40St 9:1 microbubble could not save its stability at 0.42 Pa shear stress and its concentration decreased to zero as seen in Figure 4.7 (a) . For 30 min circulation time, even under 0.028 Pa shear stress 9:1 microbubble could not survive. After 15 min circulation time at 0.42 Pa while 8:2, 7:3 and 6:4 microbubbles lost approximately 85% of their initial concentrations, 5:5 microbubble lost nearly 50% of its initial concentration. After 30 min circulation time, decrease in the concentrations of the microbubbles was close. When size distribution changes of microbubbles were considered, in general, trend showed that microbubbles with large diameters were less stable compared to smaller

ones. Generally, decrease in concentration result from bursting of large microbubbles. However, shear stress can also cause bubble coalescence.

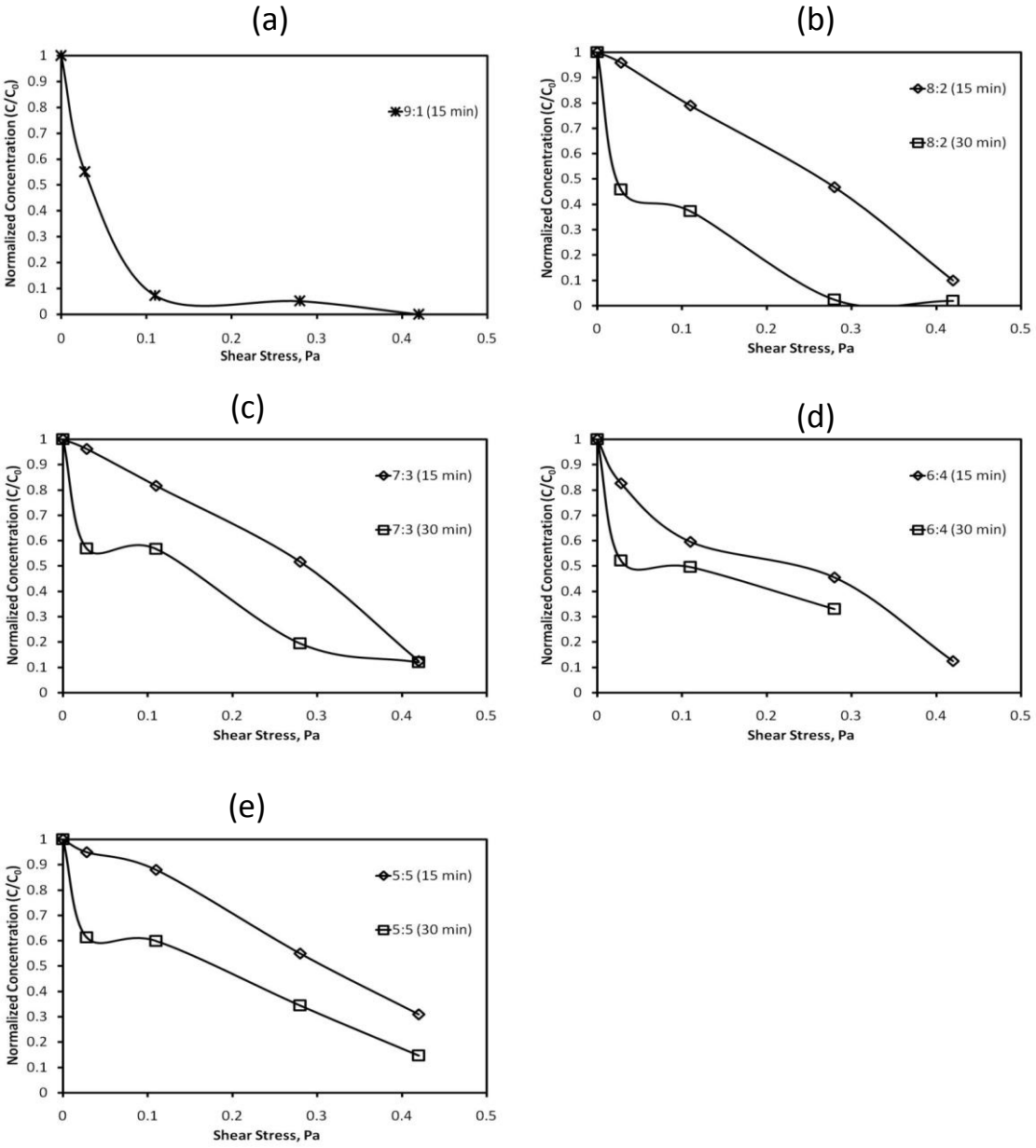

Figure 4.7. Change of microbubble concentration with shear stress for 15 and 30 min circulation of DSPC/PEG40St molar ratio of (a) 9:1, (b) 8:2, (c) 7:3, (d) 6:4 and (e) 5:5

In Figure 4.8 the changes in concentration of DSPC/PEG40St microbubbles at molar ratio of 5:5, 6:4, 7:3, 8:2 and 9:1 microbubbles' concentration change compared for 15 and 30 min circulation. Based on the results, it was concluded that, among the

microbubbles, DSPC/PEG40St 5:5 microbubbles were more resistant against the shear stress compared to other compositions.

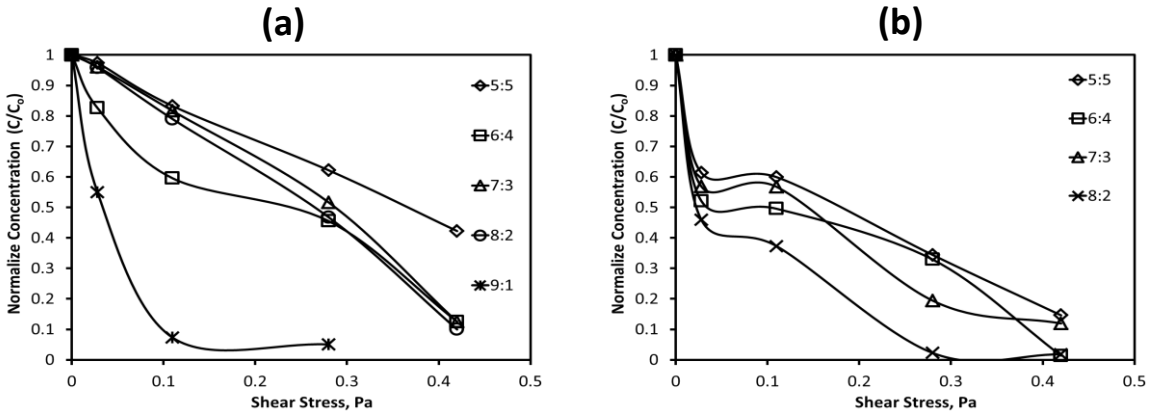

Figure 4.8. Change of microbubble concentration shear stress for (a) 15 and (b) 30 min circulation

4.1.2. Effect of Emulsifier Type on Microbubble Stability

Emulsifiers are omnipresent in microbubble formulations since they provide increase in the yield and stability of microbubbles. As emulsifying agent generally PEG attached phospholipids such as DSPE-PEG2000 and stearate-lipid attached like PEG40St are used (Kwan & Borden, 2012a). Since emulsifier type is an important parameter for microbubble stability, in this part of the study effect of emulsifier type was investigated. As illustrated in Figure 4.8, DSPC/PEG40St molar ratio of 5:5 microbubbles were more stable under shear stress compared to other compositions. Addressing this conclusion, effect of emulsifier type was investigated by mixing DSPC with DSPE-PEG1000 and DSPE-PEG2000 at 5 to 5 molar ratio. Experiments were performed at the same conditions for 15 min circulation time.

In Figure 4.9, cumulative percentages of microbubbles are illustrated. As seen in figure, sizes of microbubbles show tendency to decrease for both of the emulsifier types. Since PEG40St has a single tail acly chain and less hydrophobic compared to lipopolymer DSPE-PEG2000 (Kwan & Borden, 2012b), DSPC/PEG40St microbubbles got smaller compared to DSPC/PEG1000 and DSPC/PEG2000 microbubbles. Moreover, since DSPE- DSPE-PEG2000 has double tail, it is expected form a more cohesive microbubble shell compared to PEG40St (Lozano & Longo, 2009). Based on this reason, it may be concluded that when DSPC/DSPE-PEG2000 microbubbles were

exposed to shear stress, gas diffusion from the microbubbles was less compared to DSPC/PEG40St.

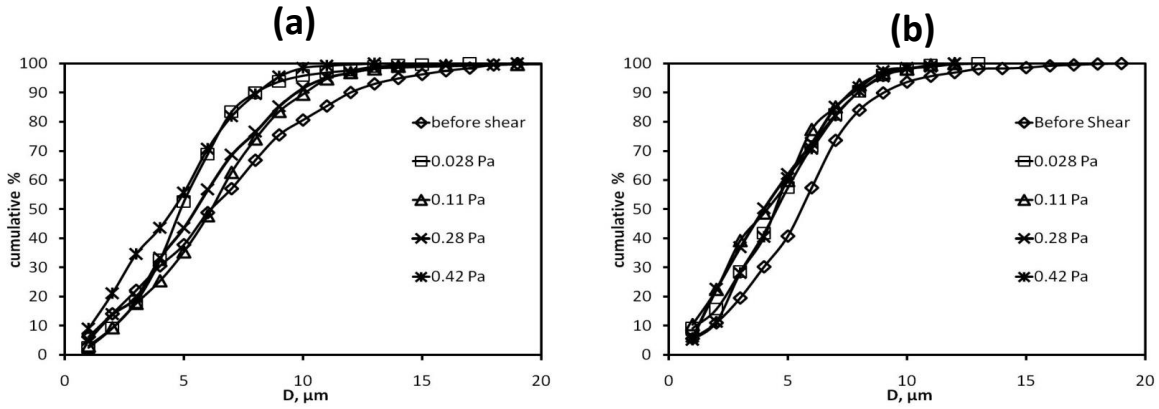

Figure 4.9. Size distribution of (a) DSPC/DSPE-PEG1000 and (b) DSPC/DSPE-PEG2000 5:5 microbubbles after circulation under shear stress for 15 min at T=25 ^{o}C

Change in concentrations of microbubbles after exposing the shear stress are revealed in Figure 4.10. After circulating under 0.028, 0.11 and 0.28 Pa shear stresses, concentration loss of DSPC/PEG40St microbubbles were lower compared to DSPC/PEG1000 and DSPC/PEG2000 microbubbles. However, under 0.42 Pa shear stress, decrease in the concentration was approximately same for DSPC/PEG40St and DSPC/PEG2000. Surprising result observed with DSPC/DSPE-PEG2000 microbubbles was attributed to shape of the emulsifier. While DSPE-PEG2000 has cylindrical shape, PEG40 St is in conical shape, filling the spaces between cylindrical phospholipid molecules covering spherical microbubble surface. Since DSPE-PEG1000 has shorter PEG chain compared to DSPE-PEG2000, this effect was more distinct in DSPC/DSPE-PEG1000 microbbubles, supporting our argument.

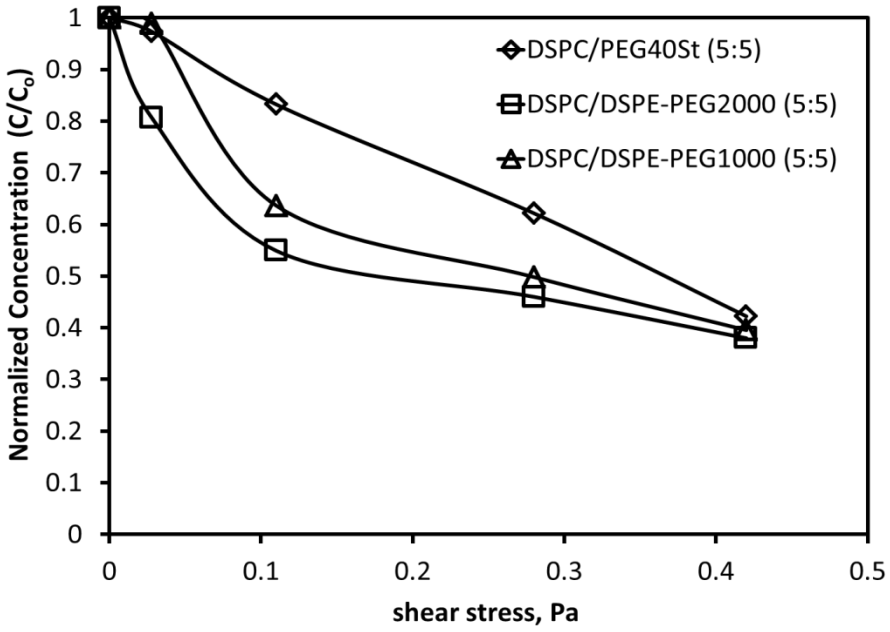

Figure 4.10. Comparison of DSPC/PEG40St, DSPC/DSPE-PEG1000 and DSPC/PEG2000 5:5 microbubbles concentration change with respect shear stress

In order to investigate effect of temperature on microbubble stability, change in microbubble diameters were observed under microscope for 2 hours at 38 ^{o}C. As illustrated in Figure 4.11, size of microbubbles did not changed significantly for both microbubbles with initial diameter 8 μm and 6 μm.

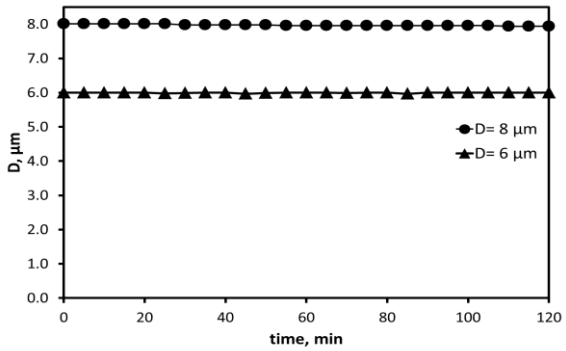

Figure 4.11. Change of diameter of DSPC/PEG40St 5:5 microbubbles with initial diameter 8 μm and 6 μm at T=38 ^{o}C without shear stress

Considering that in the experiments presented above, the effect of shear stress and temperature may have been coupled. In this part of the study, shear stress

experiments were repeated at 4 ^{o}C, 25^{o}C and 38 ^{o}C for DSPC/PEG40St 5:5 microbubbles.

In the experiments performed in our group it was observed that DSPC/PEG40St 5:5 microbubbles, 5:5 microbubbles' size distribution and concentration were found to be stable more than 24 hours at 4 ^{o}C. Based on these results, when shear experiments were performed at 4^{o}C, the change in the concentration and size distribution of microbubble resulted from effect of shear stress. Experiments were implemented for 5, 10 and 15 min circulation times under physiological shear stresses at.

Change in the size distribution of DSPC/PEG40St 5:5 microbubbles at 4 ^{o}C under different shear stresses and circulation times are illustrated in Figure 4.12. Change in the size distribution of microbubbles did not show any trend. However, microbubbles generally tended to shrink.

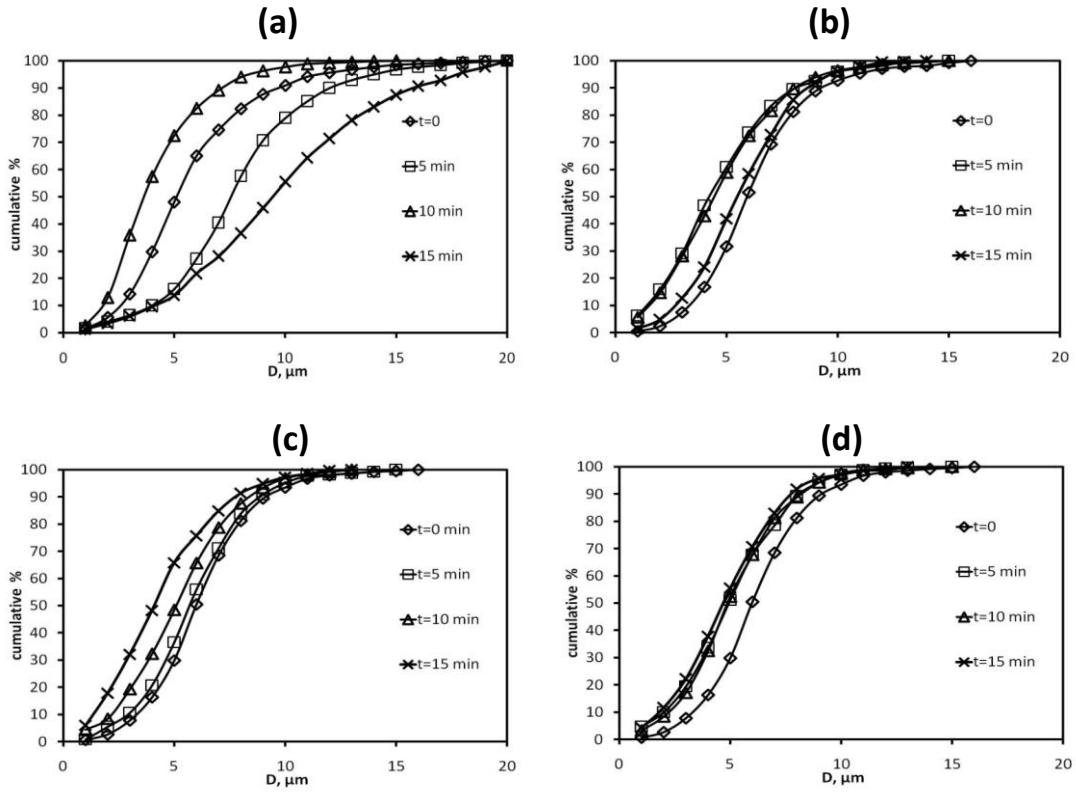

Figure 4.12. Size distribution of DSPC/PEG40St 5:5 microbubbles after circulation under (a) 0.028 Pa, (b) 0.11 Pa, (c) 0.28 Pa and (d) 0.42 Pa shear stress 5 for 15 min at T=4 ^{o}C

As revealed in Figure 4.13**,** increase in the shear stress and circulation time result in more rapid decrease in the microbubble concentration. After circulation of

microbubbles for 15 at 0.028 Pa shear stress, loss of concentration is only 3%. While no concentration loss was observed under 0.028 Pa shear stress after 5 and 10 min circulation times, under 0.11, 0.28 and 0.42 Pa shear stresses concentration of microbubbles started to decrease after 5 min circulation. Concentration loss after 15 min circulation was, 10% at 0.11 Pa, 20% at 0.28 Pa and 40% at 0.42 Pa.

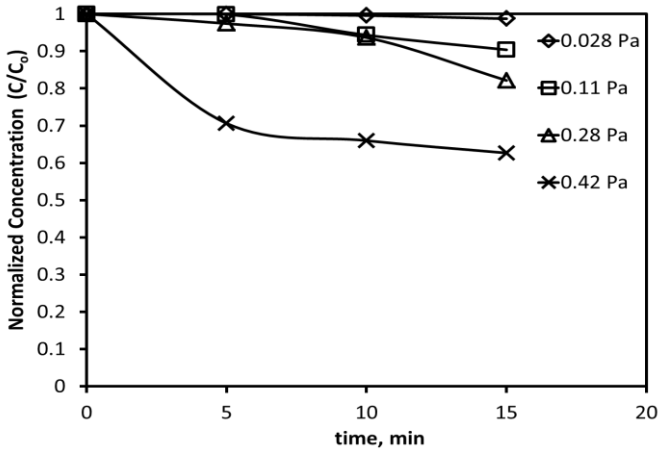

Figure 4.13. Comparison of DSPC/PEG40St 5:5 microbubble concentration change after subjecting different shear stresses at T=4 ^{o}C

At 25 ^{o}C, no considerable change was observed in size distribution of microbubbles under 0.028 Pa shear stress for different circulation times as seen in Figure 4.14. When microbubbles were subjected to 0.28 Pa shear stress, after 5 and 10 min circulation size distribution of microbubbles were approximately same. However, after 15 min circulation of the microbubbles, size of microbubbles decreased conspicuously. Under 0.42 Pa shear stress, decrease in the size distribution of microbubbles observed started after 5 min circulation and got smaller with the increasing circulation time since number of large microbubbles decreased. As discussed in previous results, decrease in the concentration of microbubbles attributed to dissolution of large microbubbles and shifting to large diameters results from coalescence of small microbubbles with the effect of shear stress.

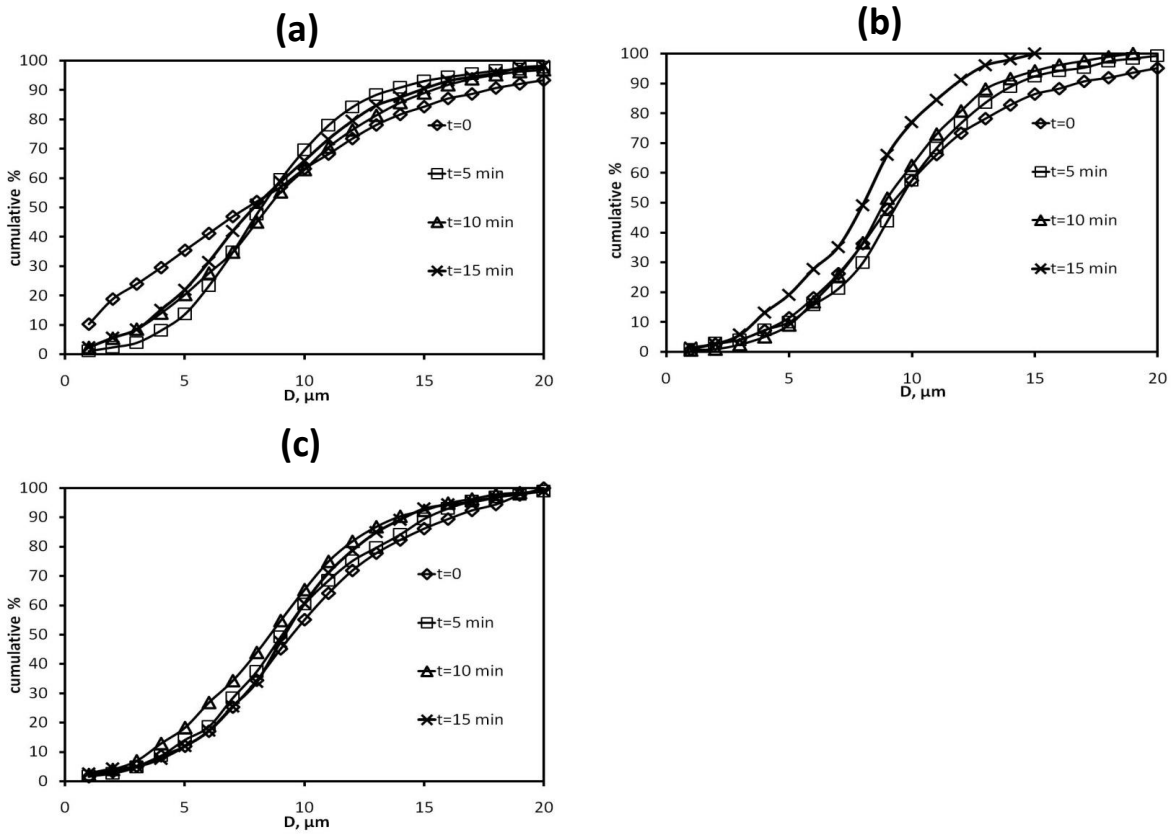

Figure 4.14. Size distribution of DSPC/PEG40St 5:5 microbubbles after circulation under (a) 0.028 Pa, (b) 0.28 Pa and (c) 0.42 Pa shear stress for 15 min at T=25 ^{o}C

Concentration changes of microbubbles with respect to circulation time under various shear stresses are illustrated in Figure 4.15. As seen in Figure 4.15, with the increasing circulation time and shear stress, decrease in the microbubble concentration quickened.

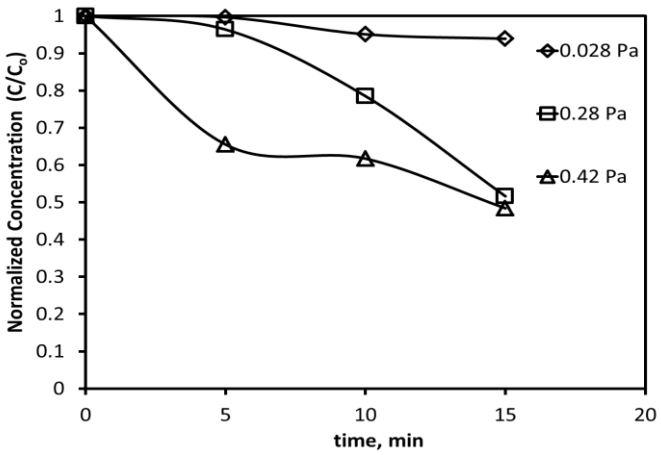

Figure 4.15. Comparison of DSPC/PEG40St 5:5 microbubble concentration change after subjecting different shear stresses at T=25 ^{o}C

Since microbubbles are injected to the body, it is necessary to investigate their dynamic stability at 38 ^{o}C which is close to body temperature. Because of this reason, same experiments were performed at 38 ^{o}C. As seen Figure 4.16 (a), microbubble size distribution did not changed significantly but show tendency to shift smaller diameters and as revealed in Figure 4.17, microbubbles lost their concentration rapidly. As illustrated in Figure 4.16 (b), after circulation under 0.28 Pa shear stress, microbubbles became smaller with increasing circulation time and concentration loss of microbubbles was higher compared to 0.028 Pa shear stress.

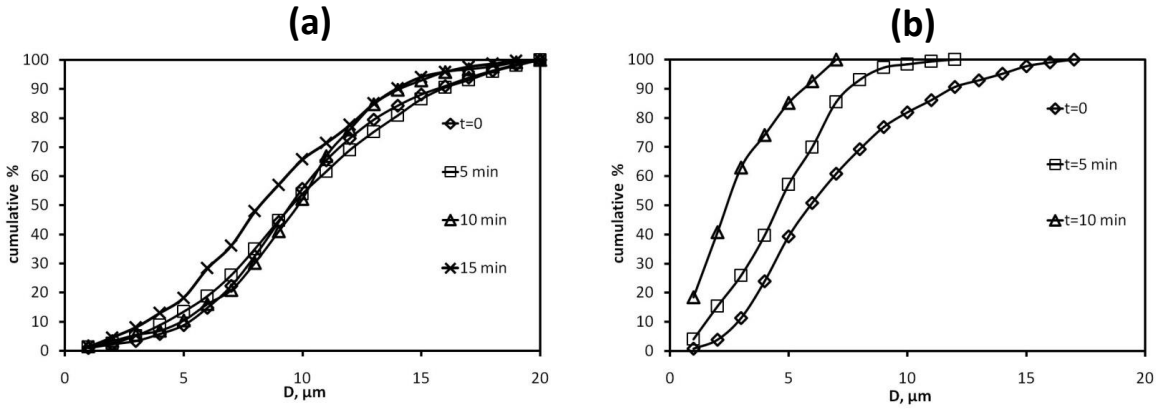

Figure 4.16. Size distribution of DSPC/PEG40St 5:5 microbubbles after circulation under (a) 0.028 Pa and (b) 0.28 shear stress for 15 min at T=38 ^{o}C

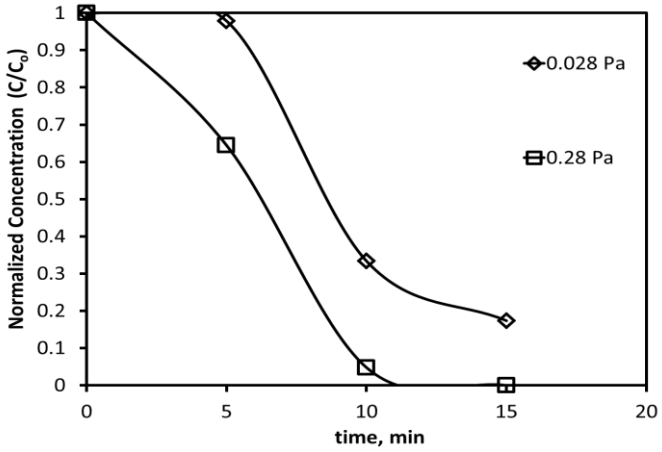

Figure 4.17. Comparison of DSPC/PEG40St 5:5 microbubble concentration change after subjecting different shear stresses at T=38 ^{o}C

In Figure 4.18 microbubble concentration changes at 4, 25 and 38 ^{o}C after circulation under shear stress are compared. As shown in Figure 4.18 (a), (b), (c), increasing temperature result in more rapid decrease in concentration of microbubbles. At low temperatures like 4 ^{o}C, van der Waals interaction between shell components are stronger (Kwan & Borden, 2012b), so that microbubble shell is in the more condense form and more resistive against shear stress. As increasing temperature, DSPC and PEG40St pass to expand phase since area per molecule increased due to weakening of van der Waals forces. So that, at high temperatures microbubble shell cannot save its stiffness.

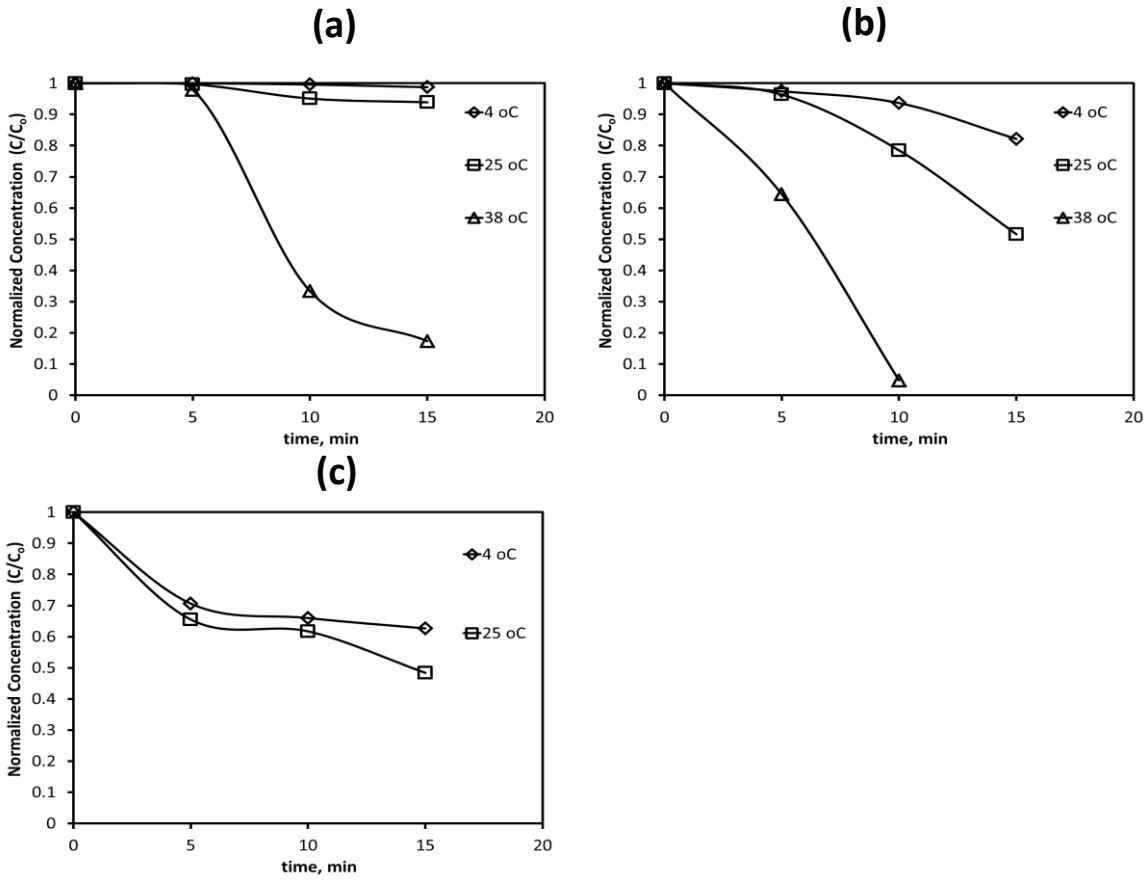

Figure 4.18. Comparison of microbubble concentration after subjecting (a) 0.028 Pa, (b) 0.28 Pa, (c) 0.42 Pa shear stress at 4 ^{o}C, 25 ^{o}C and 38 ^{o}C

4.1.3. Effect of Gas core on Microbubble stability

The filling gas of microbubble is one of the most important factors that make microbubbles functional in biomedical applications. In ultrasound imaging, due to acoustic impedance difference between filling gas and red blood cells image of structures of body delineated. Low solubility of filling gas in the surrounding medium prolongs the lifetime of microbubbles. To obtain stable microbubbles it suggested filling gas to be nonpolar, hydrophobic and have high molecular weight (Kwan & Borden, 2012b). Perfluorocarbon gas is one of the gases providing these properties.

DSPC/PEG40St 9:1, 7:3 and 5:5 microbubbles were prepared by using PFC as filling gas. Effect of shear stress on PFC filled 9:1, 7:3 and 5:5 microbubbles were investigated at 38 ^{o}C and compared with air filled 9:1, 7:3 and 5:5 microbubbles.

As discussed before, as the temperature increases, attractive interactions like van der Waals forces, hydrophobic interactions between shell components decrease. Despite the 38 ^{o}C temperature, size distribution of DSPC/PEG40St 9:1 microbubbles did not changed significantly. Emulsifier prevents the coalescence of microbubbles (Kwan & Borden, 2012a). Since 9:1 microbubbles have less emulsifier, 9:1 microbubbles were expected to be larger compared to 5:5 and 7:3 microbubbles. When air was used as filling gas, obtained 9:1 microbubbles were larger compared to other microbubbles. On the other hand, PFC filled 9:1 microbubbles were as small as 5:5 and 7:3 microbubbles due to hydrophobic interaction between the microbubble shell and PFC gas. As seen in Figure 4.19, while size distribution of 7:3 microbubbles also did not affected by shear stress, size of PFC filled 5:5 microbubbles tend to shrink.

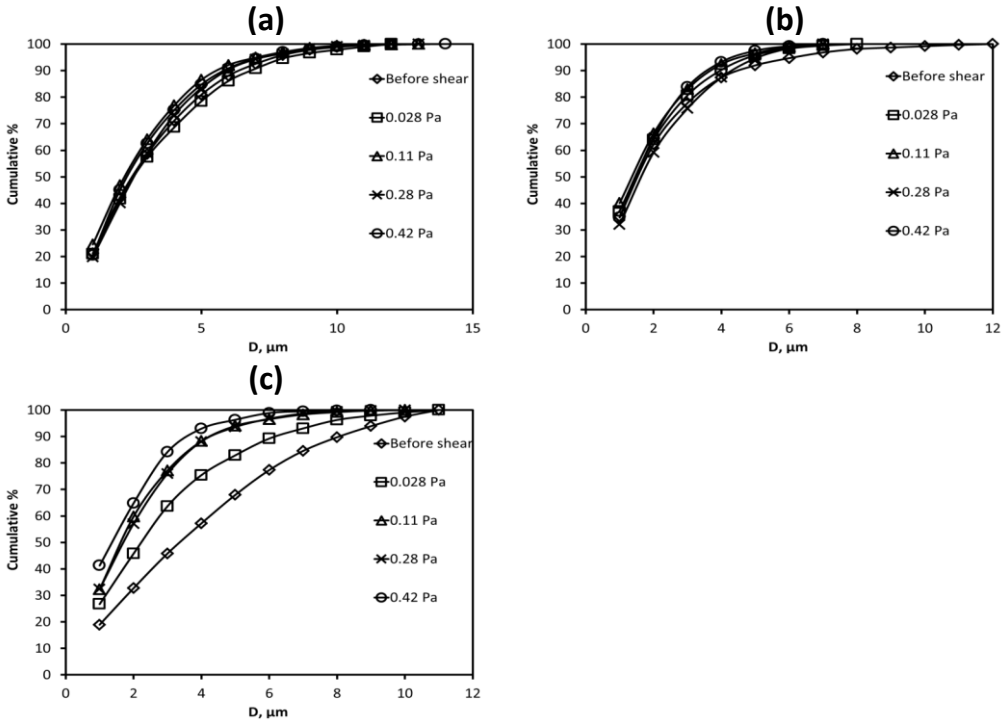

Figure 4.19. Size distribution of PFC filled DSPC/PEG40St (a) 9:1, (b) 7:3 and (c) 5:5 microbubbles after subjecting shear stress 15 min at T=38 ^{o}C

In Figure 4.20, concentration change of 9:1, 5:5 and 7:3 microbubbles are illustrated. As comprehended from the figure, starting from 0.028 Pa, microbubble concentration started to decrease for each microbubble type. Microbubble loss was not considerably different after circulation under higher shear stresses. In PFC filled

DSPC/PEG40St filled microbubbles, as the DSPC concentration increased, microbubbles become more resistive against to shear stress. As seen in figure, under same shear stress conditions, decrease in the microbubble concentration is higher compared to 7:3 and 9:1 for 5:5 microbubbles.

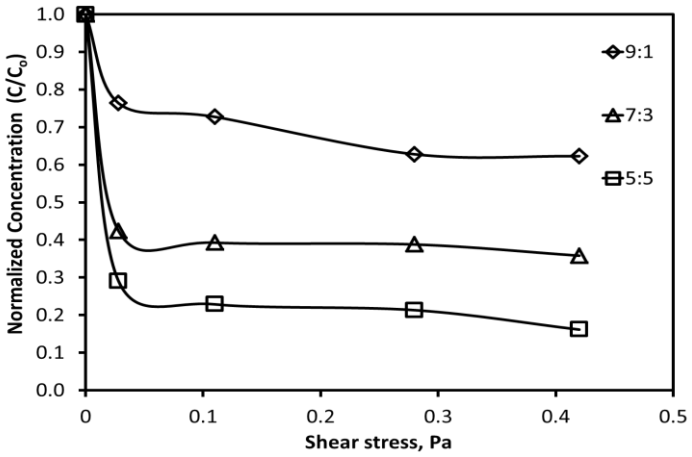

Figure 4.20. Comparison of PFC filled DSPC/PEG40St microbubble concentration change with respect shear stress at T=38 ^{o}C

In 5:5 microbubbles, as seen in Figure 4.19 and Figure 4.20, although the concentration change is approximately after subjecting the 0.11, 0.28 and 0.42 Pa shear stresses, size of microbubbles were decreased. These behaviors show that 5:5 microbubbles dissolve according to Ostwald ripening principle. Ostwald ripening occurs when one of the shell component's interfacial tension is higher than the mixture of shell components. In our case, PEG40St has higher interfacial tension than the DSPC and PEG40St mixture. Based on Ostwald ripening principle, due to high Laplace pressure small microbubbles get smaller while large bubbles become larger. Talu et al. also observed Ostwald ripening behavior for DSPC/PEG40St microbubbles (Talu, Lozano, Powell, Dayton, & Longo, 2006).

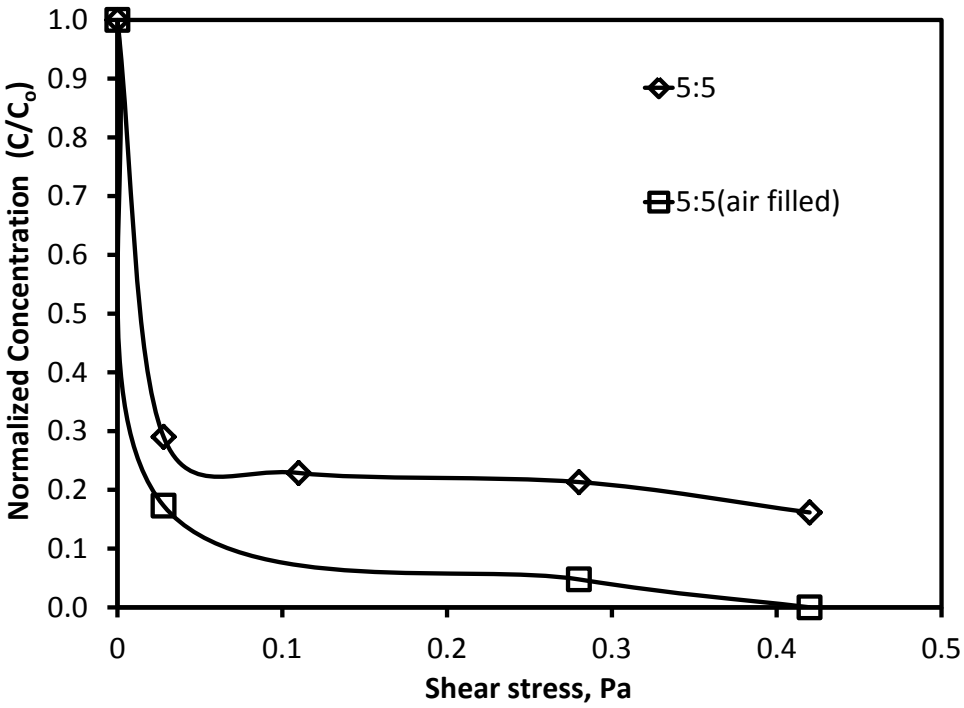

Figure 4.21. Comparison of air filled and PFC filled DSPC/PEG40St microbubble's concentration change with respect to shear stress at T=38 ^{o}C

In Figure 4.21, the response of air filled and PFC filled 5:5 DSPC/PEG40St microbubbles are revealed. As seen in figure, using PFC in the gas core of 5:5 microbubbles instead of air, enhanced the shell stability and made microbubbles more resistive against to shear stress.

As discussed before, 9:1 air filled microbubbles were not durable under shear stress at 38 ^{o}C. On the other hand, when 9:1 microbubbles were filled with PFC, they became more resistant against shear stress and temperature. These enhancements in the shell stability can be attributed to hydrophobicity, low solubility of PFC and increase in the microbubble elasticity because of PFC (Szíjjártó, Rossi, Waton, & Krafft, 2012).

4.2. Protein Adsorption to Ethylene Oxide Monolayers

Poly(ethylene glycol) (PEG) has been extensively used to cover surfaces of invivo injected biomaterials due to its low toxicity, low immunogenicity and low adhesion to proteins. PEG chains form a protective hydration layer around the surface of the material, providing steric repulsion for proteins. Literature studies showed that, PEG

does not influence the cohesive and mechanical properties of the microbubbles and lioposmes, however it significantly increases the circulation life (Tirosh, Barenholz, Katzhendler, & Priev, 1998).

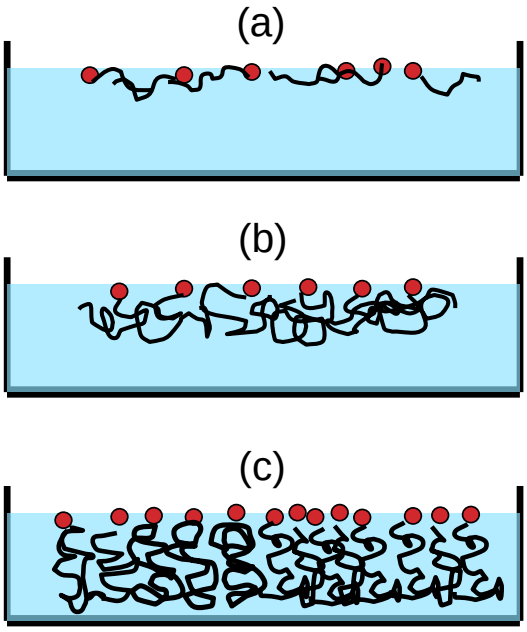

Figure 4.22. Shematic illustration of (a) pancake, (b) mushroom, (c) brush conformations of PEG

PEG chains attached to a surface may have different conformations in water phase such as pancake, mushroom and brush as shown in Figure 4.22. In mushroom conformation, the surface coverage is low (Sukhishvili et al., 2000) and in this conformation PEG cannot prevent the protein adsorption. In the mushroom conformation, PEG chains are arbitrarily oriented and a low packing density is preserved (Levin, Bishnoi, Grady, & Halas, 2006). When the distance between the chains gets smaller, PEG chains become gradually crowded and stretched away from the surface forming a brush conformation (Zhao & Brittain, 2000). In the brush conformation, molecular layer maintains approximately 10 fold greater packing density than the mushroom conformation (Levin et al., 2006) and resist to protein adsorption (Hucknall, Rangarajan, & Chilkoti, 2009).

In our microbubble formulations, PEG40St was used as emulsifying agent which is controversial in the literature. While Borden et al. asserts PEG40St squeeze out from the monolayer at high packing densities (after 35 mN/m) surface pressure (Mark A Borden, Pu, et al., 2004), El-Khouri et al. claimed that PEG40St's head group is large

enough to achieve conformational change (El-Khouri et al., 2011). We aimed to elucidate this dilemma in literature by using protein resistive property of PEG and we investigated the protein adsorption behavior of PEG40St with increasing packing density and temperature by using LB technique and SPR technique.

4.2.1. Protein Adsorption to DSPC/PEG40St monolayers in Langmuir Blodgett System

In this part of the study, effect of PEG40St molar ratio to protein resistance was investigated. Borden et al. studied the monolayers of 90% lipids with different acly chain length mixed with 10% PEG40St in LB system and plateau regions were observed at approximately at 35 mN/m surface pressure. Borden et al., interpreted the observed plateau as the squeeze out of the PEG40St from the monolayer (Mark A Borden, Pu, et al., 2004). In other words, microbubbles cannot be produced with a highly condensed shell. In order to elucidate this point, protein adsorption experiments were performed by compressing mixed monolayers up to 30 mN/m and 40 mN/m surface pressures. Thereby, the difference in protein adsorption before and after plateau region was examined. In order to investigate the effect of temperature, experiments were carried out at 20 ^{o}C and 38 ^{o}C.

In order to understand the changes in surface pressure resulting from BSA adsorption, BSA was injected to the subphase in the absence of the monolayer. Although BSA is water soluble protein, when BSA was injected to the water, surface pressure increased very rapidly within the first 20 min as seen in Figure 4.23 both at 20 ^{o}C and 38 ^{o}C. After 20 min, increase in the surface pressure was more gradual.

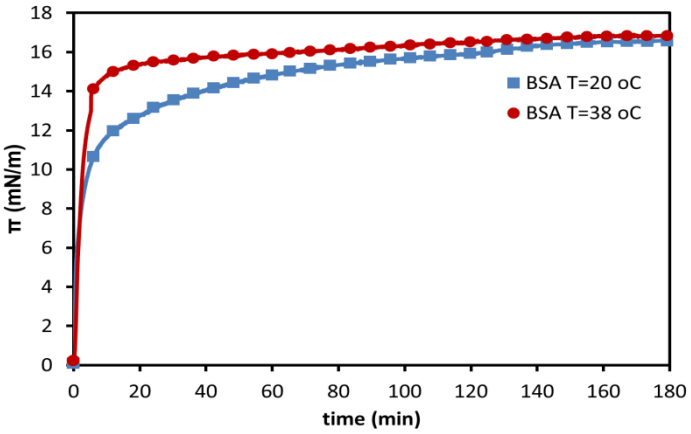

Figure 4.23. Surface pressure change with respect to time when BSA injected to subphase in the absence of monolayer

Based on these results, after protein injection in the presence of the monolayer, surface pressure change was measured for 1 hour. To calculate change in the surface pressure due to protein adsorption, at the same conditions surface pressure of monolayers measured with respect to time without protein injection to the subphase. Change in the surface pressure was calculated by subtracting surface pressure of monolayer without BSA injection from surface pressure data obtained upon BSA injection into the subphase.

Before examining mixed monolayer behavior of DSPC and PEG40St, their response to BSA in the subphase was investigated at 20 ^{o}C and 38 ^{o}C by compressing them up to 30 mN/m surface pressure. As seen in Figure 4.24, the change in surface pressure of PEG40St was negative (Figure 4.24 (b)) both at 20 ^{o}C and 38 ^{o}C. Negative $\Delta\pi$ may results from no protein adsorption to monolayer or pulling of PEG40St molecules down with gravity due to adsorbed BSA. At 38 ^{o}C, monolayer was disturbed due to weakening of van der Waals interactions at high temperature. On the other hand, PEG40St became more hydrophobic while DSPC monolayer passes to a relaxed state. Positive change in surface pressure in DSPC monolayer can be attributed to relaxation of DSPC monolayer to disordered state and thus, as seen in Figure 4.24 (a), more BSA adsorbed.

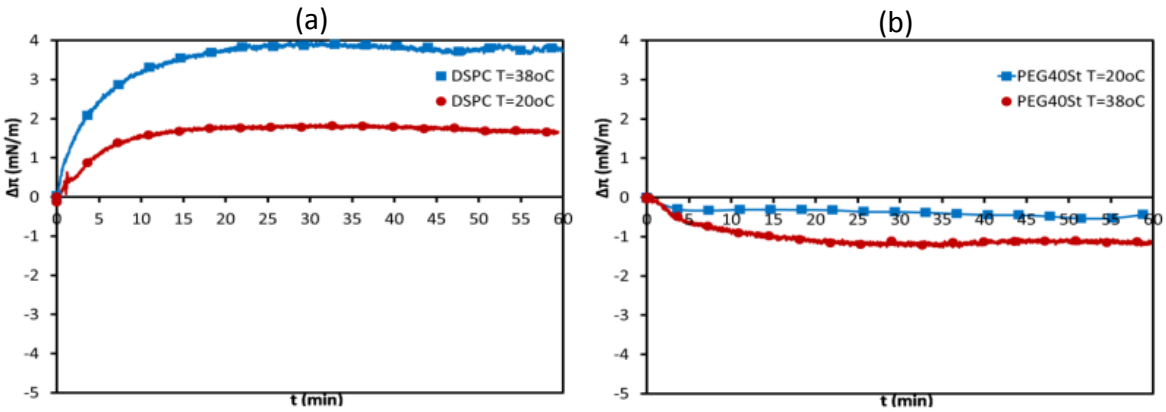

Figure 4.24. BSA adsorption to precompressed (a) DSPC and (b) PEG40St monolayer at 20 ^{o}C and 38 ^{o}C

In Figure 4.25, 9:1, 7:3 and 5:5 compositions of DSPC/PEG40St mixed monolayers were compared. As comprehended from the results, PEG40St conformation change is induced by surface pressure, temperature and molar ratio of PEG40St in the monolayer. At 20 oC, protein adsorption to 9:1 monolayer was higher compared to 38 ^{o}C for both at surface pressure 30 mN/m and 40 mN/m (Figure 4.25). At 20 ^{o}C 30 mN/m surface pressure (Figure 4.25 (a)), first 15 min BSA adsorbed to the monolayer and surface pressure reached to equilibrium. Due to presence of 9:1 film at the air-water interface, injection of BSA did not increased the surface pressure as much as increased in film free surface (Figure 4.23). At 20 ^{o}C 40 mN/m surface pressure, surface pressure increased linearly and did not reach to equilibrium as seen in Figure 4.25 (b). This increase in the surface pressure may result from the squeeze out of the PEG40St from monolayer. When PEG40St composition was higher than 10%, conformational change of PE40St from mushroom to brush became more possible and BSA adsorption to monolayer was more hindered as seen in Figure 4.25. At surface pressure 40 mN/m, except for 9:1 mixed monolayer, each mixed monolayer became more resistant against to protein adsorption. At 38 ^{o}C, change in the surface pressure was negative (Figure 4.25 (c) and (d)). As discussed before, negative $\Delta\pi$ may result from pulling down of PEG40St by adsorbed BSA or prevention of protein adsorption. In order to elucidate the negative changes in surface pressure better, mixing Gibbs free energies of mixed monolayers were calculated by using π-A isotherm data obtained before protein injection at 20 ^{o}C and 38 ^{o}C. As revealed in Figure 4.26 (a), at 20 ^{o}C, due to van der Waals interactions between head groups of DSPC and PEG40St for each mixture,

attractive interactions were dominant and PEG40St could retain in the monolayer. However, at 38 ^{o}C, van der Waals interactions weakened and interaction between monolayer components decreased (Figure 4.26 (b)). Since PEG40st become more hydropohobic, it may remain at air water interface. On the other hand, DSPC monolayer relaxed and its interaction with PEG40St decreased. Based on these results, pulling down of PEG40St by the adsorbed BSA is more possible.

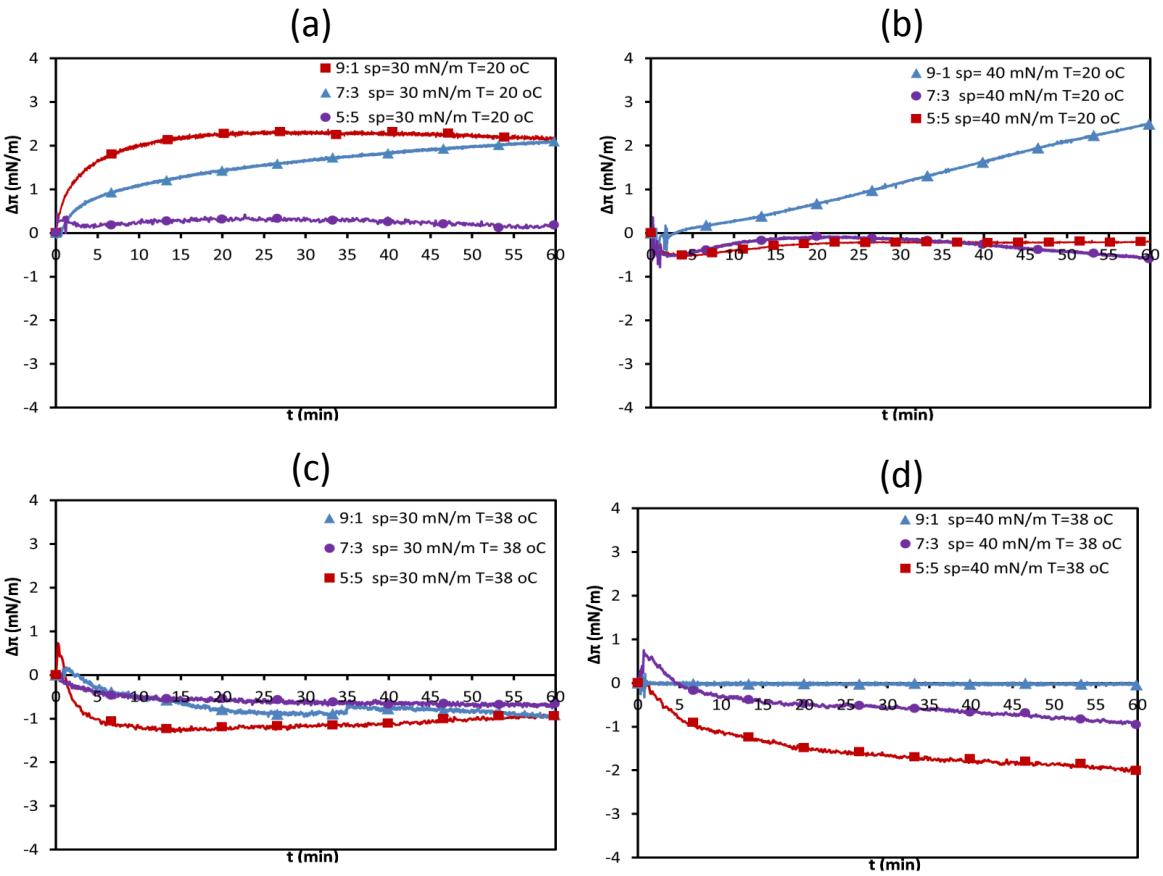

Figure 4.25. Comparison of BSA adsorption to DSPC/PEG40St mixed monolayer with 10%, 30% and 50% PEG40St at T=20 ^{o}C (a) π=30 mN/m, (b)) π=40 mN/m and at T=38 ^{o}C (c) π=30 mN/m, (d)) π=40 mN/m

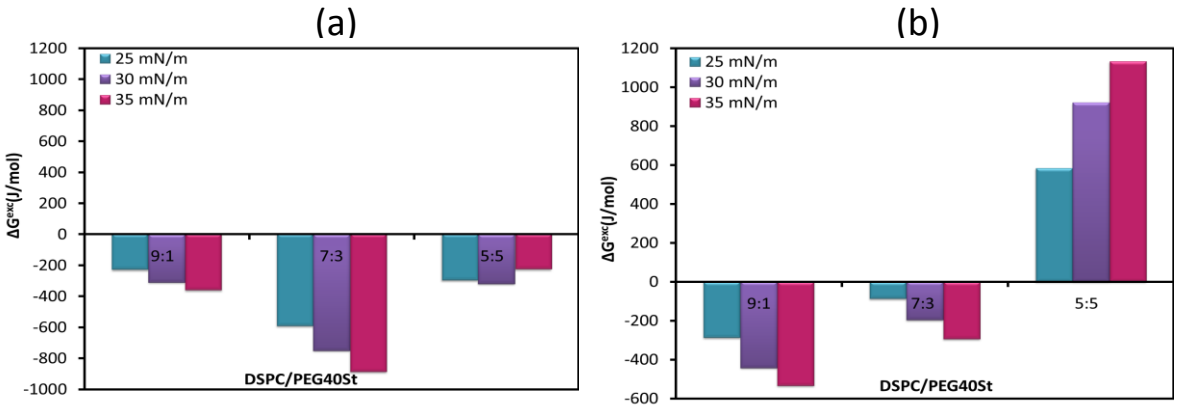

Figure 4.26. Excess Gibbs free energies of DSPC/PEG40St mixed monolayers at (a) T=20 ^{o}C, (b) T=38 ^{o}C

4.2.2. Protein Adsorption to DSPC/PEG40St monolayers in SPR

As comparative method to protein adsorption experiments to DSPC/PEG40St monolayers implemented in LB through, SPR technique was used to measure protein adhesion. In order to investigate effect of packing density, octanethiol modified gold substrates coated DSPC/PEG40St mixtures at 30 mN/m and 40 mN/m surface pressures using LB deposition technique. Effect of temperature on protein adsorption was also investigated by performing experiments at 20 ^{o}C and 38 ^{o}C respectively. As control experiment, only octanethiol modified surfaces were also tested at 20 ^{o}C and 38 ^{o}C and indicated as blank in Figure 4.27.

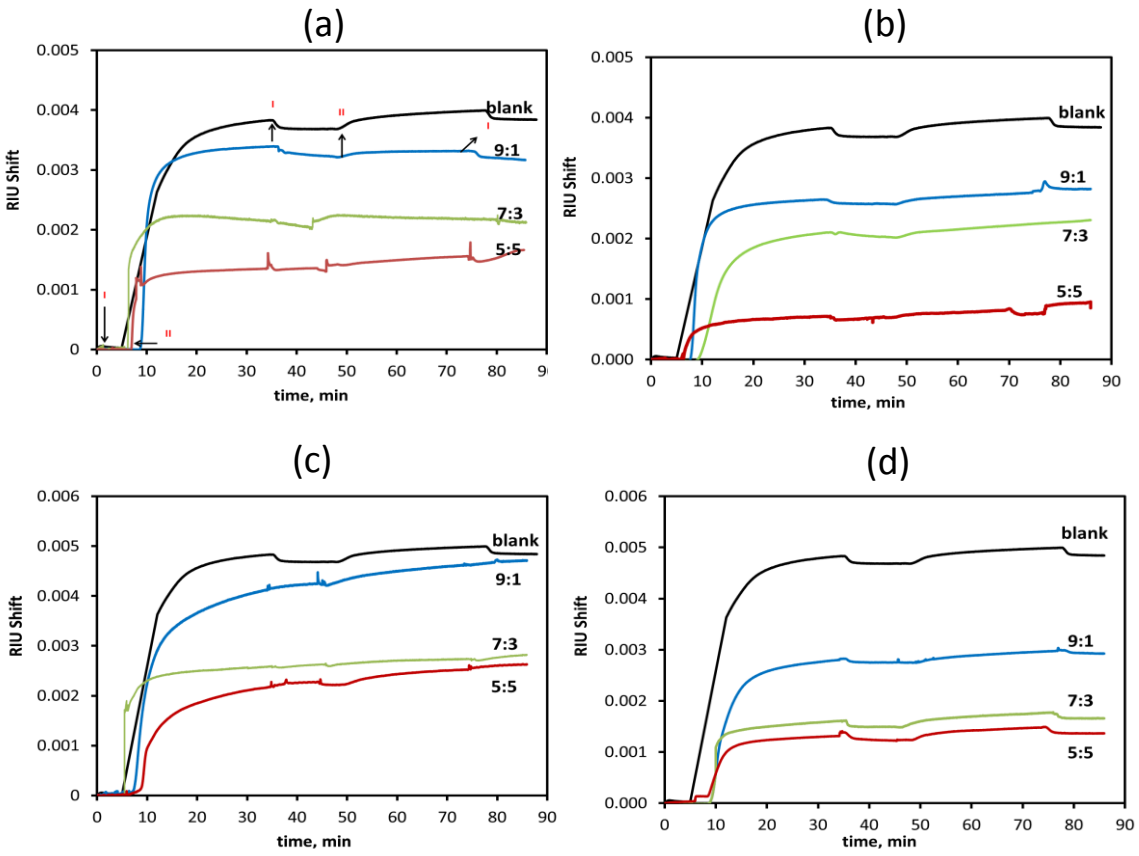

Figure 4.27. SPR sensograms of DSPC/PEG40St 9:1, 7:3 and 5:5 coated surfaces at 20 ^{o}C (a) sp=30 mN/m, (b) sp=40 mN/m and 38 ^{o}C (c) sp=30 mN/m, (d) sp=40 mN/m, I water injection, II protein injection

In Figure 4.27, comparison of SPR sensograms of DSPC/PEG40St mixtures with 10%, 30% and 50% PEG40St molar ratio are illustrated. Adsorbed amount of BSA calculated measuring the change in the refractive index unit (RIU shift). For both temperatures and surface pressure, it was observed that, increasing PEG40St molar ratio result in less RIU shift. As shown in Figure 4.27 (c) and (d) At 38 ^{o}C since monolayer less ordered state, higher RIU shift values obtained. As seen in Figure 4.27 (c), when BSA solution washed out with water, RIU shift value did not decreased. This data showed that, with 10% PEG40St molar ratio BSA adhesion cannot be prevented at 30 mN/m surface pressure and 38 ^{o}C.

Adsorbed BSA amount per area for each mixture is revealed in Figure 4.28. Only octanethiol coated surface (blank) adsorbed more BSA than each DSPC/PEG40St mixture coated surfaces. This was an expected result due to hydrophobic nature of the octanethiol layer and existence of hydrophobic moieties in BSA (Plant, Brighamburke,

Petrella, & Oshannessy, 1995). Increasing PEG40St molar ratio brought about less protein adsorption. At 20 ^{o}C (Figure 4.28 (a)), protein adsorption was less compared to 38 ^{o}C Figure 4.28 (b)) since molecules are at more ordered state at low temperatures. As surface pressure increased, protein adhesion to surfaces decreased due to high packing density for all mixtures. At 20 ^{o}C,5:5 coated surface at 40 mN/m surface pressure , as BSA solution pass through the flow cell and replaced with ultrapure water change in the resonance angle was low due to minor binding of BSA to the surface (Figure 4.27 (b)). Increase in the PEG40St molar ratio and packing density made the surfaces more protein repellant. These results suggest that, 10% PEG40St may not be enough to achieve conformational change at 30 mN/m surface pressure, so that it cannot show resistance to protein adhesion. At 38 ^{o}C, increasing PEG40St content of the monolayer result in more protein resistive surfaces as happened in 20 ^{o}C.

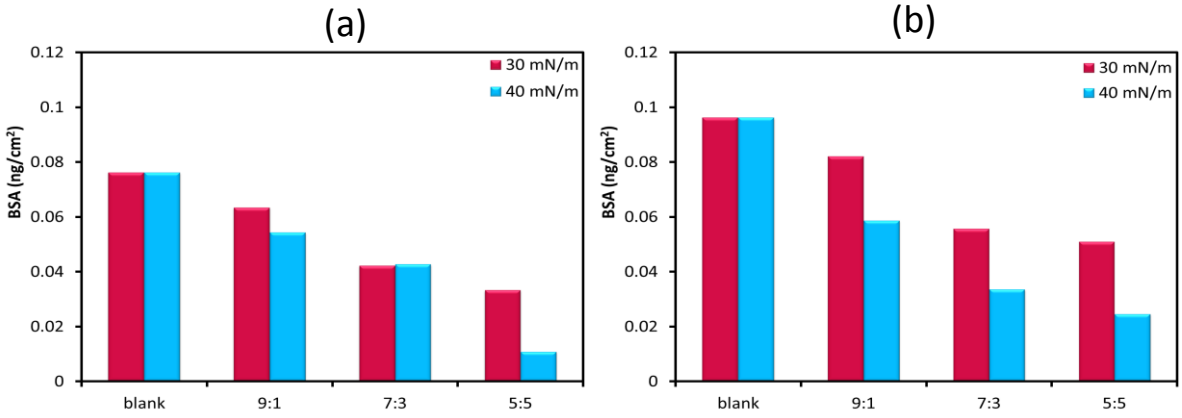

Figure 4.28. BSA adsorption to DSPC/PEG40St 9:1, 7:3 and 5:5 coated surfaces at sp= 30 mN/m and 40 mN/m (a) T=20 ^{o}C and (b) T=38 ^{o}C

When LB method and SPR method results are considered, both method showed that as the PEG40St molar ratio is increased the possibility of PEG40St to change its conformation and retain in the monolayer. However, while negative changes were observed in surface pressure in LB experiments (Figure 4.25 (b) and (c)), in SPR experiments, as seen in Figure 4.28(b) BSA adsorption was higher compared to 20 ^{o}C. These differences may be elucidated by considering the difference between two systems. With the effect of gravity, as schematized in Figure 4.29 (a) and discussed above, while BSA pull down the PEG40St molecules, in SPR BSA molecules sit on the SPR substrate (Figure 4.29 (b)).

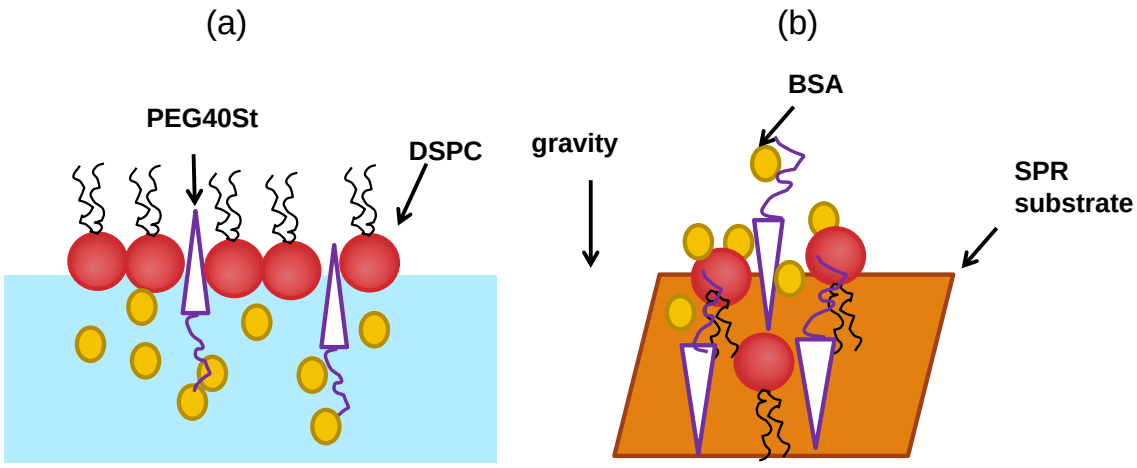

Figure 4.29. Schematic illustration of protein adsorption experiments (a) LB and (b) SPR system at T=38 ^{o}C

As reported in literature studies, a plateau was observed in DSPC/PEG40St mixtures at approximately 35 mN/m surface pressure which is collapse pressure of pure PEG40St monolayer and this plateau was interpreted as squeeze out of PEG40St from the monolayer (Mark A Borden, Pu, et al., 2004). However, in our experiments in both LB and SPR methods we observed that with increasing PEG40St molar ratio protein adsorption characteristic of monolayers changed. From these results we can conclude that not all PEG40St, even some do, squeezed out from the monolayer at the surface pressures above 35 mN/m.

4.3. Effect of Secondary Forces on Microbubble Shell Structure

Microbubble shell components determine the stability and drug delivery properties of microbubbles. Secondary forces like ionic interactions and hydrogen bonding may increase the microbubble shell stability and if microbubbles are to be used as drug or gene delivery vesicles, drugs or genes can be conjugated to microbubble shell with the help of a charge dependent non covalent bonding (Dijkmans et al., 2004).

In Figure 4.30, π-A isotherms of DSPC/PEG40St mixed monolayers are illustrated performed by one ofour research group member (Bölükçü, 2013). As seen in Figure 4.30, at the beginning of the compression, increasing PEG40St molar ratio shifted the π-A isotherms larger mean molecular areas. However, after approximately

40 $Å^2$, monolayers became more condensed with increasing PEG40St molar ratio. We also reported that, for air filled microbubbles, increasing PEG40St molar ratio resulted in more stable microbubbles against shear stress. From these results, we surmise that holding PEG40St molar ratio as 50% in mixtures results in more cohesive microbubble shell.

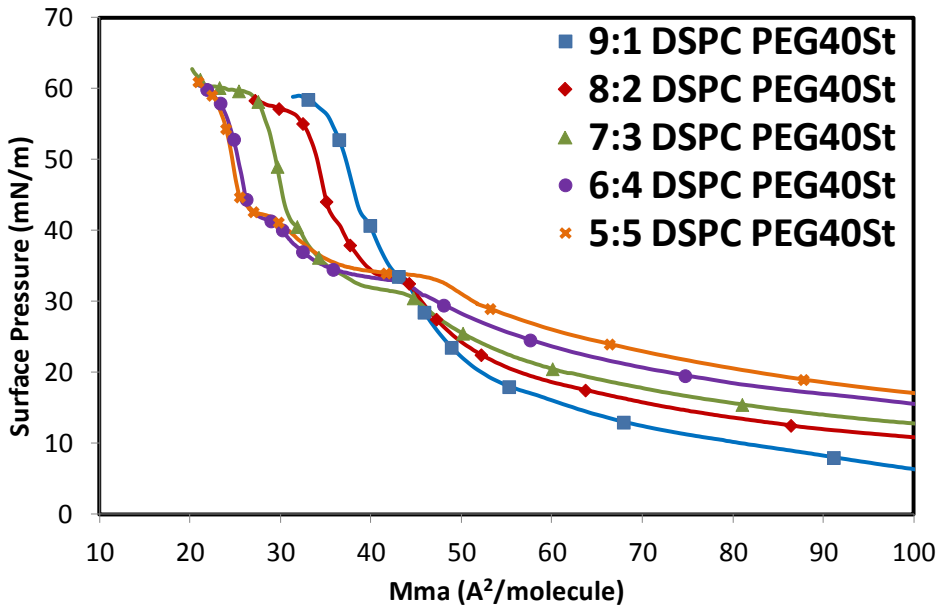

Figure 4.30. π-A isotherms of DSPC/PEG40St monolayers T=20 ^oC

In this part of the study, we investigated the effect of secondary forces on microbubble shell stability by addition of a third component to DSPC/PEG40St mixture. In mixtures, because of the reasons discussed above PEG40St molar ratio generally hold as 50%.

In experiments, Langmuir Blodgett technique was used and phase behavior of monolayers was visualized via Brewster Angle Microscopy. As a third component to DSPC and PEG40St mixture, 1-steoyl-rac-glycerol (StGly), Stearylamine ($StNH_2$), 1,2-distearoyl-sn-glycero-3-(phospho-l-serine) (DSPS), 1,2-stearoyl-3-trimethylammonium-propane (DSTAP). Among third components, StGly have ability to make hydrogen bonding, DSPS is anionic and capable of making hyrogen bonding, $StNH_2$ and DSTAP are cationic.

4.3.1. Phase Behavior and Morphology of DSPC/PEG40St/Stgly Monolayers

1-steoyl-rac-glycerol (StGly) is a single tail nonionic surfactant and generally used as food emulsifier (Ruiz Domínguez, Narváez, & Rodríguez Patino, 1998). As seen in Figure 4.31, it has hydroxyl groups in its chemical structure. So that, it was expected to make hyrogen bonding with DSPC and PEG40St.

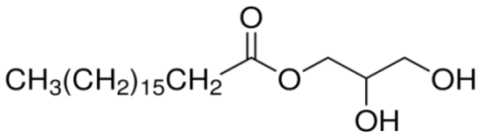

Figure 4.31. Chemical structure of 1-steoyl-rac-glycerol

In this part of the study, effect of StGly addition to DSPC/PEG40St mixture on monolayer stability, flexibility and morphology was investigated by using Langmuir – Blodgett technique. For this purpose, mixtures of DSPC/PEG40St/StGly were prepared at different molar ratios.

Figure 4.32 shows π-A isotherms of pure components and mixtures of DSPC/PEG40St/StGly monolayers measured at T=20 ^{o}C. PEG40St π-A isotherm is in good agreement with previous literature studies (Mark A Borden, Pu, et al., 2004; Xing et al., 2010). As seen in Figure 4.32, PEG40St exhibited expand phase behavior due to repulsive interactions between its large hydrophilic chains and collapsed approximately at 35 mN/m surface pressure. Obtained DSPC π-A isotherm is also consistent with the current literature studies (Mark A Borden, Pu, et al., 2004; Greenough & Blanchard, 2009). At large mean molecular areas, DSPC exhibited 0 mN/m surface pressure. Further compression of DSPC resulted in a dramatic increase in the surface pressure with a lift off at approximately 56 Å^2 mean molecular area and eventually the monolayer collapsed at around 63 mN/m surface pressure. As seen in Figure 4.32 isotherm of StGly showed more condense phase behavior compared to that of PEG40St and DSPC, exhibiting no increase in surface pressure up to 60 Å^2 mean molecular area and it collapsed nearly at 55 mN/m surface pressure. π-A curves of mixed films of DSPC, PEG40St and StGly when PEG40St molar ratio kept 0.5 was presented in Figure 4.32. In each mixture isotherm, a plateau region was observed at 35 mN/m (± 2) which is collapse pressure of PEG40St. In a literature study, Borden et. al studied the surface

phase behavior of lipid/PEG monolayers by mixing acyl chain length of lipid from $diC_{12:0}PC$ to $diC_{24:0}PC$. They reported that, when PEG40St was mixed with $diC_{12:0}PC$,$diC_{14:0}PC$, lipids plateau region was not observed in π-A isotherms. On the other hand, $diC_{16:0}PC$,$diC_{18:0}PC$ and $diC_{20:0}PC$ exhibited the plateau. Borden et al. attributed this plateau to squeeze out of PEG40St from the monolayer and they reported that plateau was more evident for $diC_{18:0}PC$/PEG40St monolayer (Mark A Borden, Pu, et al., 2004). Observed plateau in mixture isotherms (Figure 4.32) may result from conformational change of PEG40St or squeeze out of PEG40St from monolayer. When protein adsorption experiments were considered, conformational change of PEG40St As shown in Figure 4.32 since StGly exhibits more condense behavior compared to DSPC and PEG40St, increase in the molar ratio of StGly resulted in shift to smaller mean molecular areas in mixture isotherms, therefore, more condensed film was obtained.

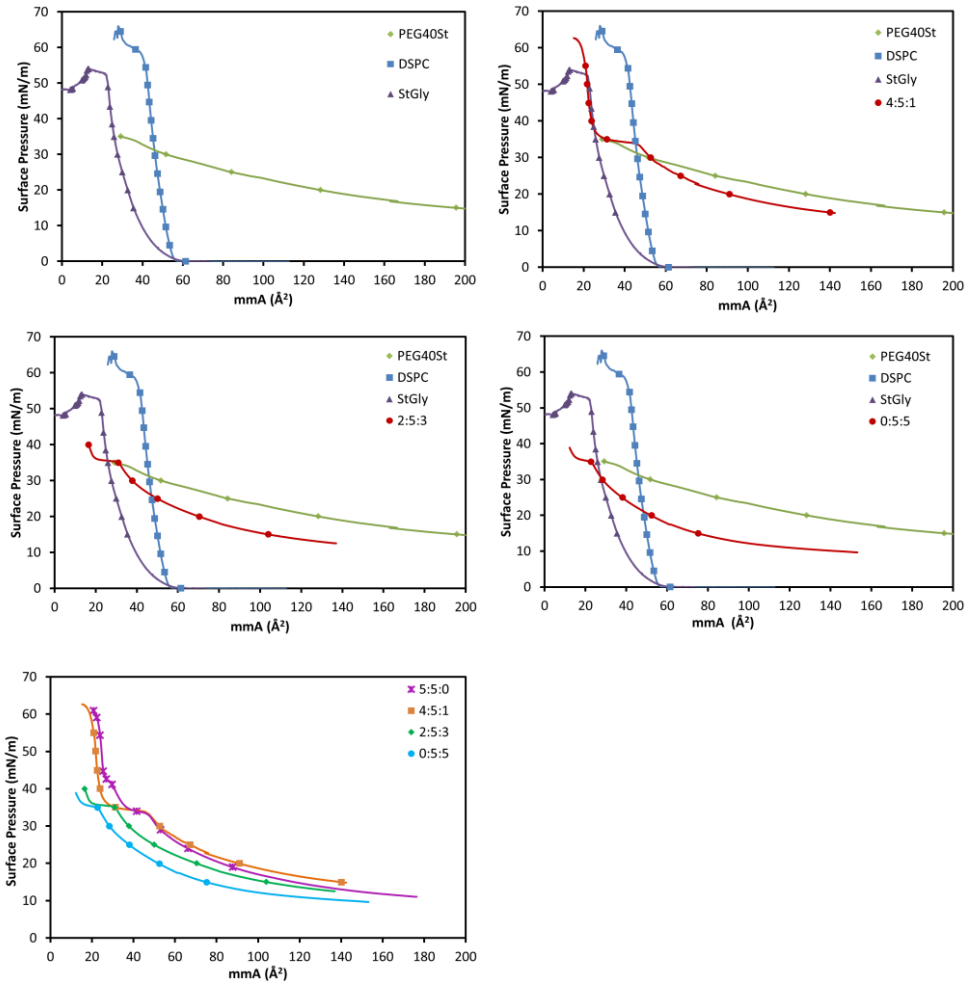

Figure 4.32. π-A isotherm of pure and DSPC/PEG40St/StGly mixtures at T=20 ^{o}C

In order to gain information about interaction and miscibility of DSPC/PEG40St/StGly mixtures, mixing Gibbs free energies were calculated.

Figure 4.33 represents the comparison of excess Gibbs free energies of mixed films. Each mixed film of DSPC/PEG40St/StGly showed non-ideal mixing behavior. In 4:5:1 mixture repulsive interactions between head groups of molecules were dominant. With the increasing surface pressure, a decrease in the mixing free energy was observed since molecules get closer. When StGly mol fraction was 30% attractive interactions between head groups of molecules dominated the mixing behavior of the monolayer. Even though pure StGly isotherm exhibits more condensed behavior compared to pure DSPC, 0:5:5 mixed film's mixing free energy values were less negative compared to 2:5:3 mixed film. From these results it may be concluded that, interaction between DSPC and StGly may provide more packed monolayer when StGly mol fraction is higher than 10%.

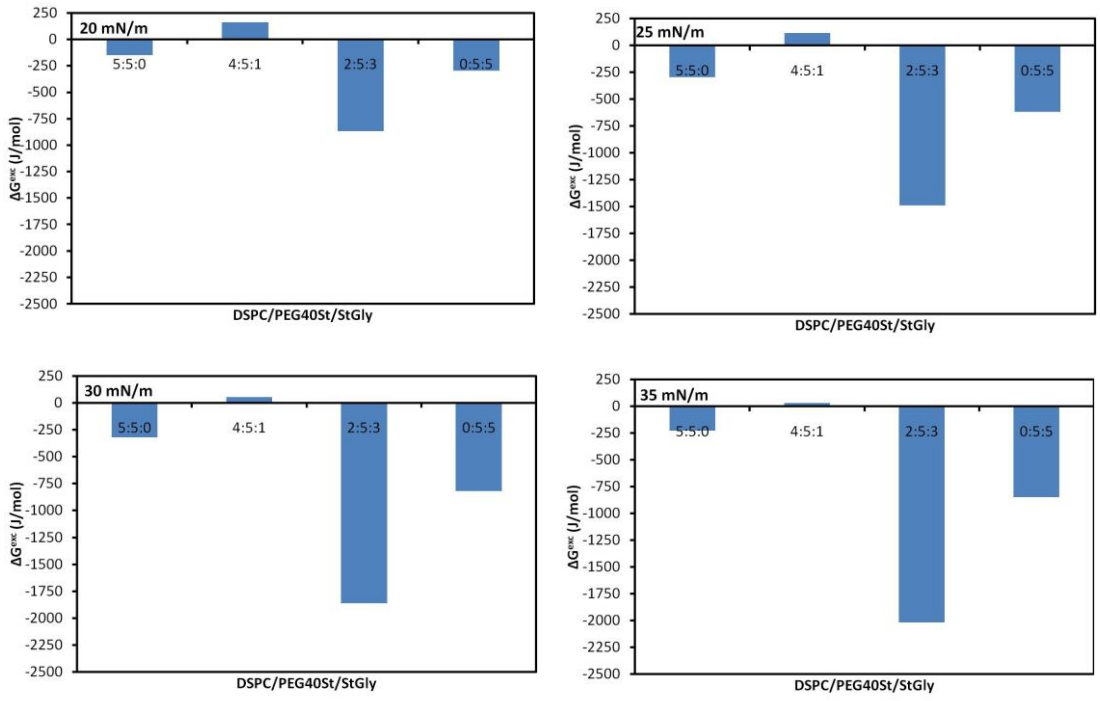

Figure 4.33. Excess free energy of mixing (ΔGExc) values of DSPC/PEG40St/StGly mixed monolayers calculated at π=20 mN/m, π=25 mN/m, π=30 mN/m, π=35 mN/m surface pressures.

Elasticity behaviors of DSPC/PEG40St/StGly mixed films are illustrated in Figure 4.34. Although StGly exhibits more condense phase behavior in π-A isotherms,

it provided more elastic behavior. Approximately at 45 mN/m surface pressure, StGly monolayer displayed a peak at 120 mN/m compressional modulus due to liquid condense phase. After that peak, with increasing surface pressure, compressional modulus started to decrease since StGly monolayer approached to collapse. Compressional modulus values of mixtures were similar except for 0:5:5 mixture. 0:5:5 mixture showed a more elastic behavior compared to other mixtures since there was no DSPC in it. Each mixture exhibited liquid expand phase behavior up to 35 mN/m surface pressure. Exhibited a minimum in compressional modulus at 35 mN/m surface pressure may be due to configurational change of PEG chains. After the minimum point, compressional modulus values of the mixtures were increased indicating liquid condensed phase.

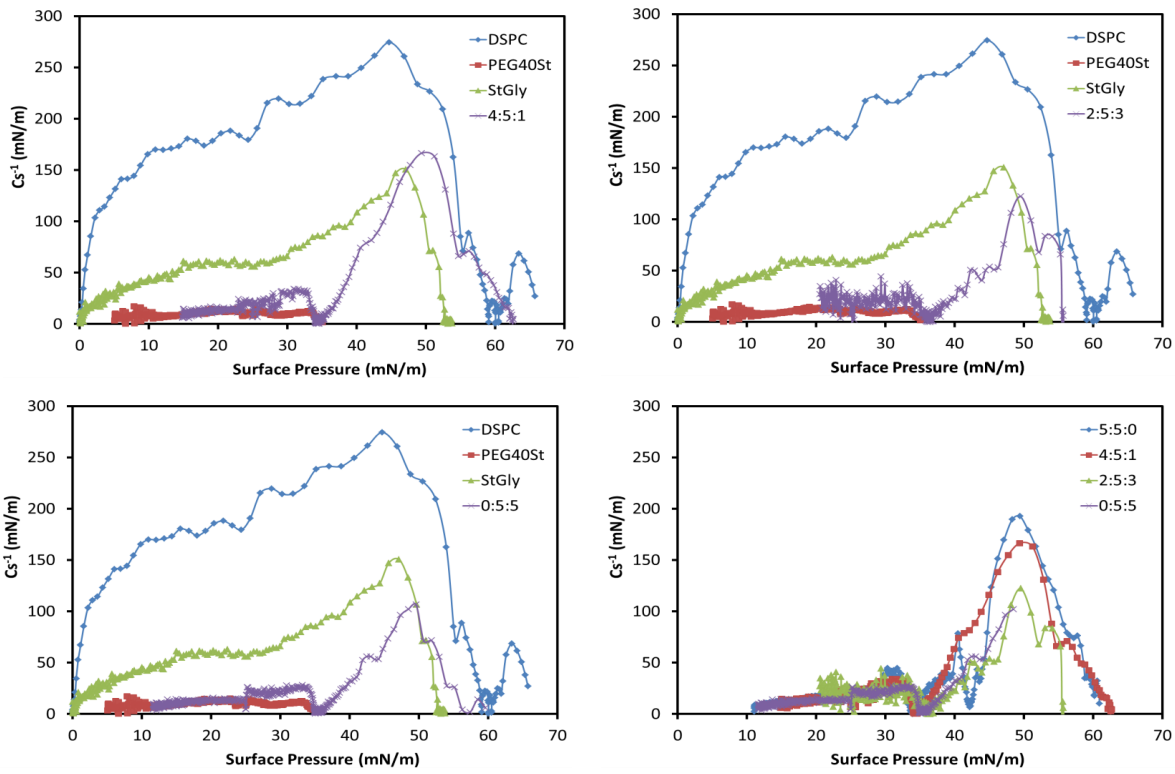

Figure 4.34. The compression modulus (Cs^{-1}) plots of DSPC/PEG40St/StGly mixed films

In order to visualize phase behavior of DSPC/PEG40St/DSPC mixed films which does not reverberate to the π-A isotherm (like local collapses), BAM images of the mixed films taken at the same conditions with LB experiments.

Phase behavior of StGly surfactant was observed via BAM at air water interface. As represented in Figure 4.35, at low surface pressures StGly gave cardioid and circular shaped domains. With increasing surface pressure, solid domains were detected. After 40 mN/m surface pressure, liquid condensed homogeneous phases were observed. However, at 50mN/m surface pressure phase separations were observed again and monolayer collapsed. During the collapse of monolayer, solid stick like domains and liquid condense phases were coexist.

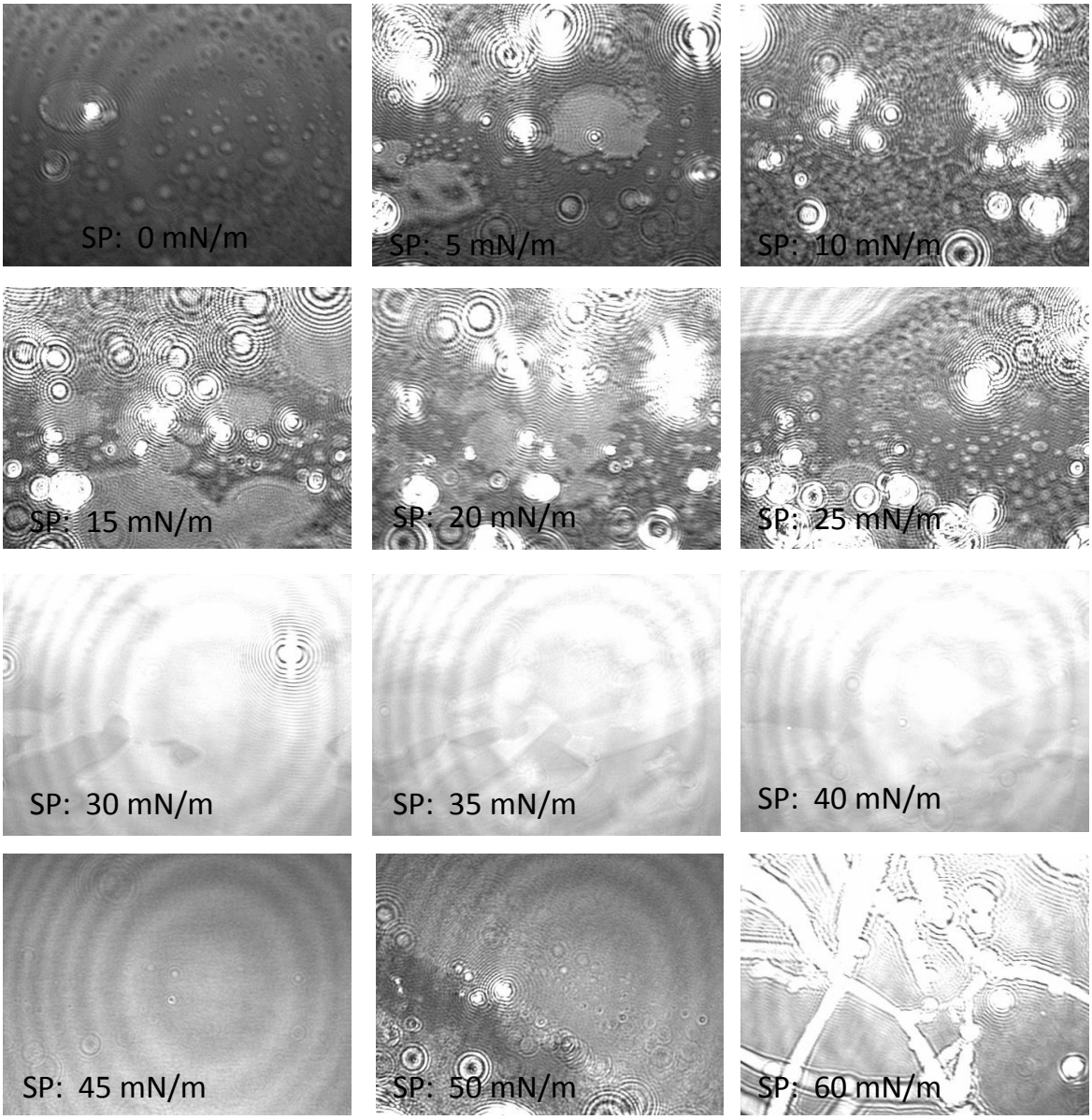

Figure 4.35. BAM images of pure StGly monolayer at T=20 ^{o}C

BAM images of 4:5:1 mixture is illustrated in Figure 4.36. As indicated in Figure 4.33, repulsive interactions were dominant between molecules in 4:5:1 mixture. Being consistent with the thermodynamic analysis, dark images were observed in BAM images due to repulsive interactions. During compression of the mixed film, generally liquid expand and gas phases were detected.

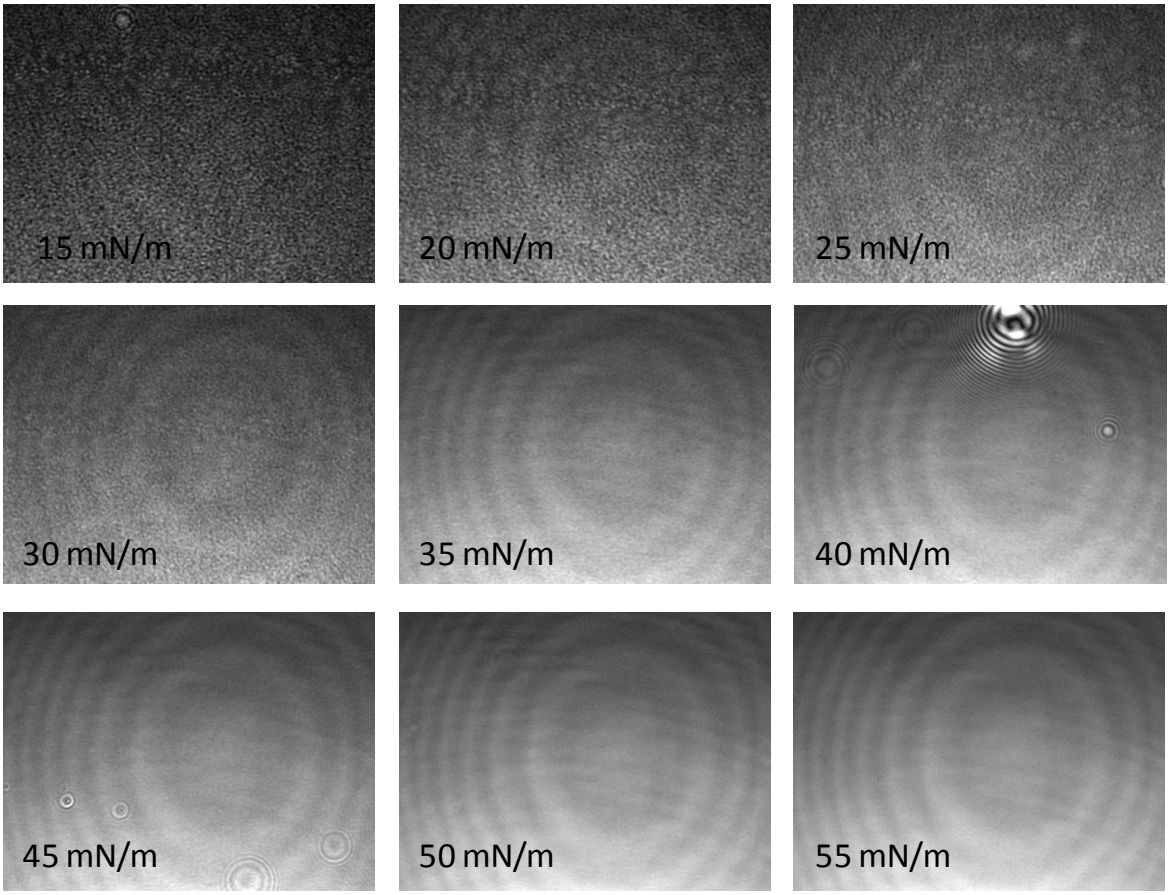

Figure 4.36. BAM images of DSPC/PEG40St/StGly 4:5:1 mixed film at T=20 ^{o}C

Although 2:5:3 mixed film π-A isotherm reveal more negative mixing free energy (Figure 4.33), in BAM images phase separations were observed. Obtained images were not homogeneous generally. At the plateau region bright domains were detected which may result from formation of thick domains or local collapses at PEG40St rich regions.

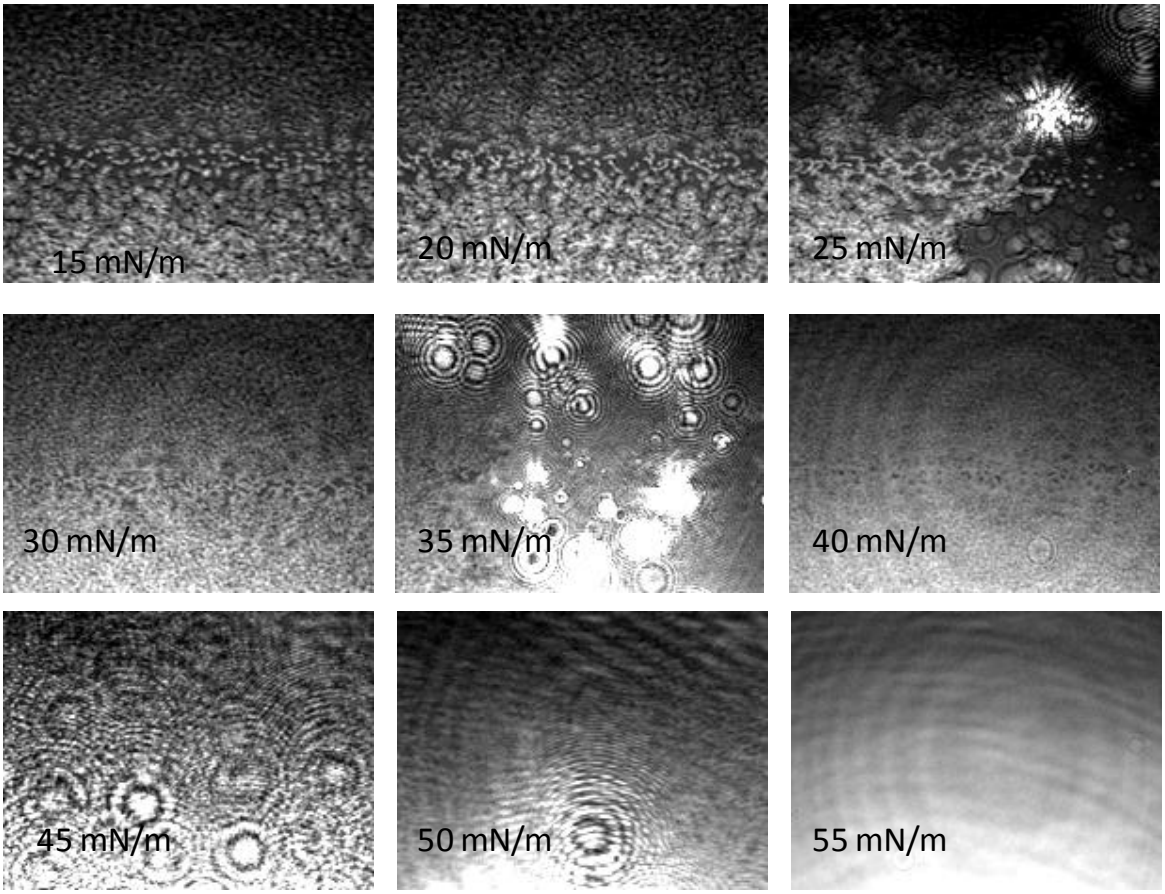

Figure 4.37. BAM images of DSPC/PEG40St/StGly 2:5:3 mixed film at T=20 ^{o}C

As seen in Figure 4.35, pure StGly molecule has specific images. In order to investigate what changes in plateau region, cycle experiments were performed with 0:5:5 mixed film and visualized with BAM. 0:5:5 mixture was compressed up to 50 mN/m surface pressure and expanded down to 25 mN/m surface pressure. Between each compression and expansion process monolayer equilibrated for 20 min at constant surface pressure. As illustrated in Figure 4.38, in the first compression of the monolayer, a broad plateau was detected. However, in the second compression, the plateau region was not observed and π-A isotherm was shifted to smaller mean molecular area exhibiting more condense phase behavior. Lack of plateau at the second compression may stem from squeeze out of PEG40St since it did not reincorporate to monolayer during expansion. Another reason for lack of plateau may be the irreversible conformational change of PEG40St from mushroom to brush. As shown in Figure 4.38, each compression reaches to 50 mN/m surface pressure at the same mean molecular area. This behavior may be attributed to conformational change in PEG chains of

PEG40St rather than squeeze out of PEG40St molecules from the monolayer. It may also be possible that some PEG40St molecules were squeezed out while some went through the conformational change.

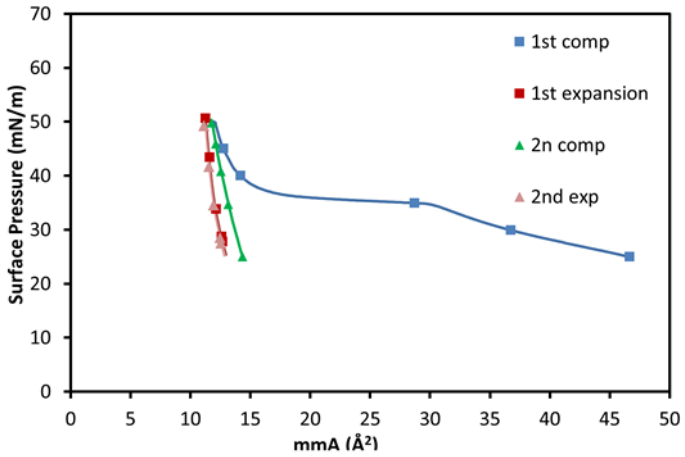

Figure 4.38. DSPC/PEG40St/StGly 0:5:5 compression-expansion cycle experiment T=20°C

During first compression of the 0:5:5 mixed film, from BAM images shown in Figure 4.39, phase separations were clearly observed. At the further stages of the compression solid domains were detected. Especially at 35 mN/m surface pressure where the plateau region exists, bright solid domains were increased. Up to 50 mN/m surface pressure, generally phase separations were observed consisting of solid and liquid condensed domains. Existence of solid domains may result from local collapse of the monolayer which may not reverberate to π-A isotherm. During the expansion process from 50 mN/m to 25 mN/m surface pressure, same solid domains were observed up to 40 mN/m surface pressure. However, at 35 mN/m, there were no bright domains and taken images were approximately homogeneous. This result may be attributed to presence of irreversible conformational change in the monolayer during first compression as well as local collapses of PEG40St molecules. Decrease in this size of bright domains in the second compression may man that, due to the conformational change of PEG chains, more PEG40St molecules become miscible with the other molecules in monolayer. At 25 mN/m surface pressure, molecules were more closely packed compared to first compression being consistent with the π-A isotherm. During second compression, observed solid domains were less compared to first compression.

Generally homogeneous liquid condensed domains were detected during the second compression.

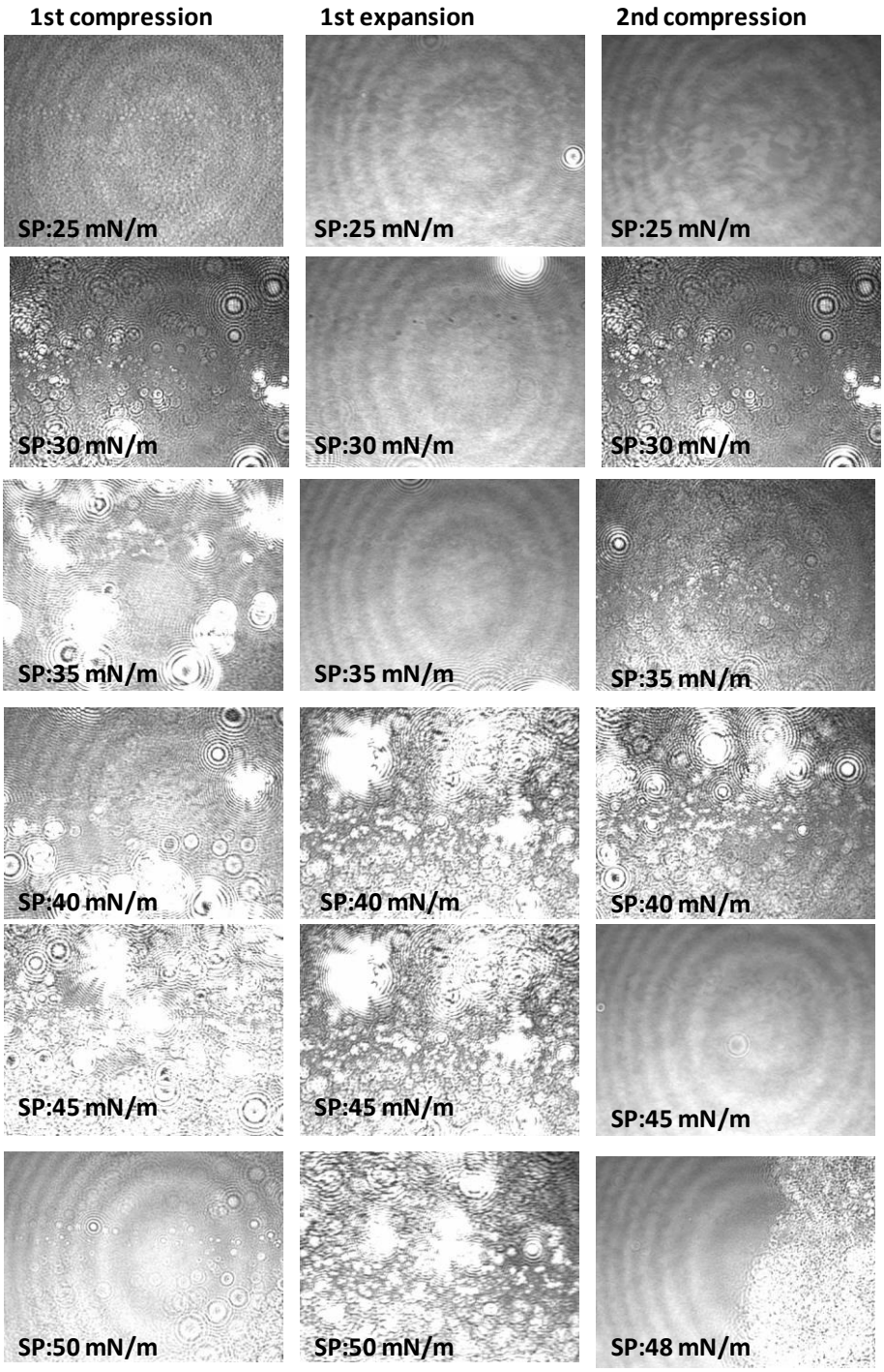

Figure 4.39. Compression – expansion cycle BAM images of DSPC/PEG40St/StGly 0:5:5 mixed film T=20 ^{o}C

The performed experiments by holding PEG40St molar ratio as 0.5 showed that, interaction between DSPC and StGly form a condense monolayer when mixed in proper molar ratio.

In order to elucidate the interaction between StGly and PEG40St, DSPC molar ration was held constant as 0.5. Π-A isotherms of DSPC/PEG40St/StGly 5:4:1, 5:3:2 and 5:2:3 mixed films are revealed in Figure 4.40. In mixture Π-A isotherms as the PEG40St molar ratio increased, the broadness of plateau region increased. Before plateau region, 5:2:3 mixture exhibited more condensed behavior compared to 5:4:1 and 5:3:2 mixtures. After plateau region, 5:2:3 and 5:3:2 Π-A isotherms showed same behavior while 5:4:1 Π-A isotherm was shifted smaller mean molecular areas. Collapse pressures of the three mixtures were close to each other.

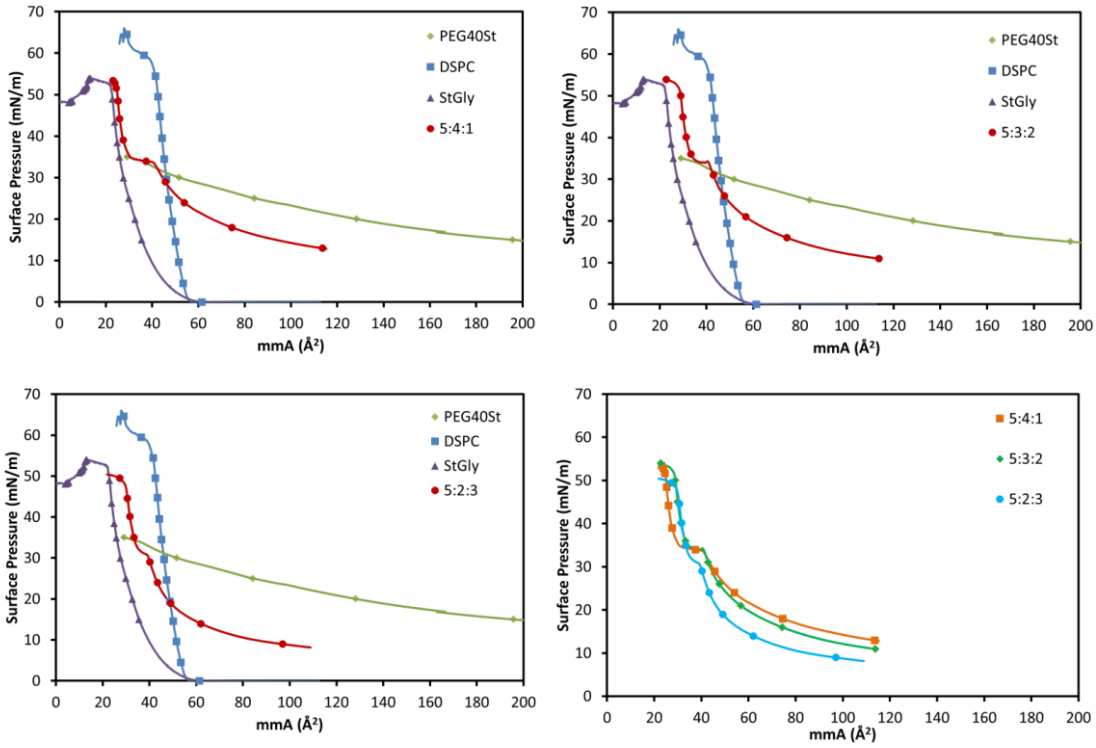

Figure 4.40. π-A isotherms of pure and DSPC/PEG40St/StGly mixtures

Miscibility analysis of the mixed film are illustrated in Figure 4.41. Each mixture's excess mixing free energies were negative representing a miscible behavior. Increase in the surface pressure resulted in more negative mixing free energies especially for 5:2:3 mixture.

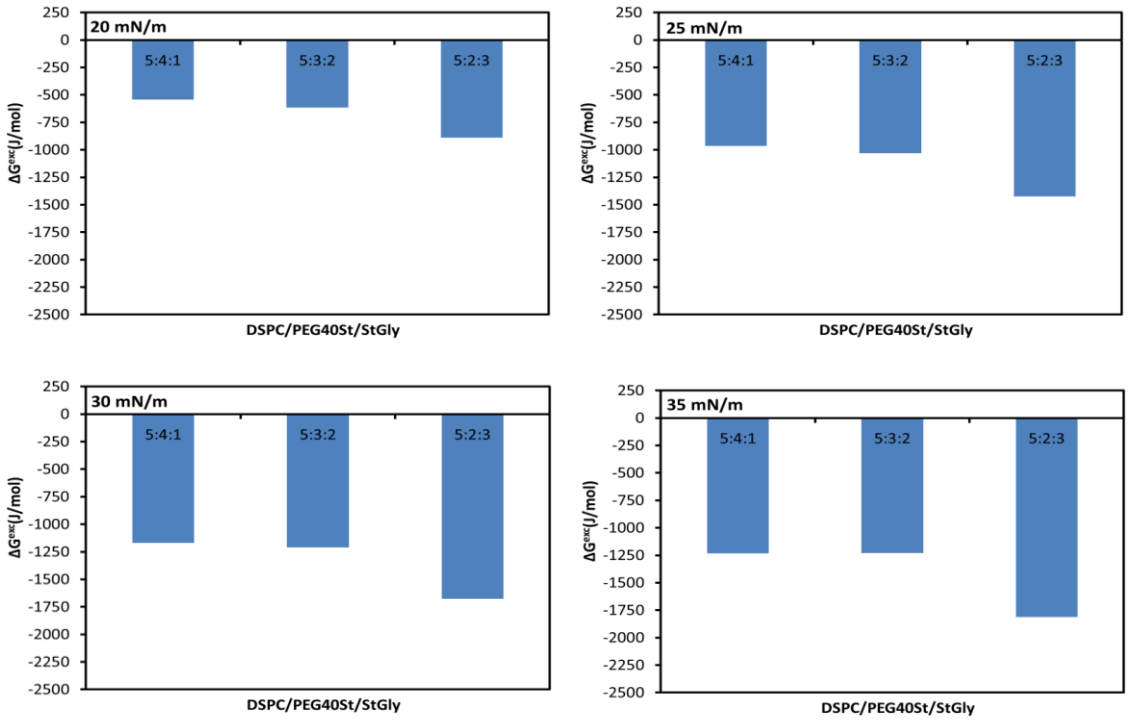

Figure 4.41.Comparison of excess free energy of mixing (ΔGExc) values of DSPC/PEG40St/StGly mixed monolayers calculated at π=20 mN/m, π=25 mN/m, π=30 mN/m, π=35 mN/m surface pressures.

Fluidity behaviors of the mixed monolayers were determined by calculating the compressional modulus. At the early stages of the compression, mixed films exhibited more elastic behavior. At the plateau region, a minimum point was observed due to phase transition. Despite 5:2:3 mixed film includes higher molar fraction of StGly, it exhibited more flexible monolayer compared to 5:4:1 and 5:3:2. From these results it can be conclude that PEG40St interaction with StGly and DSPC is stronger for 5:2:3 mixture. Another prominent detail is minimum points which represent phase transition of mixed film. While the minimum point is seen at 30 mN/m surface pressure for 5:2:3 mixed film, at 35 mN/m the minimum points were observed for 5:4:1 and 5:3:2. Due to strong molecular interactions between DSPC and StGly with PEG40St in 5:2:3 mixed film, more PEG40St may retain in the monolayer.

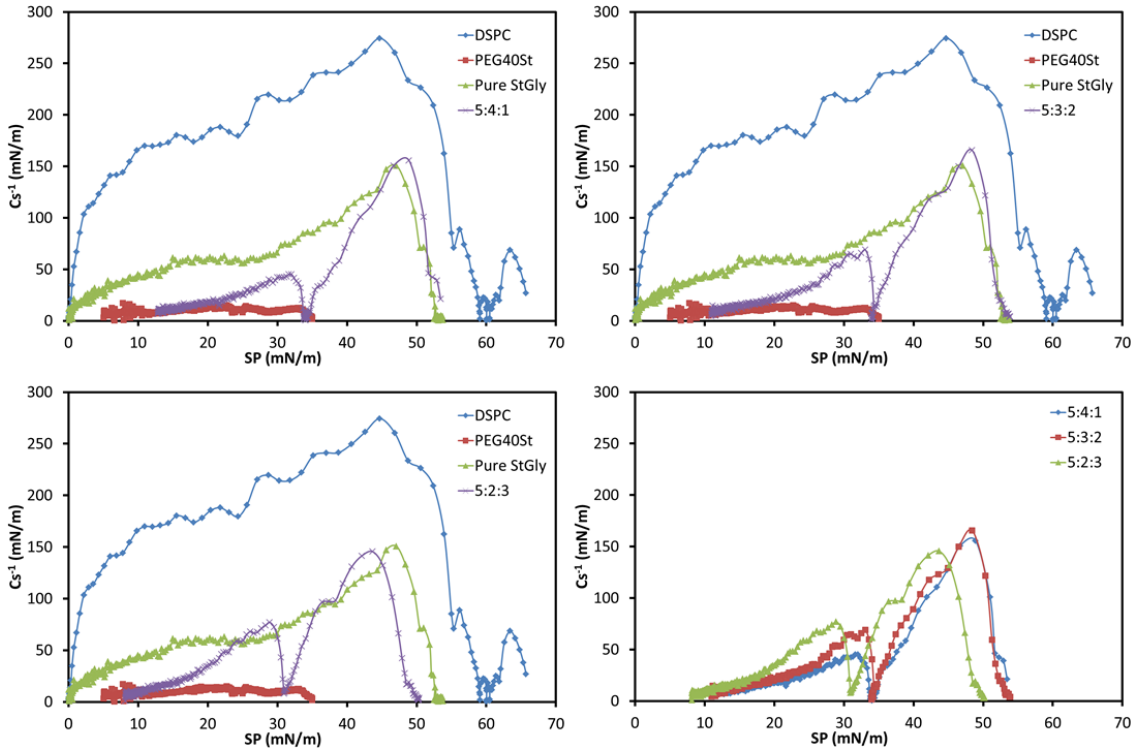

Figure 4.42. The compression modulus (Cs^{-1}) plots of DSPC/PEG40St/StGly mixed films

BAM images of the mixed films were taken at air/water interface in order to visualize phase behavior of mixed monolayers. BAM images of mixtures taken at same conditions with the isotherms.

As represented in Figure 4.43, 5:4:1 mixed film exhibited phase separations up to 32 mN/m surface pressure. Generally two dimensional gas and liquid expanded phases were detected. Starting from 30 mN/m, condense phases gathered and formed a bright domains representing solid phase. With increasing surface pressure, field of view covered with bright domains owing to collapse of monolayer.

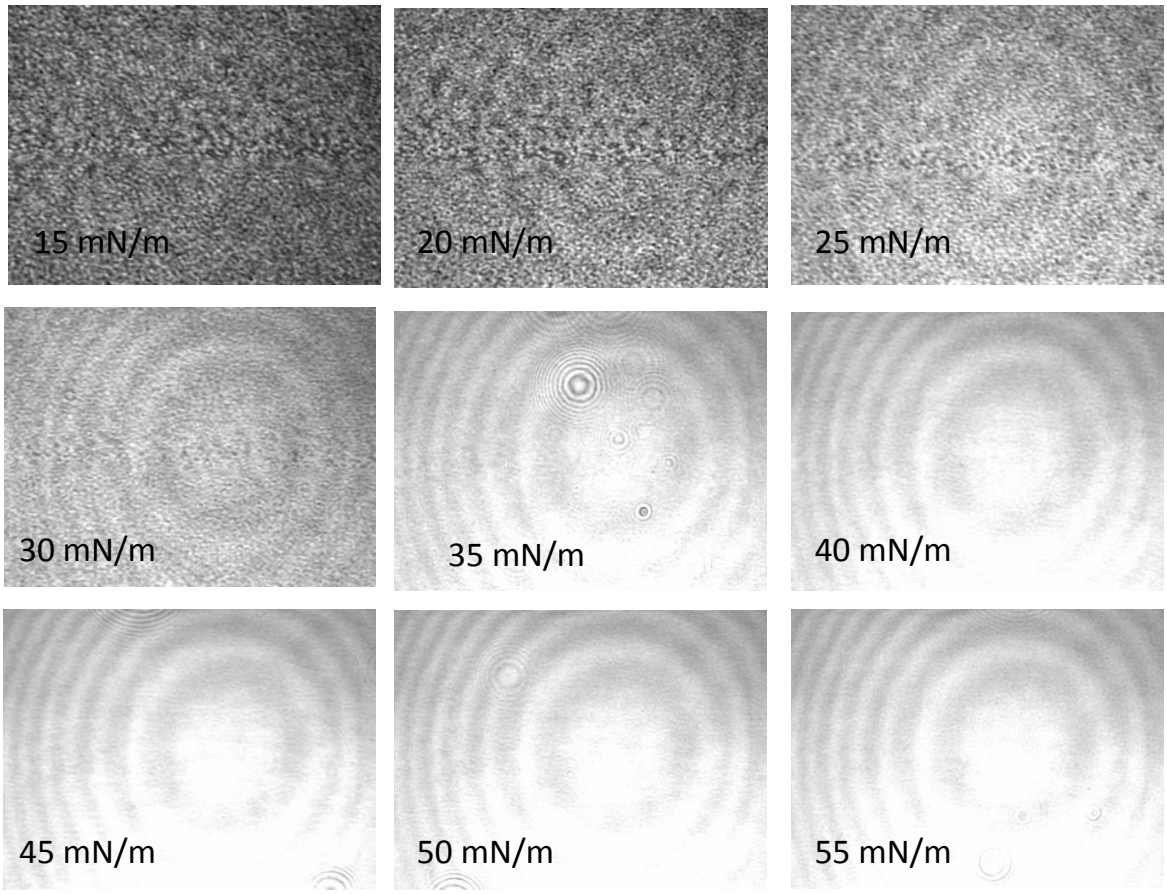

Figure 4.43. BAM images of DSPC/PEG40St/StGly 5:4:1 mixture at T=20 ^{o}C

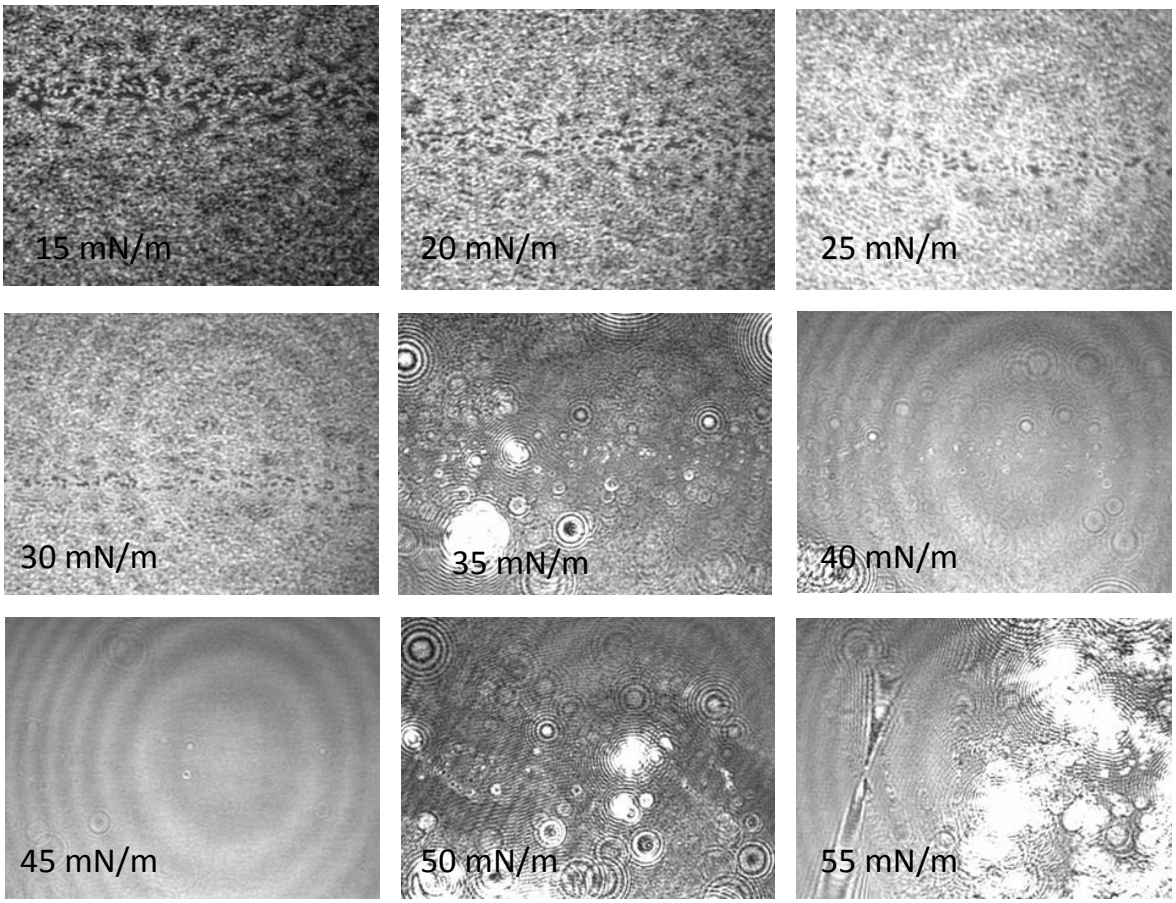

Figure 4.44. BAM images of DSPC/PEG40St/StGly 5:3:2 mixture at T=20 ^{o}C

As interpreted from Figure 4.44, in 5:3:2 mixed film, more phase separations were observed compared to other mixtures. Between 40 mN/m and 45 mN/m surface pressure, homogeneous condense phases were observed. Further compression of the mixed film result it phase separations again. Solid phases and liquid phases were coexist. During the collapse of the mixture, thickness of the monolayer increased, resulting in formation of brighter domains.

BAM images of 5:2:3 generally exhibited dark images referring to gaseous and liquid expand phases as seen in Figure 4.45. There were also small solid domains most probably belongs to StGly.

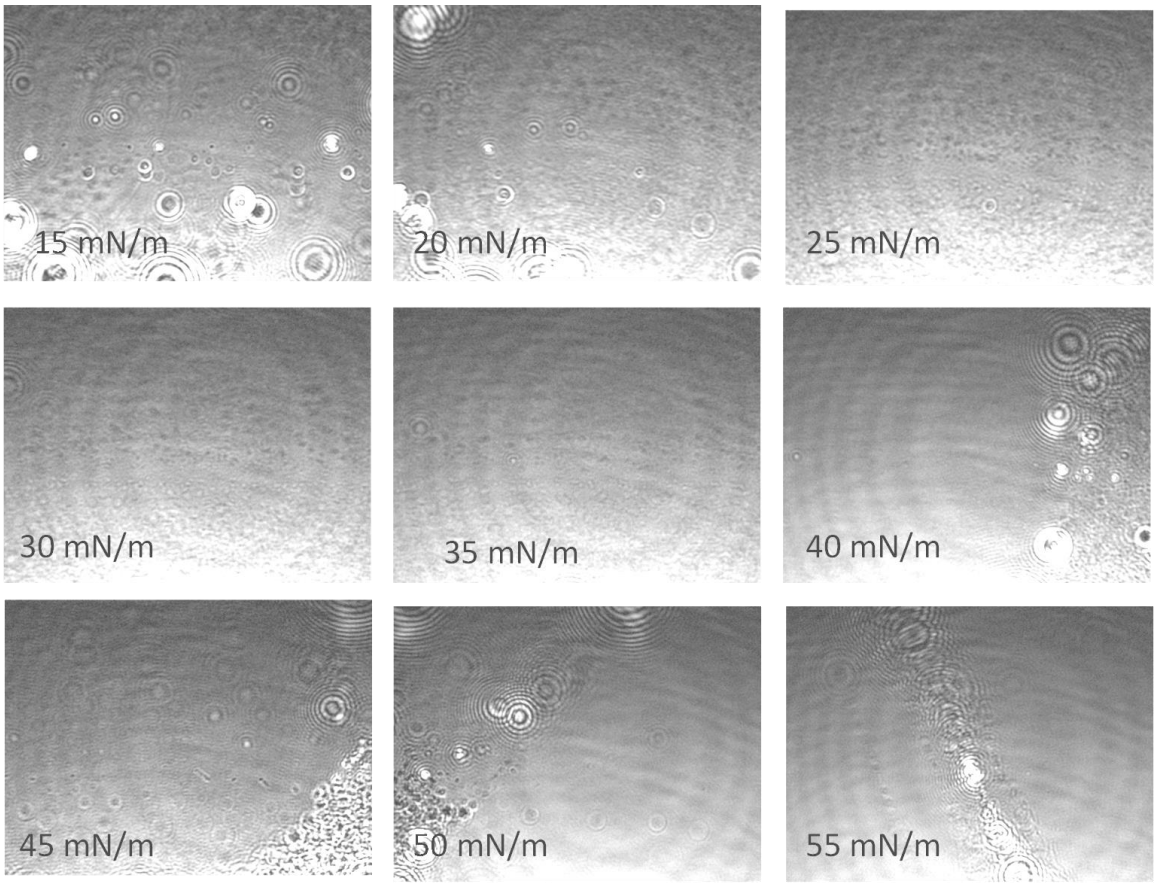

Figure 4.45. BAM images of DSPC/PEG40St/StGly 5:2:3 mixture at T=20 ^{o}C

When all DSPC/PEG40St/StGly mixed films were considered, StGly may not be a good choice for microbubble shell. Since StGly has single tail, it may not provide a good curvature on microbubble surface.

4.3.2. Phase Behavior and Morphology of DSPC/PEG40St/$StNH_2$ Monolayers

In microbubbles, the cohesiveness of the shell materials is important to provide stability to the microbubbles. In conventional formulation of phospholipid based microbubbles, this cohesiveness is obtained through secondary forces. Ionic interactions between head groups of monolayer components may have influence on the microbubble shell stability. Addition of a ionic component to the monolayer may affect the specific properties of monolayer such as electric charge density.

In this part of the study as a third component to DSPC/PEG40St mixture, $StNH_2$ was used in order to investigate the effect of ionic interaction between positively charged $StNH_2$ and zwitterionic DSPC on microbubble shell stabilityStearyl amine ($StNH_2$) is a surfactant which consists of a hydrophobic single tail and an ionizable nitrogen atom positively charged at physiological pH (Kotyńska & Figaszewski, 2007). Chemical structure of $StNH_2$ is seen in Figure 4.46. Mixture isotherms of DSPC/PEG40St/$StNH_2$ were obtained at 20 ^oC at air-water interface to examine the interaction between molecules two dimensionally.

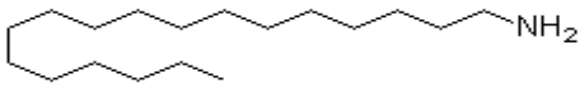

Figure 4.46. Chemical structure of stearyl amine

Pure component and mixed film π-A isotherms are illustrated in Figure 4.47 . Obtained pure $StNH_2$ isotherm is in agreement with previous the literature studies (Wan, Chovelon, & Jaffrezic-Renault, 2000). Surface pressure of $StNH_2$ was measured 0 mN/m up to 20 $Å^2$ mean molecular area. At 20 $Å^2$ mean molecular area, a rapid increase in the surface pressure was observed and monolayer shifted to liquid condensed phase. Starting from nearly 57 mN/m, $StNH_2$ monolayer collapsed. As seen in Figure 4.47**,** $StNH_2$ exhibits more condense phase behavior compared to DSPC and PEG40St. In the prepared mixed DSPC/PEG40St/$StNH_2$ films, PEG40St mole fraction was kept constant at 0.2. Due to small PEG40St content, plateau regions at 35 mN/m (±2) were narrow and as discussed before, these plateau may result from configurational change of PEG chains or squeeze out of PEG40St from the monolayer. In protein adsorption experiments discussed in previous section showed that, configurational change of PEG chains was more likely. Obtained mixed film π-A isotherms did not show considerable difference. Strong interaction between cationic $StNH_2$ and zwitter ionic DSPC polar head group was reported in literature studies (Dey, Anam, Afrin, & Ali, 2000; Teixeira et al., 2000).

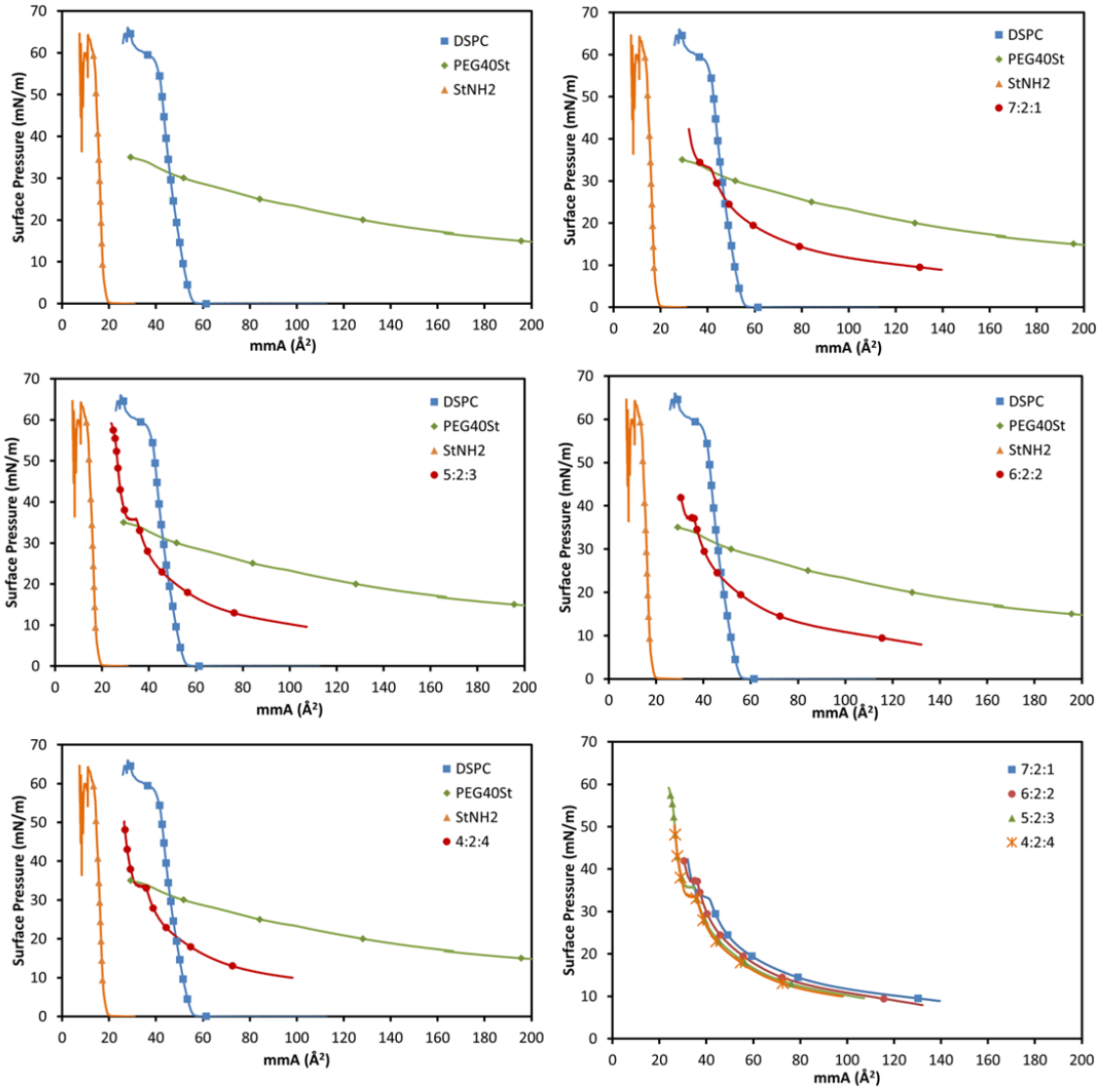

Figure 4.47. π-A isotherms of pure and DSPC/PEG40St/$StNH_2$ mixtures

Interaction between monolayer components were investigated thermodynamically. In Figure 4.48, mixing gibbs free energies of the mixed films with respect to surface pressure were shown. For all mixtures, negative ΔG^{Exc} means that attractive interactions between monolayer components were dominant. Excess Gibbs free energy of mixing values of 7:2:1 and 6:2:2 mixtures became more negative with increasing surface pressure. On the other hand, for 4:2:4 mixture, after 25 mN/m surface pressure ΔG^{Exc} values became less negative meaning that, attractive forces between component were started to decrease.

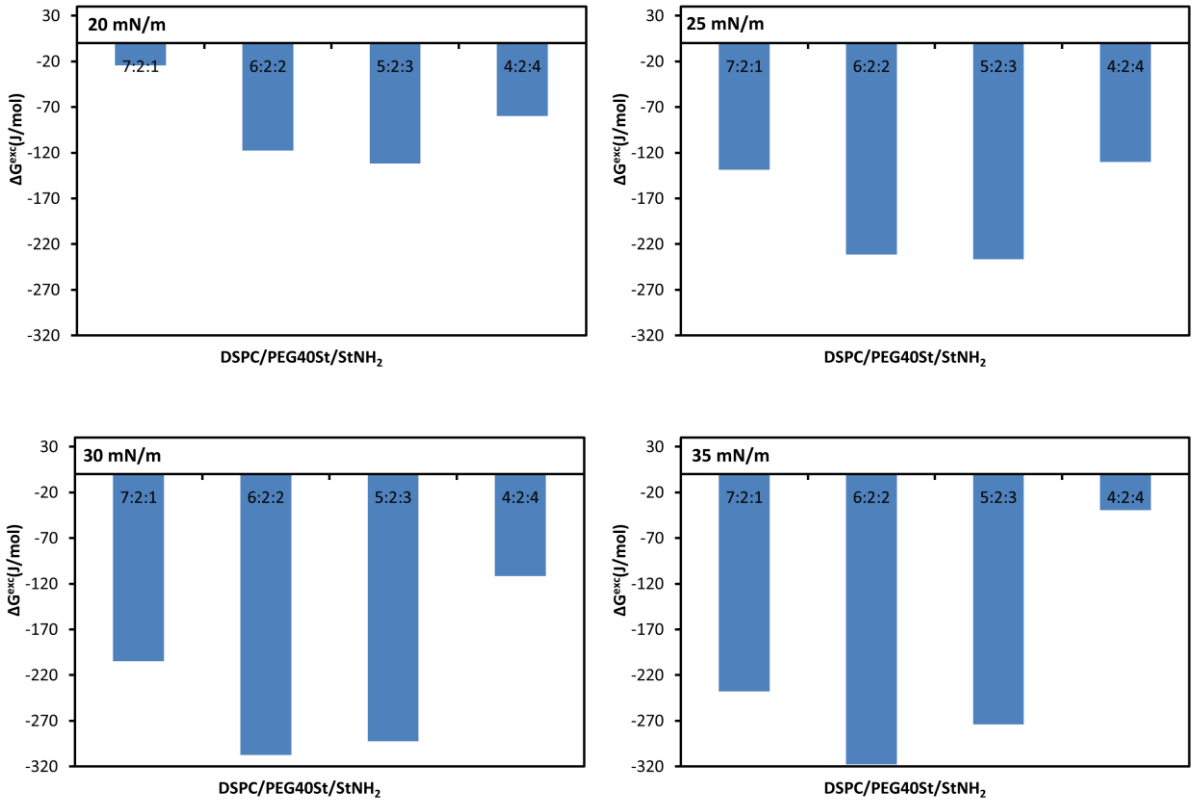

Figure 4.48. Comparison of excess free energy of mixing (ΔG^{Exc}) values of DSPC/PEG40St/$StNH_2$ mixed monolayers calculated at π=20 mN/m, π=25 mN/m, π=30 mN/m, π=35 mN/m surface pressures

Incompressibility values of DSPC/PEG40St/$StNH_2$ mixed films were quantitatively analyzed by calculating compression modulus. As illustrated in Figure 4.49, incompressibility values of DSPC/PEG40St/$StNH_2$ mixtures were close. Beginning from 10 mN/m to 35 mN/m(±2), mixed films were in gas phase since their compression modulus values were less than 100 mN/m. In each mixture, a minimum point was a minimum point due to plateau regions in π-A isotherms seen in Figure 4.47. We surmise that these minimum points coreespods to phase transition of mixed films or squeeze out of PEG40St from the monolayer. After minimum points, compression modulus values of mixtures increased dramatically and reached to 200-250 mN/m which represents the liquid condense phase behavior.

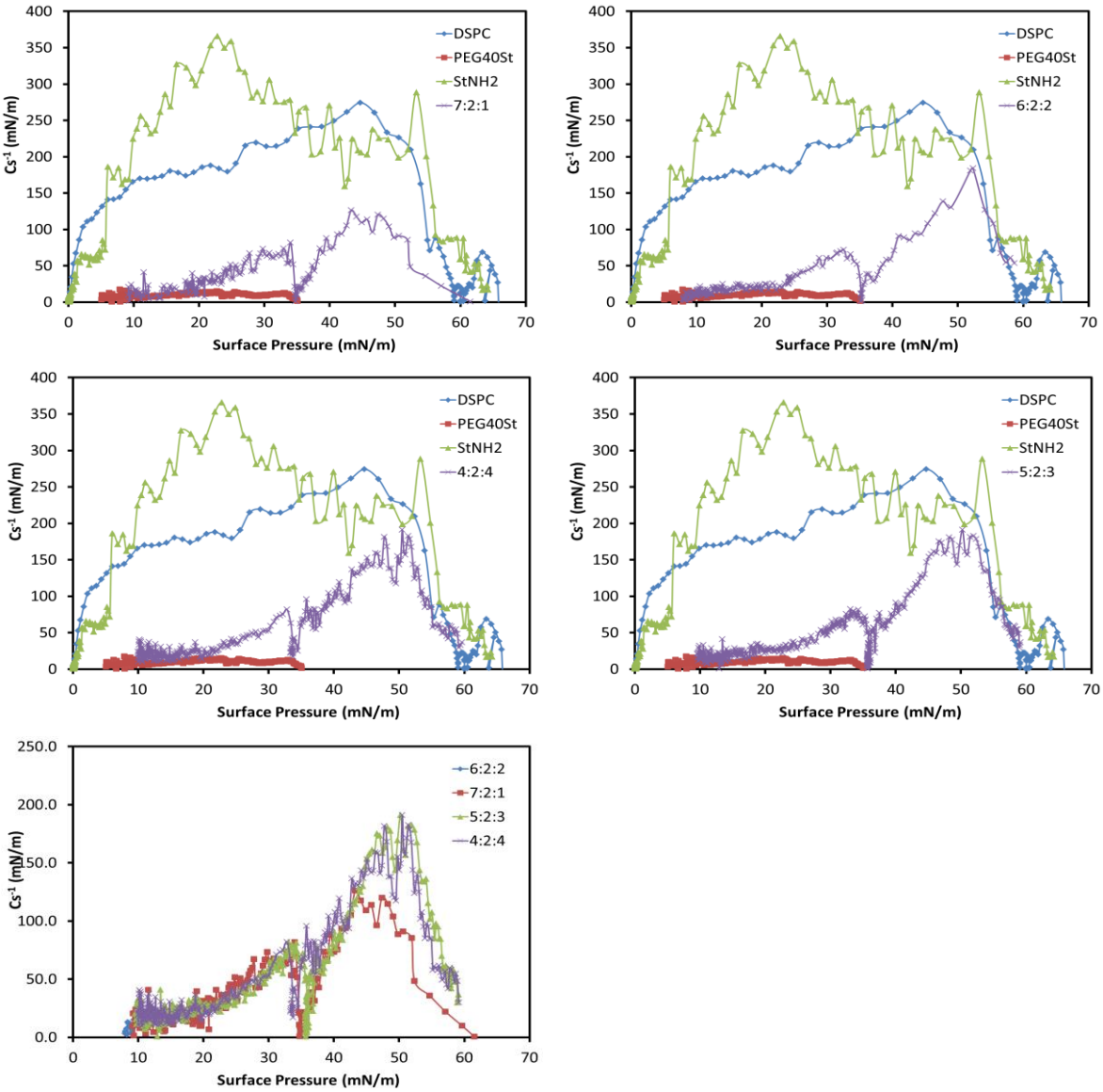

Figure 4.49. The compression modulus (Cs^{-1}) plots of DSPC/PEG40St/$StNH_2$ mixed films

Besides compression modulus calculations, phase behavior of pure $StNH_2$ and its mixtures with DSPC and PEG40St was also investigated using BAM.

BAM images of pure $StNH_2$ molecule at various surface pressures are represented in Figure 4.50. Starting from 0 mN/m to 1 mN/m phase separations were observed clearly. Two dimensional gas and liquid expand phases were exist together. With increasing surface pressure, a homogeneous surface consist of condense phase was observed up to 45 mN/m. After that, rods like condense domains were observed and with the collapse of $StNH_2$ monolayer, observed images were dark. These observations revealed that, the collapse of $StNH_2$ is through the subphase.

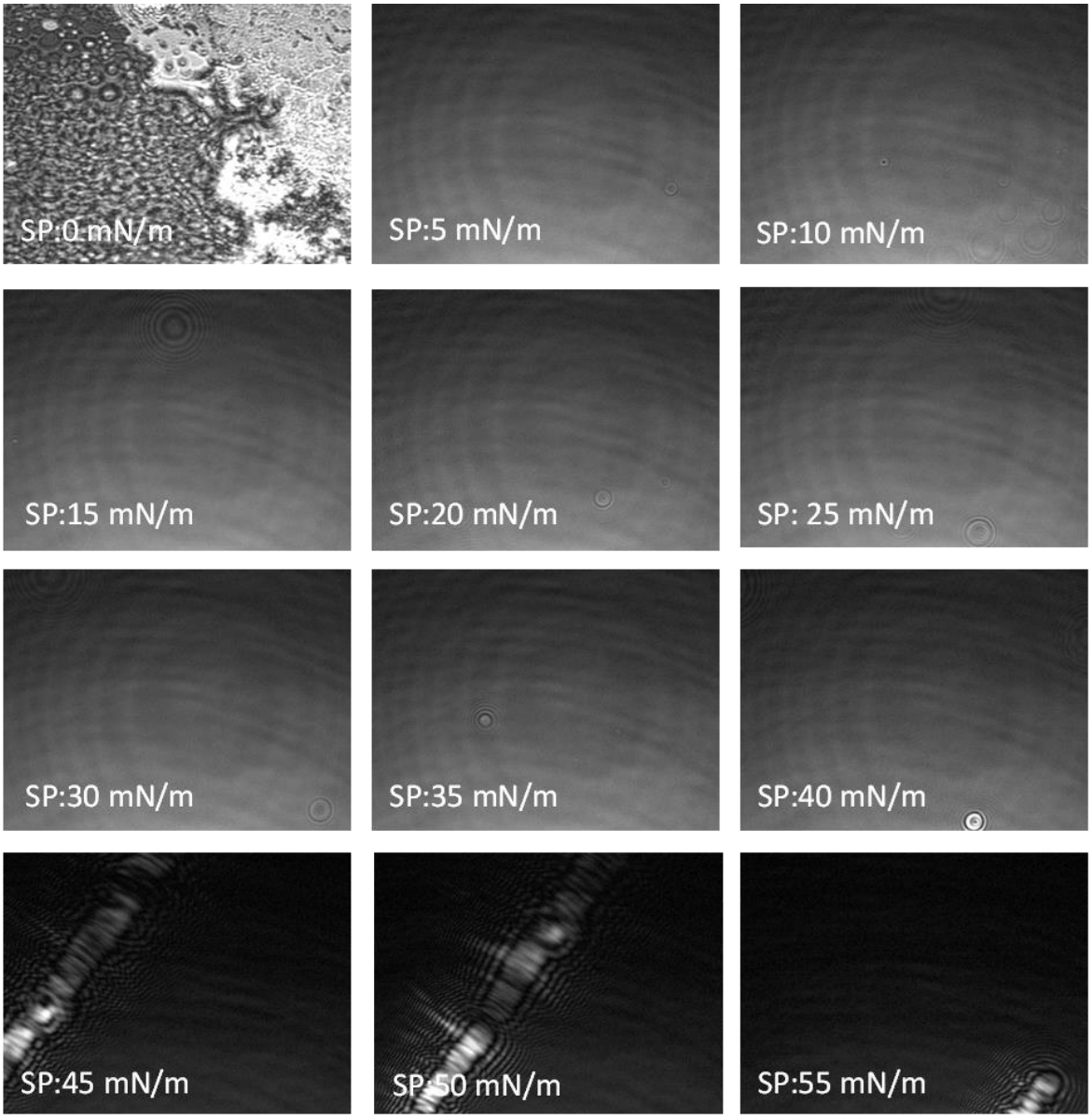

Figure 4.50. BAM images of pure $StNH_2$ monolayer at T=20 ^oC

In literature it was hypothesized that, $StNH_2$ could result in some separation of the lipidic mixture at the interface allowing the phospholipids to form the lamellar phase resultant to bridle of the structure. As a support to this hypothesis, it was shown that, in BAM images of DSPC and $StNH_2$ mixtures no phase separations were observed (Teixeira et al., 2000).

DSPC/PEG40St/$StNH_2$ 7:2:1 mixture's BAM images are illustrated in Figure 4.51. Due to weak interaction between molecules at low surface pressures, two dimensional gas and liquid expand phases were observed. As the surface pressure

increased, attractive forces between molecules also increased and homogeneous images were observed. Over the 45 mN/m surface pressure, thickness of the monolayer increased and bright regions appeared.

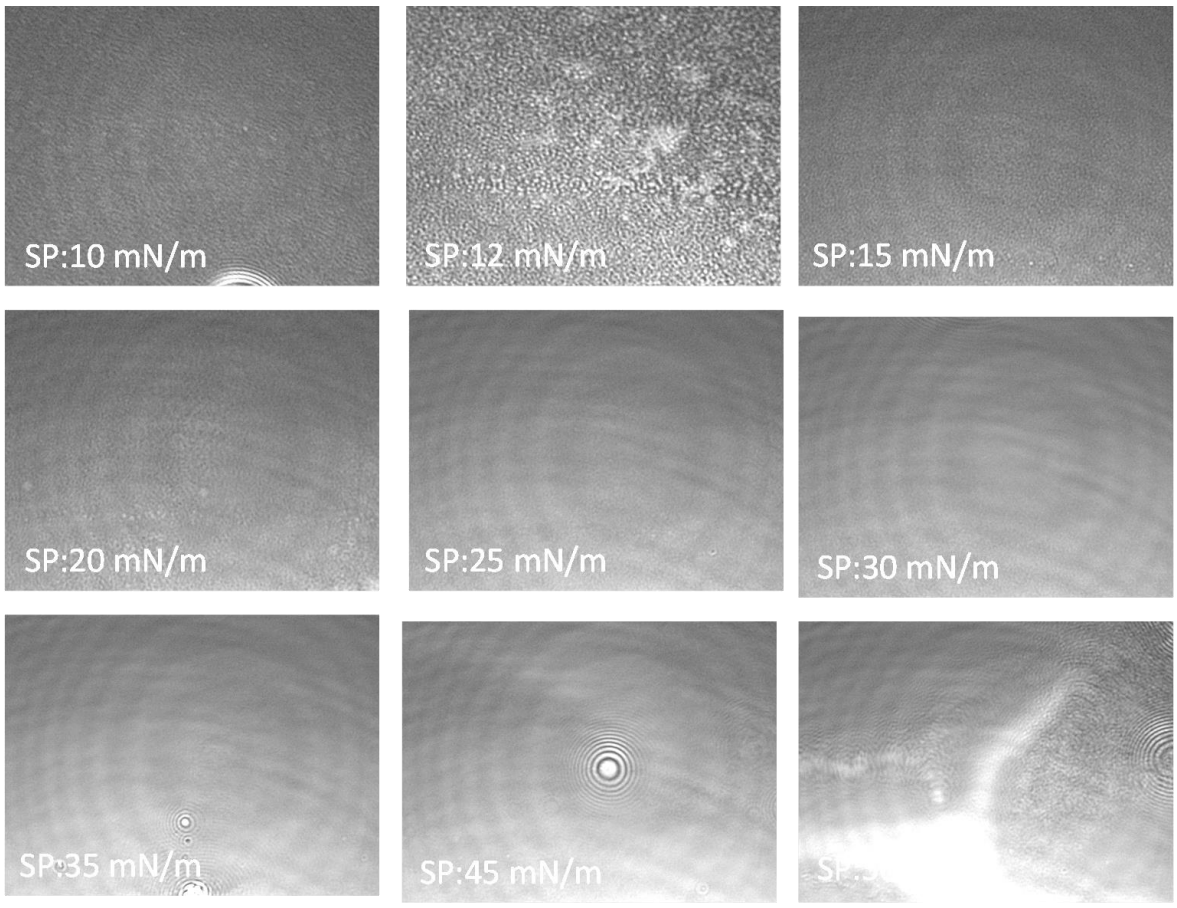

Figure 4.51. BAM images of DSPC/PEG40St/StNH2 7:2:1 mixed film at T=20 ^{o}C

In the BAM images of DSPC/PEG40St/$StNH_2$ 6:2:2 mixed film, at low surface pressures, bright patches and dark regions were coexist since up to 20 mN/m surface pressure, monolayer was not formed completely. As seen in Figure 4.52, homogeneous liquid condense phases observed between 20 mN/m-45 mN/m surface pressures.

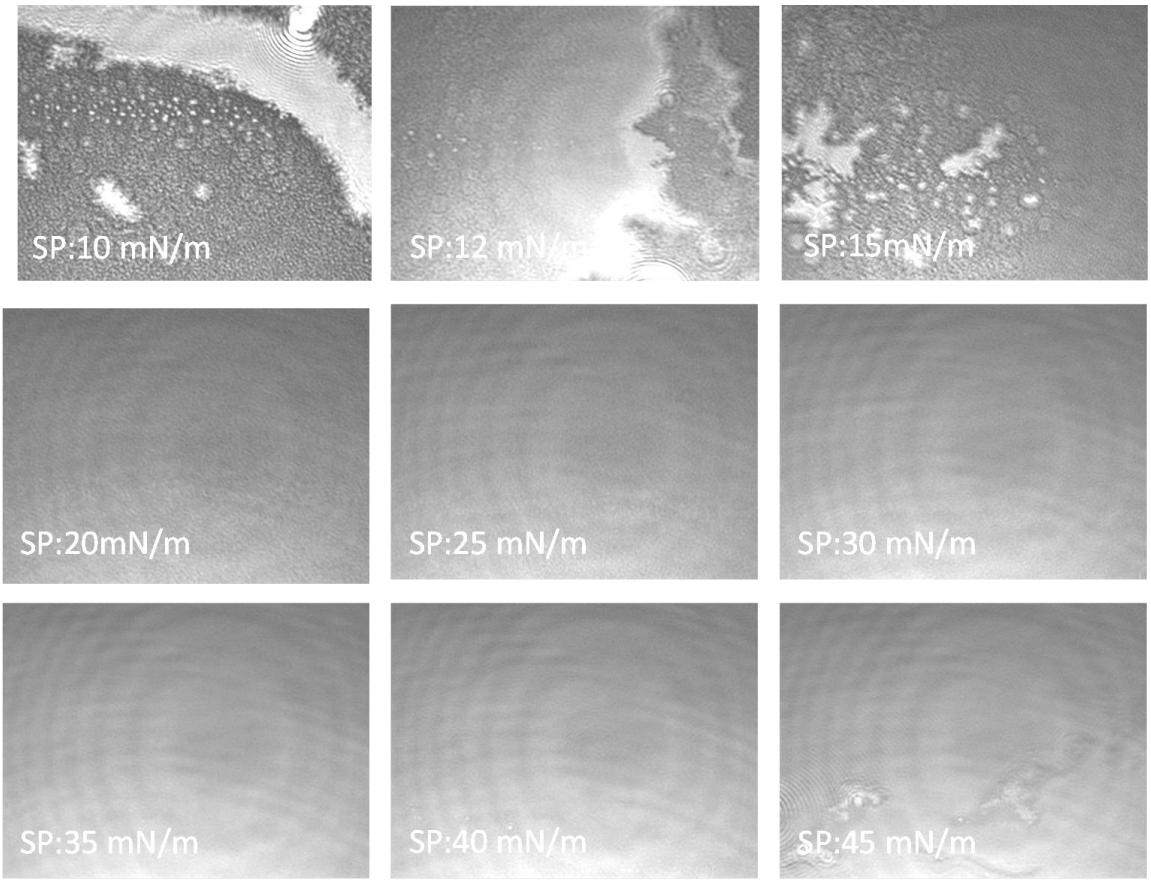

Figure 4.52. BAM images of DSPC/PEG40St/StNH2 6:2:2 mixed film at T=20 ^{o}C

As seen in Figure 4.53, in contrast to DSPC/PEG40St/$StNH_2$ 7:2:1 and 6:2:2 mixtures, 5:2:3 showed more homogeneous phase behavior even at low surface pressures. Despite the BAM images were taken at same brightness and contrast for all samples, 5:2:3 mixed film images were brighter. Bright domains represented the thick and condense phases. At the collapse of the monolayer, bright circles were observed on the surface.

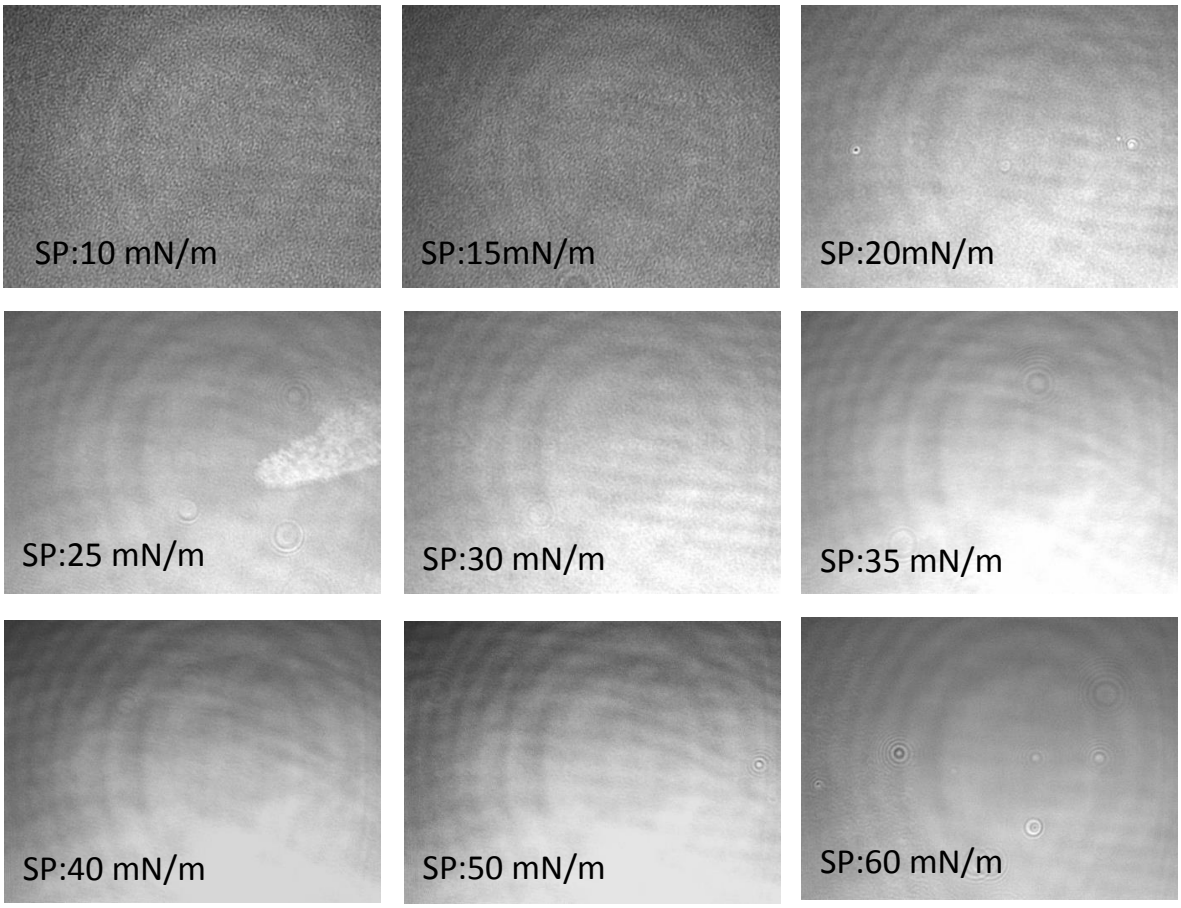

Figure 4.53. BAM images of DSPC/PEG40St/$StNH_2$ 5:2:3 mixed film at T=20 ^oC

BAM images of DSPC/PEG40St/$StNH_2$ 4:2:4 mixed film are revealed in Figure 4.54. Since molar fraction of $StNH_2$ is high with respect to other mixtures, it showed more homogeneous phase behavior. As it was also interpreted from incompressibility and thermodynamic analysis, 4:2:4 mixture forms a strong and liquid condense monolayer.

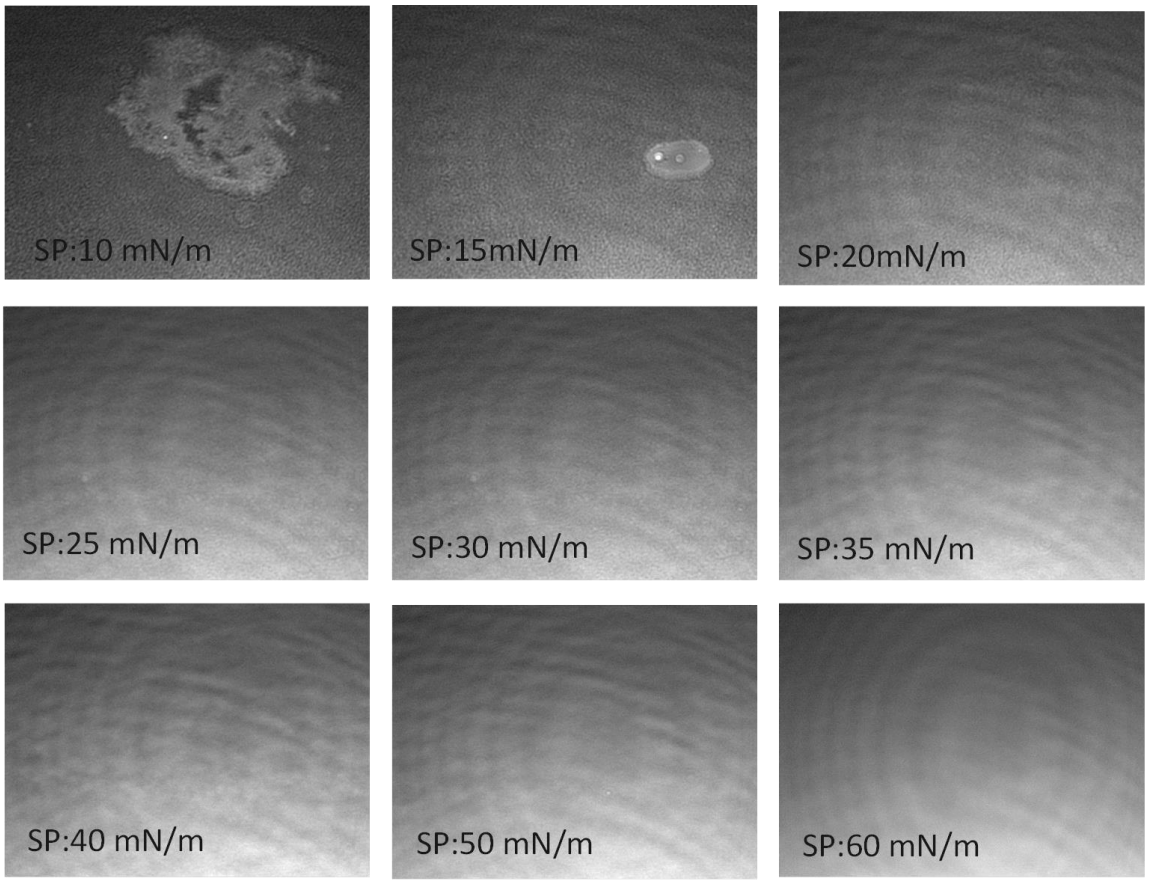

Figure 4.54. BAM images of DSPC/PEG40St/$StNH_2$ 4:2:4 mixed film at T=20 ^oC

When all obtained results were considered in, it may be conclude that, $StNH_2$ may provide a cohesive shell structure in 2-D. However, in 3-D it may not provide a good curvature since it has single tail.

4.3.3. Phase Behavior and Morphology of DSPC/PEG40St/DSPS Monolayers

Negatively charged microbubbles may be used for the delivery of positively charged drugs. Negatively charged microbubble shell can easily be produced by addition of a negatively charged phospholipid to microbubble formulation.

1,2-distearoyl-sn-glycero-3-(phospho-l-serine) (DSPS), is a negatively charged phospholipid exist in many ocaryotic cell's plasma membrane and it is capable of making hydrogen bond (Ross, Steinem, Galla, & Janshoff, 2001). Chemical structure of DSPS is illustrated in Figure 4.55 When a negatively charged phospholipid like DSPS is

mixed with zwitterionic phospholipid like DSPC, it determines the electrical and mechanical properties of the membrane (Luna, Stroka, Bermudez, & Aranda-Espinoza, 2011). In this part of the study, as a third component to DSPC/PEG40St, DSPS was added in order to investigate effect of ionic interactions on monolayer stability.

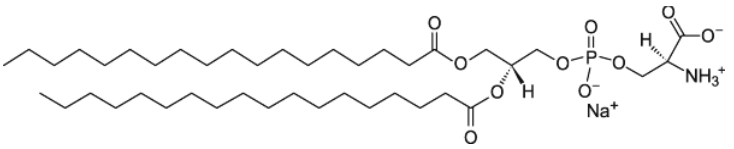

Figure 4.55. Chemical structure of DSPS

Surface pressure – mean molecular area isotherms of pure components and DSPC/PEG40St/DSPS mixed films are illustrated in Figure 4.56. At large mean molecular areas, surface pressure of DSPS remained 0 mN/m and exhibited a takeoff at 40 $Å^2$. DSPS monolayer collapsed slightly smaller molecular area approximately at 48 mN/m surface pressure. To the our knowledge, in current literature, DSPS surface pressure – mean molecular area at 20 ^oC at air-water interface is not available. However, in literature LB isotherms of DSPS exists in 37 ^oC (NEUROBLASTOMA, 2003). As expected, at 20 ^oC DSPS isotherm shifts left compared to the isotherm at 37 ^oC with same slope since molecules are at more condense form. As seen in Figure 4.56, mixture π-A isotherms were similar. All mixtures showed a plateau approximately at 35 mN/m which is collapse pressure of PEG40St due to squeeze out of PEG40St or phase transition of mixed monolayers.

Since the PEG40St content was same for the mixtures, length of plateau regions were also expected to be same. However, while the broadness of plateau was same for 4:5:1 and 0:5:5 mixtures, it was smaller for 2:5:3 mixture (Figure 4.56). As shown in Figure 4.57, ΔG^{Exc} of 2:5:3 mixed monolayer was more negative compared to other mixed monolayers meaning that more miscible. Observed short plateau may mean that, at 2:5:3 composition configurational change of PEG chains of PEG40St may be easier. These results showed the importance of composition effect on interaction between molecules and monolayer stability. According to miscibility analysis, all examined compositions showed non-ideal mixing behavior.

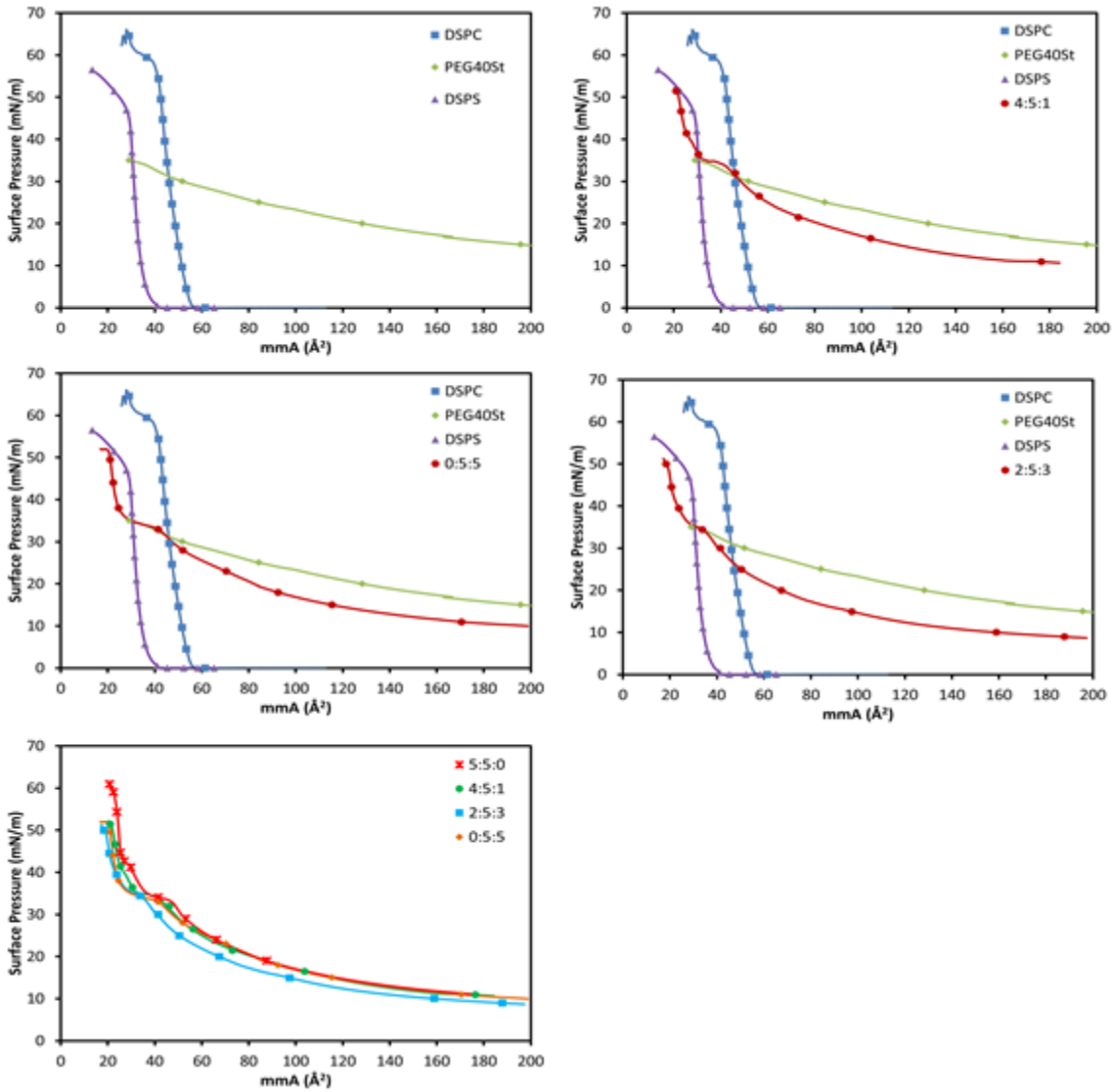

Figure 4.56. π-A isotherms of pure and DSPC/PEG40St/DSPS mixtures

Despite the π-A isotherms of DSPC/PEG40St/DSPS mixed films showed similar behavior, as seen in Figure 4.57 mixing Gibbs free energy values were different. For 4:5:1 and 2:5:3 mixtures, attractive interactions were dominant. On the other hand, for 0:5:5 mixture, free energy of mixing values were positive probably due to repulsive interaction between DSPS and PEG40St. From these results it can be concluded that, existence of DSPC in the mixture favors the attractive interactions in the mixtures.

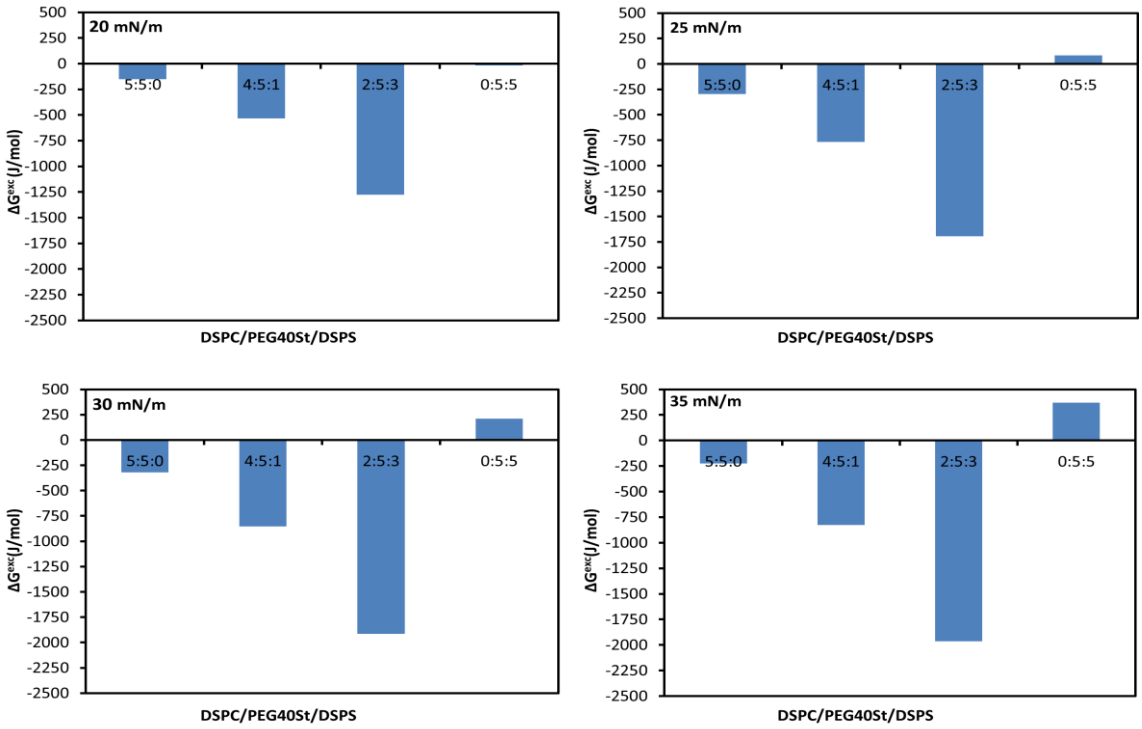

Figure 4.57. Comparison of excess free energy of mixing (ΔG^{Exc}) values of DSPC/PEG40St/DSPS mixed monolayers calculated at π=20 mN/m, π=25 mN/m, π=30 mN/m, π=35 mN/m surface pressures.

Two dimensional incompressibility values of DSPS and DSPC/PEG40St/DSPS mixed films were calculated to characterize the nature of the monolayer phases and plotted as seen in Figure 4.58. Incompressibility of pure DSPS increased sharply up to 250 mN/m and it gave another peak approximately at 300 mN/m. DSPS compressional modulus values showed typical liquid condense phase behavior. As also it can be interpreted from π-A isotherms seen in Figure 4.56, DSPS exhibits more condense behavior compared to DSPC. In mixtures, approximately at 35 mN/m surface pressure a minimum point was observed. This minimum point may result from configurational change of PEG chains. Three of the mixed films gave a peak at 45 mN/m surface pressure. At this point, while compressional modulus of 2:5:3 and 4:5:1 nearly 80 mN/m, 0:5:5 mixture's compressional modulus was 120 mN/m.

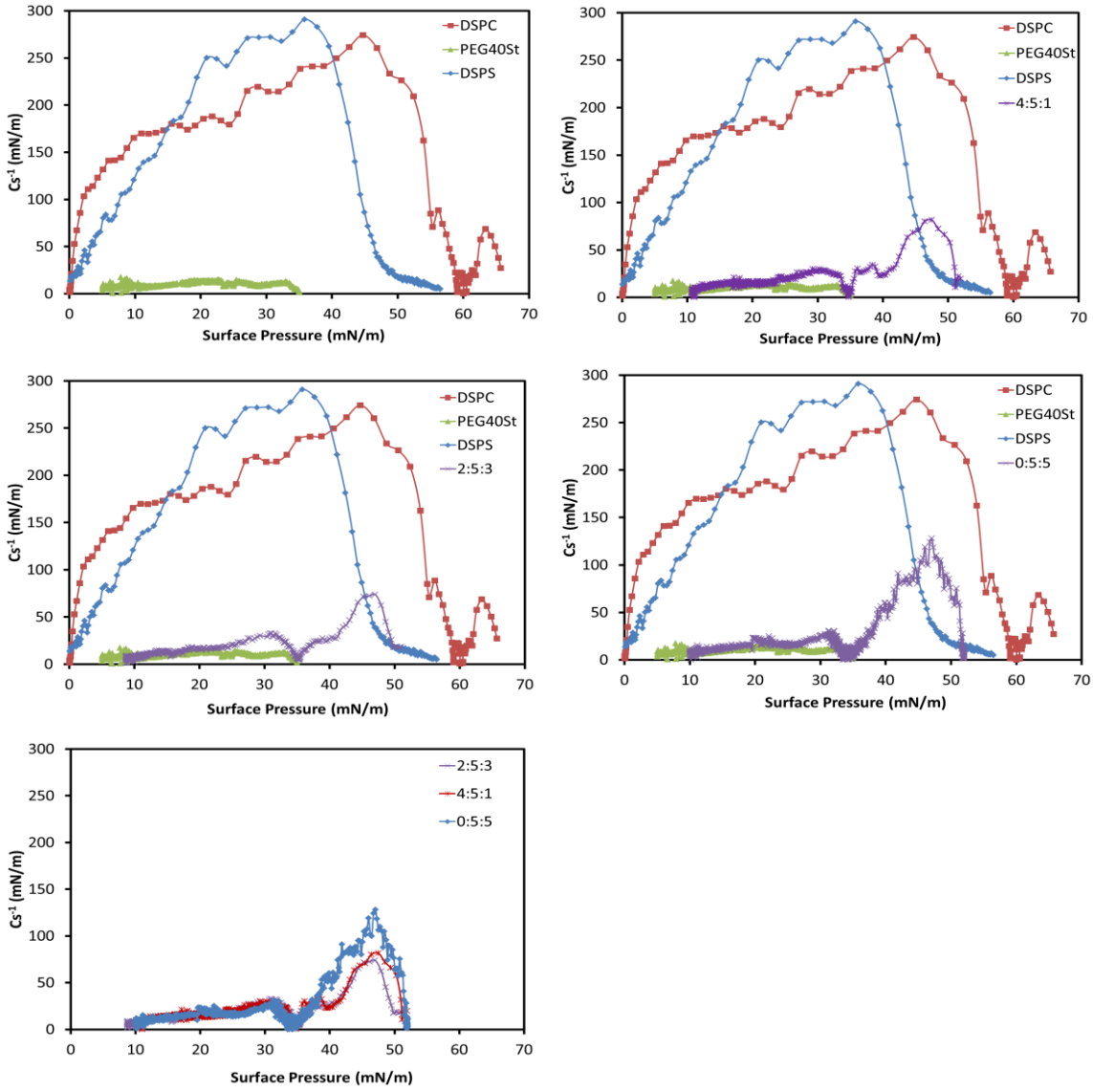

Figure 4.58. The compression modulus (Cs^{-1}) plots of DSPC/PEG40St/DSPS mixed films

In order to investigate the phase behavior of DSPS and its mixtures with DSPC and PEG40St visually, BAM images were taken. Obtained π-A isotherms obtained during BAM experimets were consistent with the isotherms shown in Figure 4.56.

In Figure 4.59, BAM images of pure DSPS molecule starting from 0 mN/m to its collapse pressure are presented. As seen in Figure 4.56, DSPS surface pressure was 0 mN/m at large mean molecular areas. At 0 mN/m surface pressure, two dimensional gas phase and liquid expand phases were coexist. With the increasing surface pressure, condense domains gathered and homogeneous morphology was observed. At 20 mN/m, phase separations were observed. These phase separations were attributed to

electrostatic repulsive interactions between DSPS head groups. DSPS molecule started to collapse 50 mN/m. During the collapse of DSPS, rod like bright domains were observed.

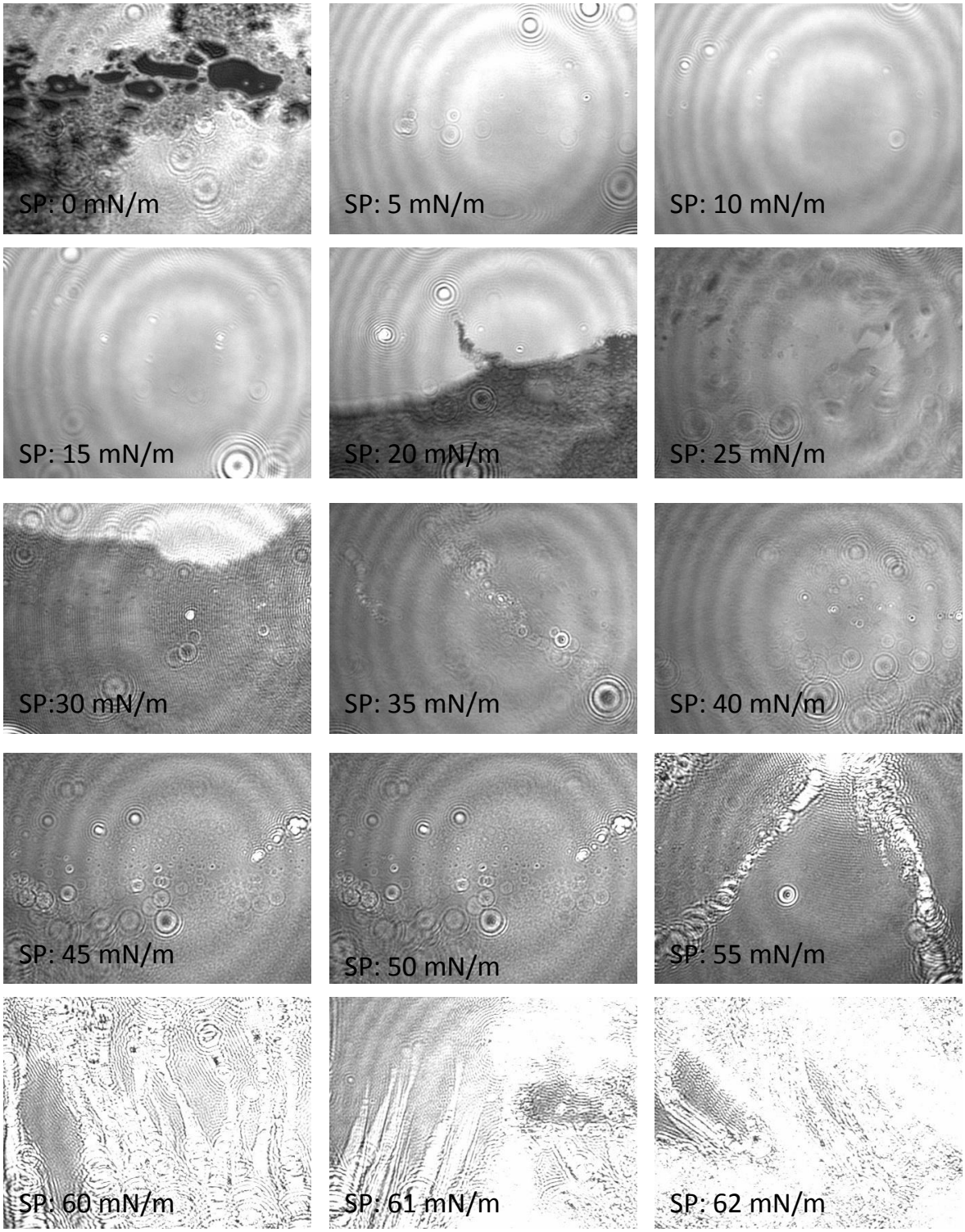

Figure 4.59. BAM images of DSPS at T=20 ^{o}C

At low surface pressures no homogeneous phase was observed in BAM images of 4:5:1 mixture (Figure 4.60). Until reaching 25 mN/m surface pressure two dimensional gas phase and liquid expanded phases were detected. At 25 mN/m surface pressure, the BAM image was dark representing liquid expand phase and these results were consistent with the compressional modulus values shown in Figure 4.58 . When the mixed film reached the plateau region (35 mN/m), very bright domains at different sizes were detected. Darker phases at 35 mN/m resembled to pure DSPC and DSPS BAM images. With the further compression of the mixed film, bright small domains gathered and film covered the surface. Homogeneous liquid condense phases were observed until collapse of the mixed monolayer.

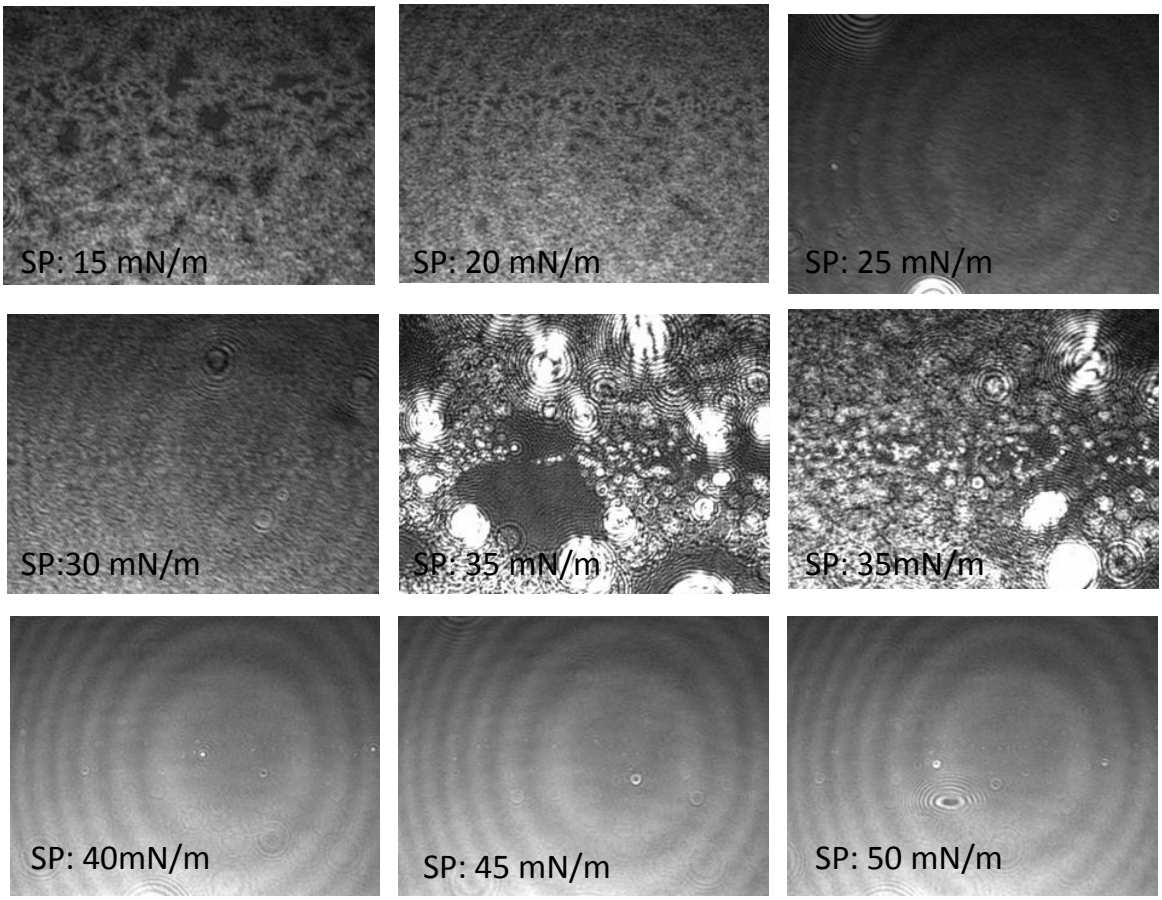

Figure 4.60. BAM images of DSPC/PEG40St/DSPS 4:5:1 mixed film at T=20 ^{o}C

In 2:5:3 mixture, as illustrated in Figure 4.61, liquid expand and liquid condense phases coexist. Being consistent with the thermodynamic analysis shown in Figure 4.57, increasing surface pressure improved the attractive interactions between molecules and

resulted in formation of liquid condensed domains. Since DSPS is capable of doing hydrogen bonding and interact with DSPC electrostatically, molecules in mixed monolayer may attract each other rapidly and form solid domains as seen in Figure 4.61. Further increase of surface pressure may result in collapse of solid domains at this may reverberate to the BAM images as bright domains (Figure 4.61).

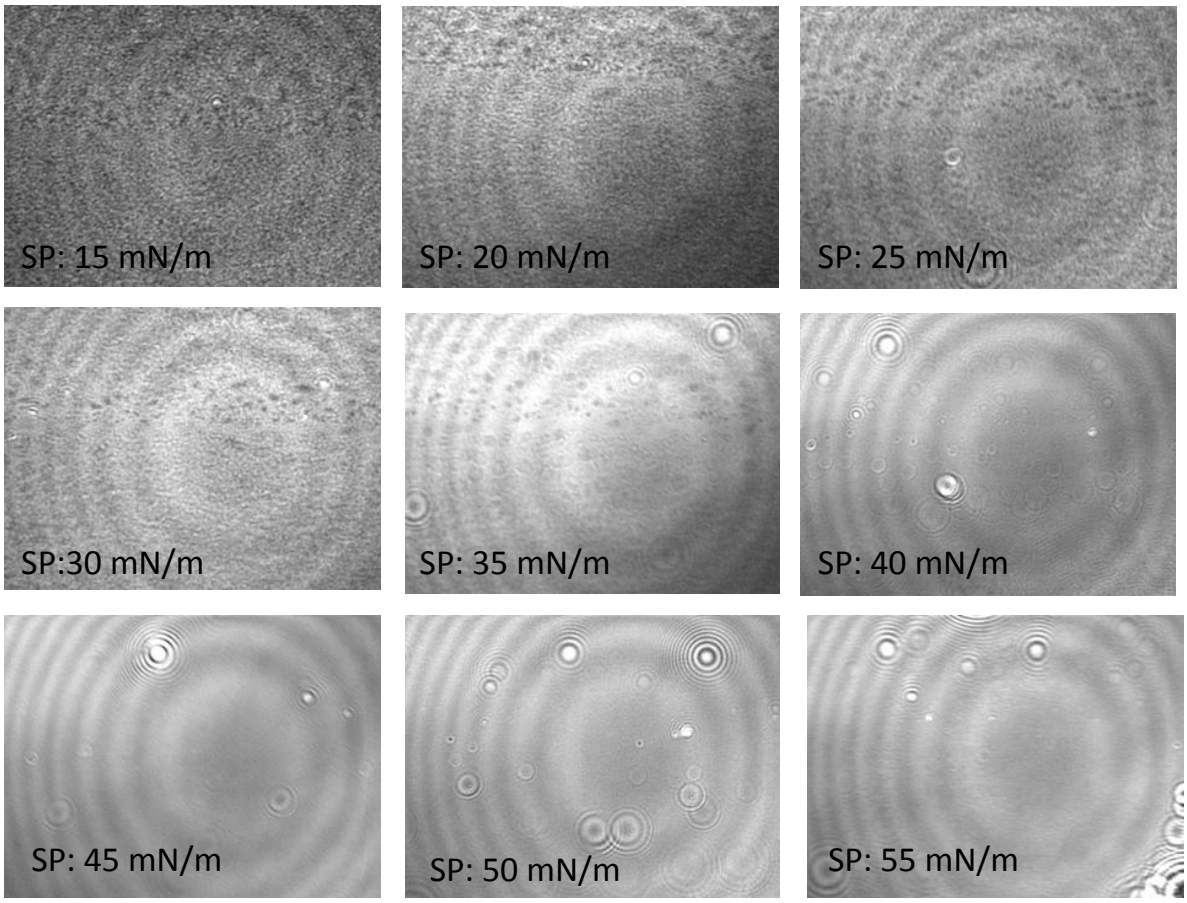

Figure 4.61. BAM images of DSPC/PEG40St/DSPS 2:5:3 mixed film at T=20 ^{o}C

In 0:5:5 mixture, two dimensional gas phases observed below 25 mN/m surface pressure (Figure 4.62). As concluded from miscibility analysis shown in Figure 4.57, DSPS and PEG40St were not miscible. Detected phase separations may result from immiscibility of DSPC and PEG40St. At 35 mN/m, solid and condensed domains were detected. Most probably, these solid domains were belong to PEG40St and at 35 mN/m, PEG40St collapsed in PEG40St rich regions. At higher surface pressures, detected phases were not homogeneous as expected.

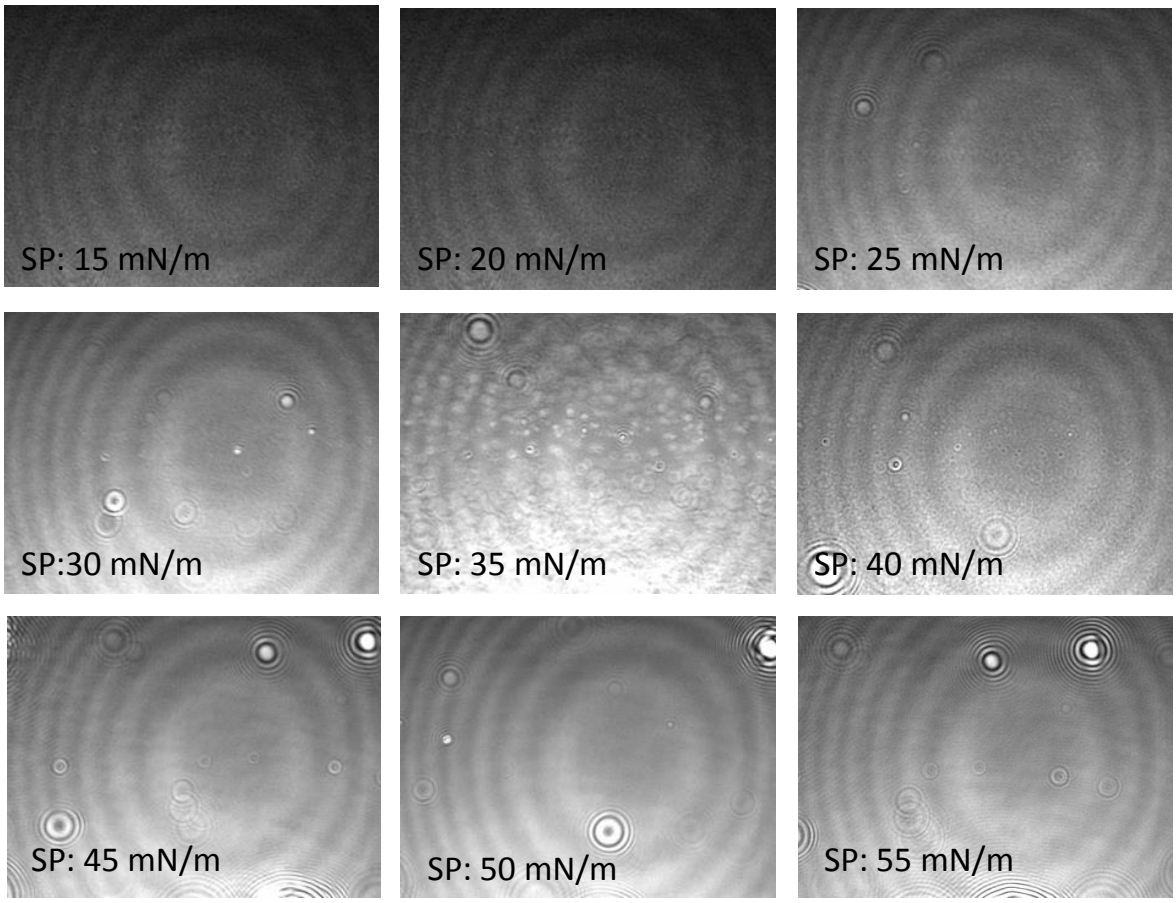

Figure 4.62. BAM images of DSPC/PEG40St/DSPS 0:5:5 mixed film

4.3.4. Phase Behavior and Morphology of DSPC/PEG40St/DSTAP Monolayers

1,2-stearoyl-3-trimethylammonium-propane (DSTAP) is a cationic lipid that body gives optimal immune response. Chemical structure of DSTAP is seen in Figure 4.63. Since DSTAP is ionic, electrostatic interaction between the zwitterionic phospholipid DSPC may influence the microbubble shell stability. The hydrophilic part of DSPC and DSTAP are completely same, the only phosphate group is missing in DSTAP. Owing to that reason, the interaction between DSPC and DSTAP result from their polar head groups. In this part of the study, DSTAP was added as a third component to DSPC/PEG40St mixture in order to investigate effect of ionic interactions on microbubble shell stability.

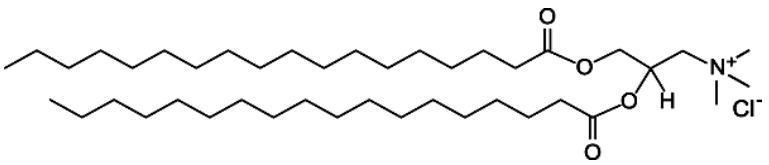

Figure 4.63. Chemical structure of DSTAP

Pure component and DSPC/PEG40St/DSTAP mixture π-A isotherms are revealed in Figure 4.64. Since head group of DSTAP is smaller than head group of DSPC, obtained DSTAP isotherm was slightly more condensed region. At large mean molecular areas DSTAP monolayer exhibits 0mN/m surface pressure. The π-A isotherm of DSTAP dramatically increased approximately at 53 $Å^2$ mean molecular area. Collapse of DSTAP occurred at 60 mN/m at approximately same mean molecular area with DSPC. Observed pure DSTAP π-A isotherm was consistent with the literature (Moghaddam, McNeil, Zheng, Mohammed, & Perrie, 2011). In the DSPC/PEG40St/DSTAP mixed films, effect of composition on monolayer stability was clearly observed. Since DSPC and DSTAP π-A isotherms are very similar, 4:5:1, 2:5:3 and 0:5:5 mixture isotherms were also similar. Before plateau region, up to 30% DSTAP molar ratio, increasing DSTAP molar ratio resulted in more condense monolayer. However, 50% DSTAP molar ratio in the mixed film lead to less condense monolayer compared to other mixtures due to ionic repulsion between DSTAP head groups. Unger et. al reported that, inclusion of charged lipid to the shell disturb the lipid packing and they noted that with cationic lipids only up to 20% molar ratio a stable microbubble shell can be obtained (Unger et al., 2004).

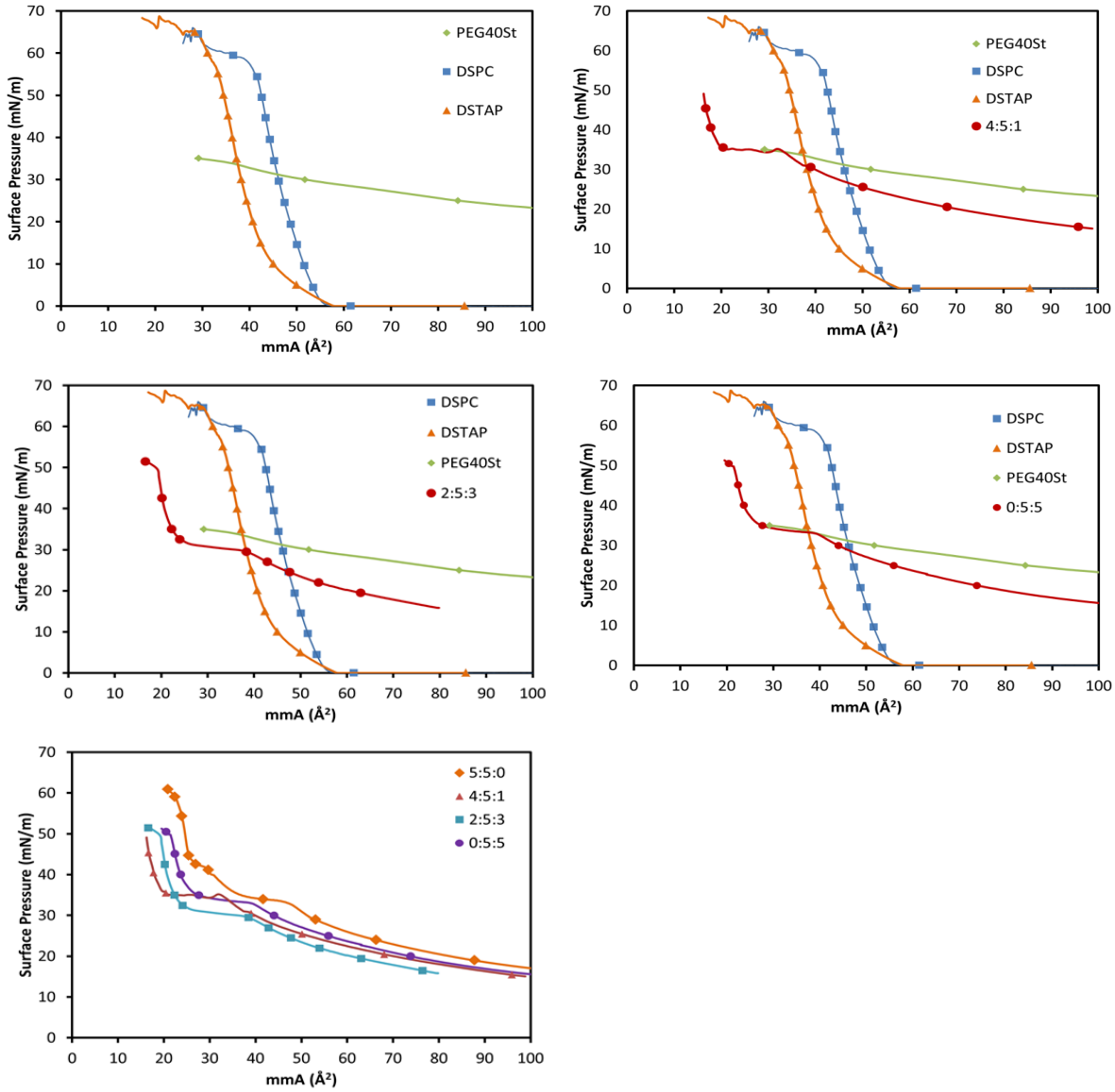

Figure 4.64. Surface pressure – mean molecular isotherm of pure and DSPC/PEG40St/DSTAP mixtures

Thermodynamic analysis showed that, all DSPC/PEG40St/DSTAP mixtures were miscible. Each mixture showed non-ideal mixing behavior. As seen in Figure 4.65, higher surface pressures result in more negative gibbs free energies. Increasing DSTAP composition more than 30% caused less negative mixing free energy due to electrostatic lateral repulsion between DSPC and DSTAP head groups. In a literature study, DSPC/PEG40St/DSTAP microbubbles were produced at different compositions by holding constant PEG40St molar ratio at 10% and changing DSTAP molar ratio between 0 to 40 %. They reported that, as the molar concentration of DSTAP increased, microbubbles with larger diameters were produced because of the electrostatic repulsion

between shell components (Mark A Borden et al., 2007). However, in our study PEG40St content was kept constant at 50% and attractive forces were found to be dominant in DSPC/PEG40St/DSTAP mixtures. Increased amount of PEG40St may have shield the repulsive forces between the components.

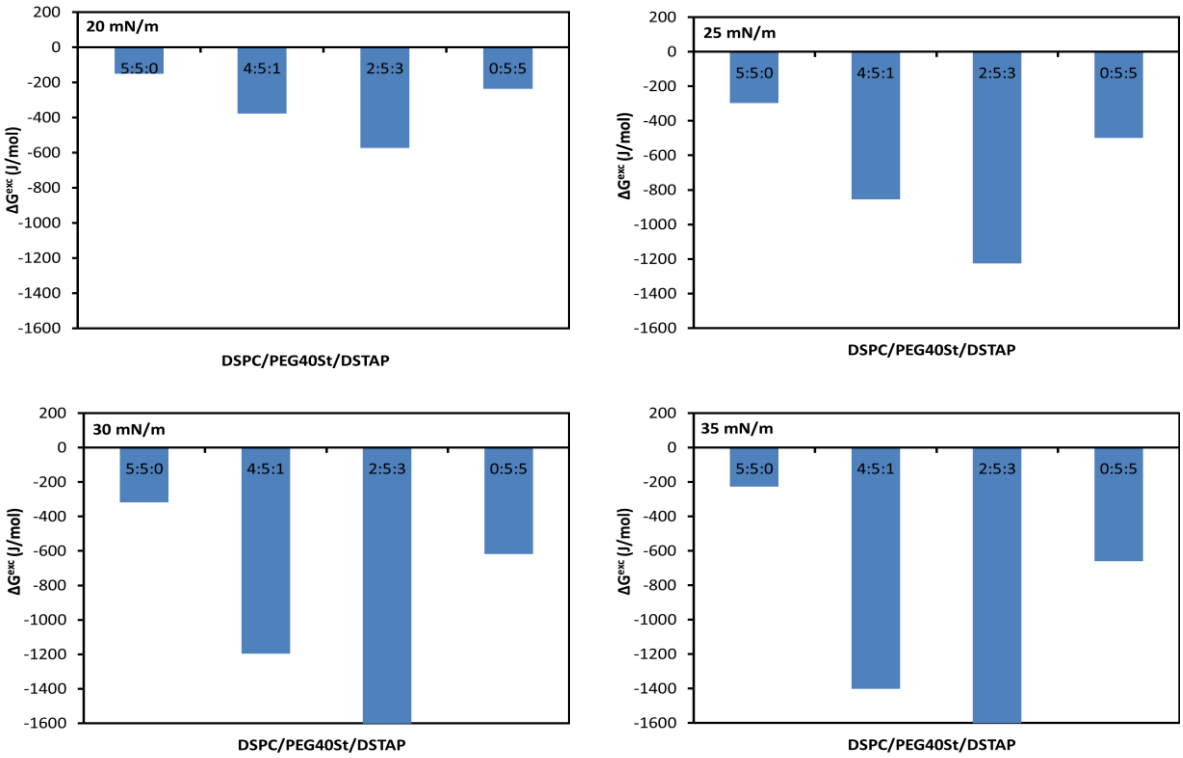

Figure 4.65. Comparison of excess free energy of mixing (ΔG^{Exc}) values of DSPC/PEG40St/DSTAP mixed monolayers calculated at π=20 mN/m, π=25 mN/m, π=30 mN/m, π=35 mN/m surface pressures.

Compression modulus graphs of DSPC/PEG40St/DSTAP mixed films are illustrated in Figure 4.66. Although DSTAP monolayer is exhibits slightly more condense isotherm than DSPC, it is more compressible compared to DSPC. Up to 32-34 mN/m surface pressure, elasticity behaviors of the mixtures were similar and at these surface pressures a minimum point was observed which may be due to phase transition of mixed monolayers or squeeze out of PEG40St as elucidated previous sections. After the minimum point, elasticity behaviors of mixed monolayers showed differences. Approximately at 46 mN/m surface pressure, 2:5:3 and 0:5:5 mixtures reached a maximum at approximately 140 mN/m compression modulus. 4:5:1 mixture reached

approximately 135 mN/m compression modulus at 50 mN/m surface pressure. At 50 mN/m surface pressure 2:5:3 mixture exhibited another peak nearly at 90 mN/m compression modulus which results from coexisting of two different phases.

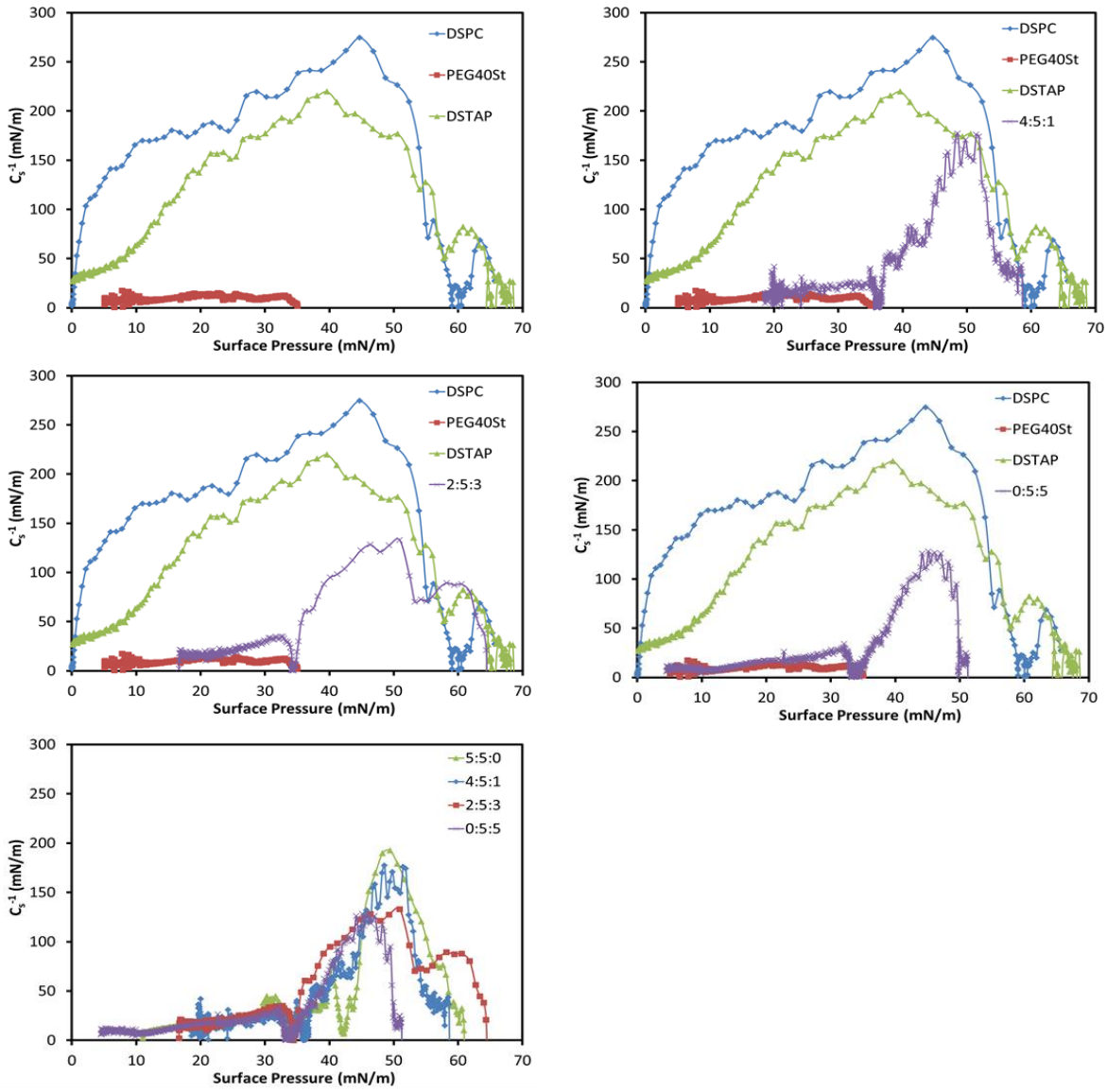

Figure 4.66. The compression modulus (Cs^{-1}) plots of DSPC/PEG40St/DSTAP mixed films

In Figure 4.67, BAM images of DSTAP is represented. Below 10 mN/m surface pressures DSTAP exhibited gas and liquid expanded phases. With the increasing surface pressure condense domains gathered and a homogeneous condense phase was formed. Until collapse reaching the collapse pressure no phase separation was observed.

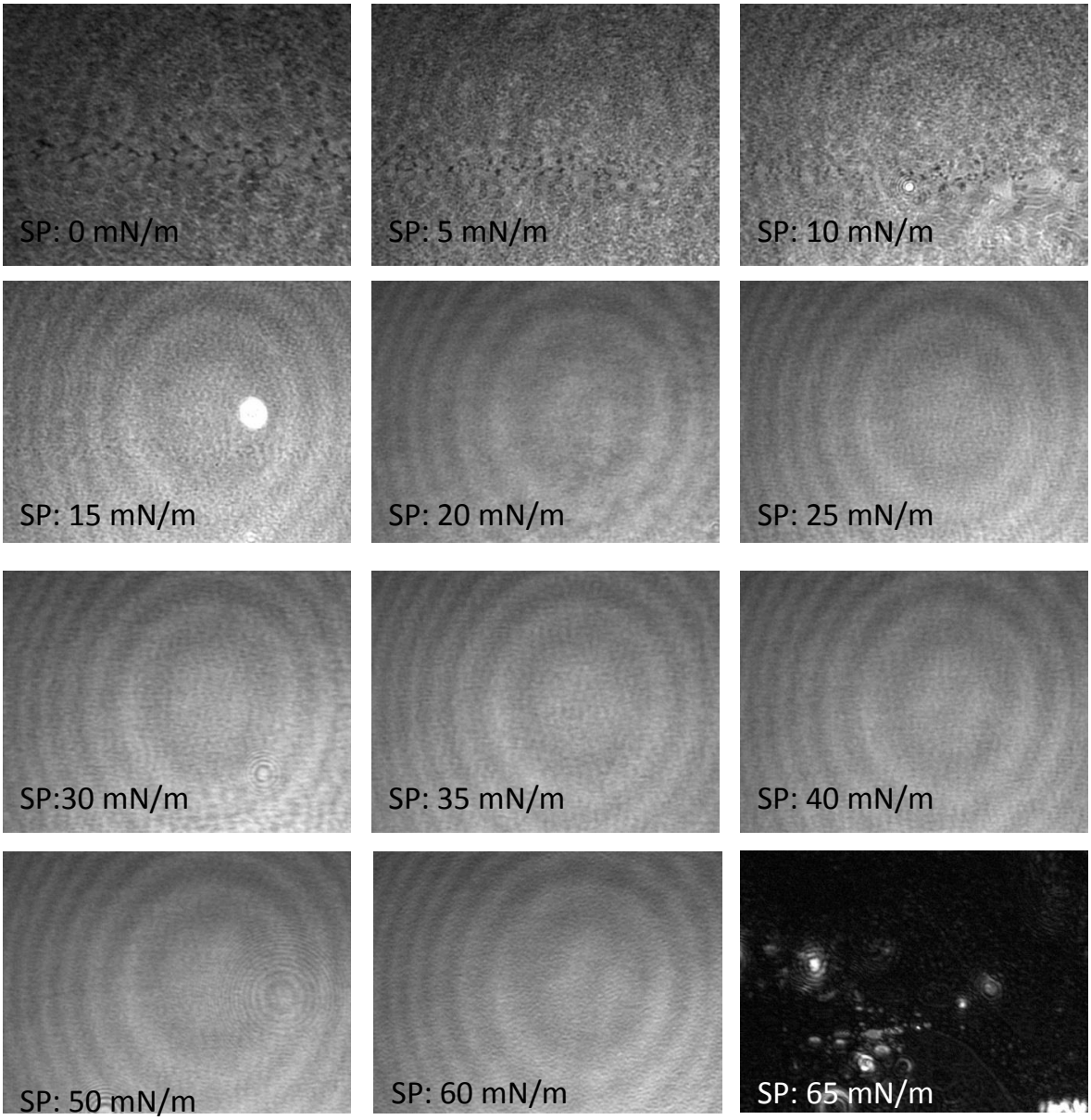

Figure 4.67. BAM images of DSTAP at T=20 ^{o}C

As illustrated in Figure 4.68, in 4:5:1 mixture starting from 25 mN/m surface pressure, small sized solid domains appeared. These solid domains gathered and formed a thick layer. At 35 mN/m surface pressure, very bright small domains were detected. After plateau region, these bright domains disappeared and resulting in condensed homogeneous phase.

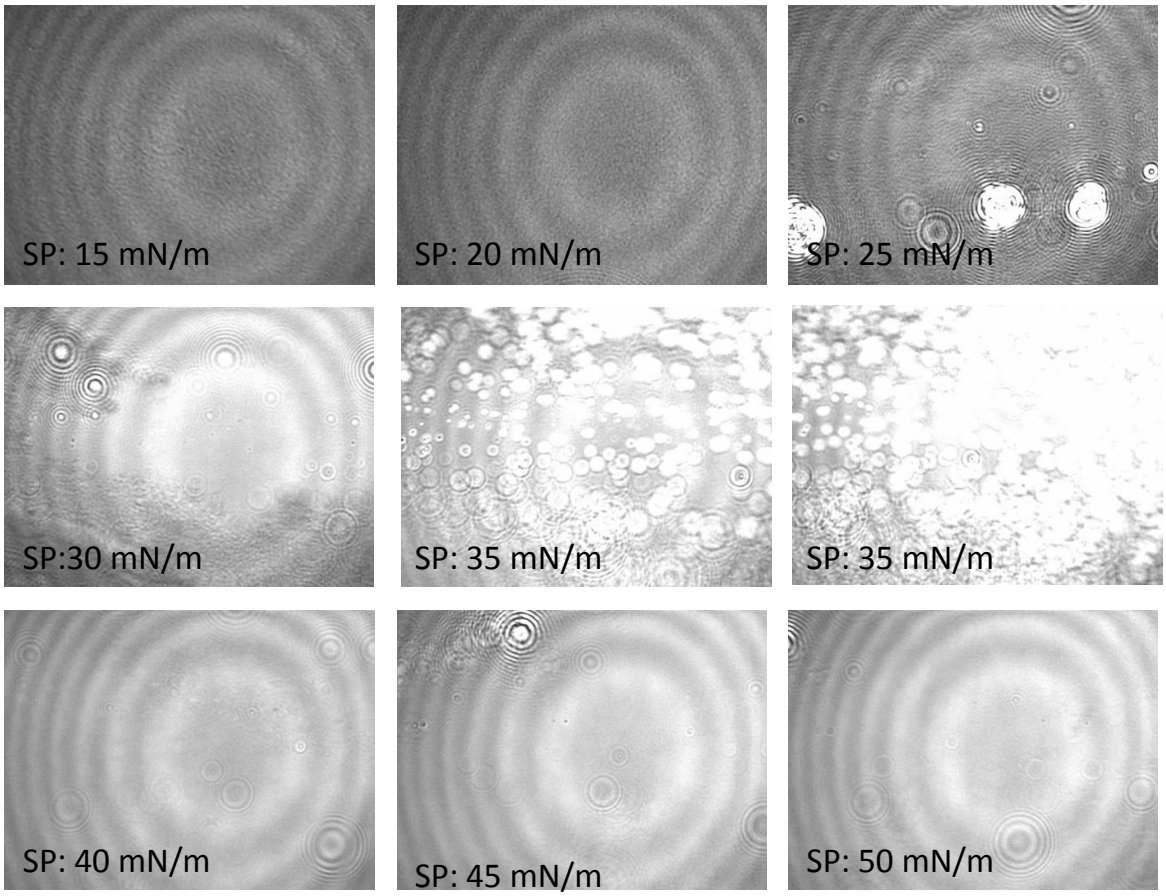

Figure 4.68. BAM images of DSPC/PEG40St/DSPS 4:5:1 mixed film T=20 ^{o}C

BAM images of 2:5:3 mixture (Figure 4.69) exhibited homogeneous liquid expand phase in the range of 15 mN/m – 24mN/m. At 35 mN/m bright, thick domains were observed local collapses. Further compression of the mixed film rendered a homogeneous liquid condensed surface.

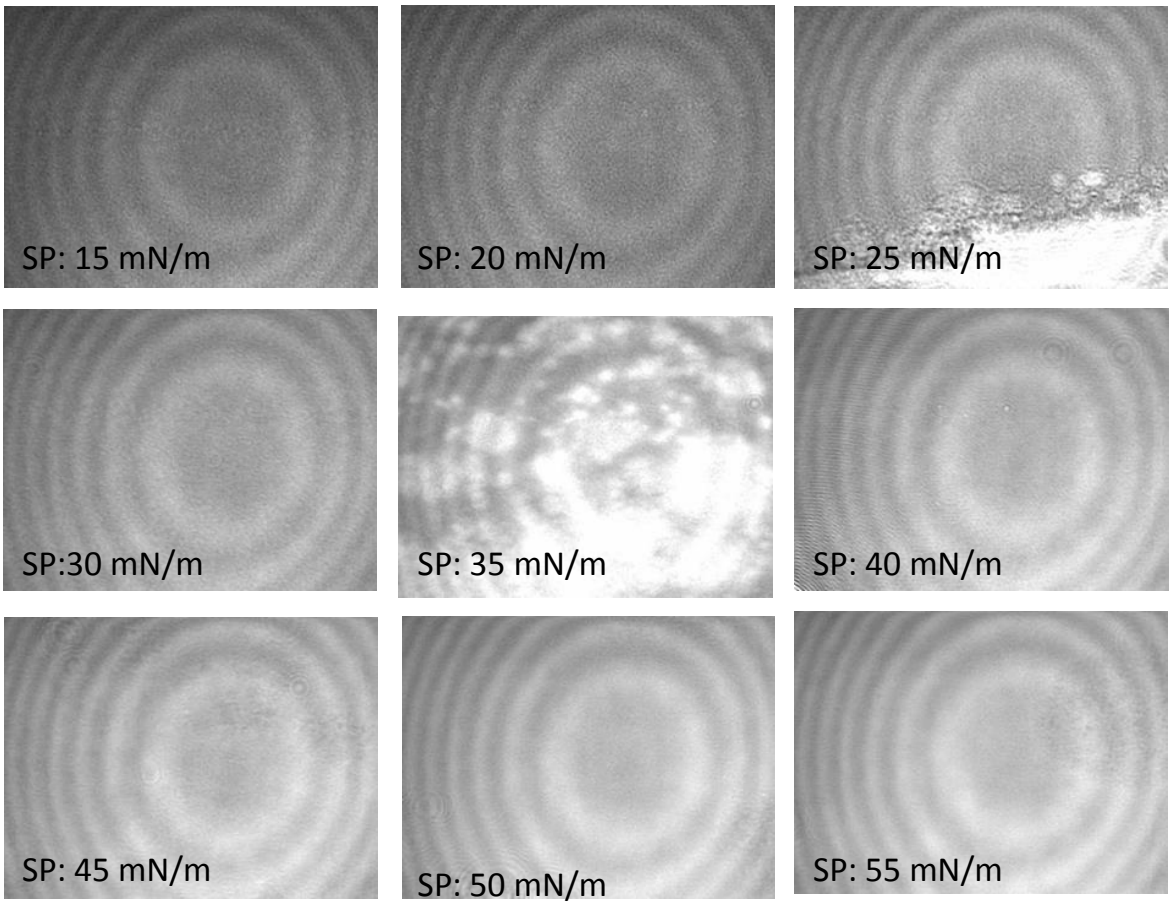

Figure 4.69. BAM images of DSPC/PEG40St/DSPS 2:5:3 mixed film at T=20 ^{o}C

As illustrated in Figure 4.70, BAM images of 0:5:5 mixed film exhibited phase separation up to 40 mN/m. At higher surface pressures obtained images were generally homogeneous.

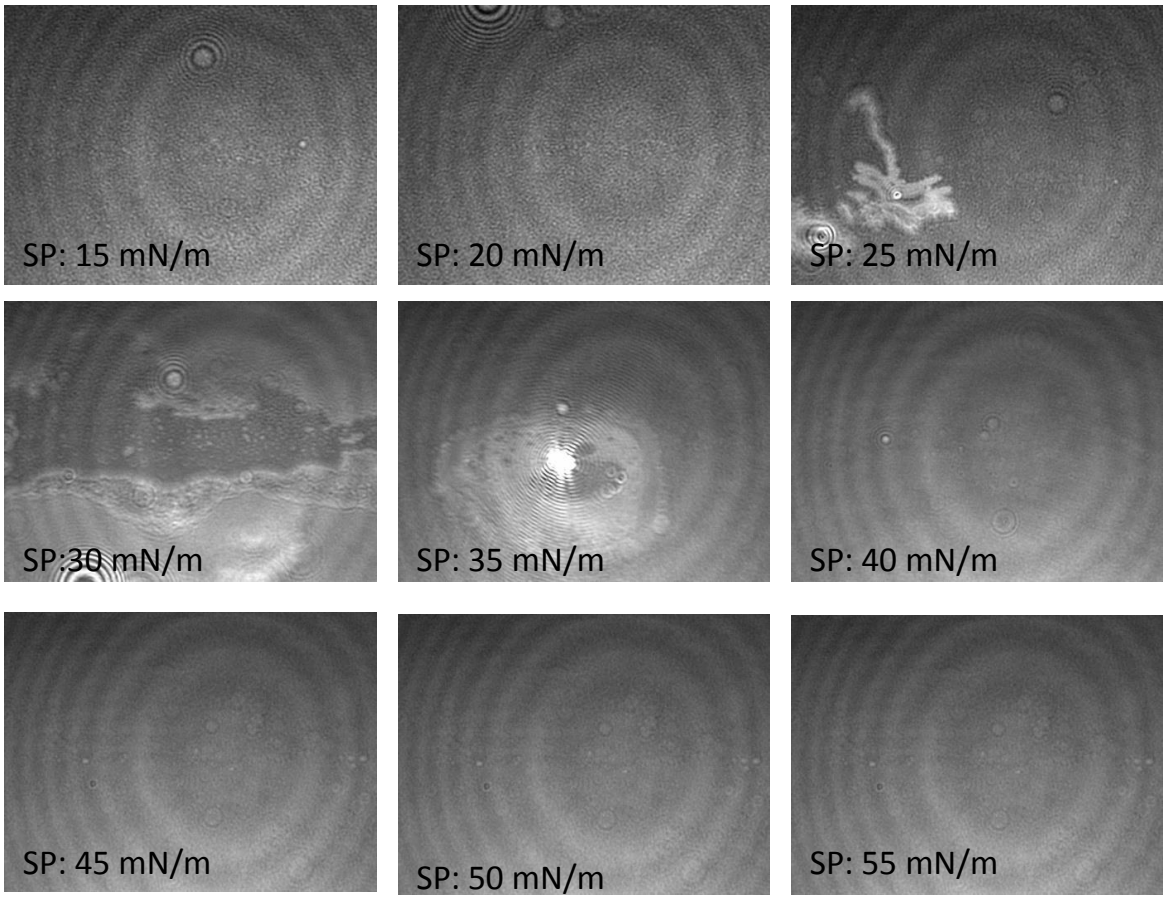

Figure 4.70. BAM images of DSPC/PEG40St/DSPS 0:5:5 mixed film at T=20 ^{o}C

From the results we may conclude that, when a microbubble shell is to be produced with the mixture of DSPC, PEG40St and DSTAP, molar ratio of DSPC or DSTAP should be low. In a literature study it was revealed that, in DSPC/PEG40St/DSTAP microbubbles produced by holding PEG40St molar ratio as 0.1 , as the DSTAP molar ratio increased, microbubble yield decreased and microbubble size increased (Mark A Borden et al., 2007). This study is consistent with our 2D LB studies.

CHAPTER 5

CONCLUSIONS

Microbubbles at varying ratio of DSPC/PEG40 St were prepared and their response to shear stress at 25 ^{o}C were investigated determining their size and concentration with respect to time. Shear stress experiments performed with air-filled DSPC/PEG40St microbubbles showed that as the PEG40St molar ratio increased, microbubbles became more resistive against shear stress. As expected, increase in circulation time under shear stress resulted in higher decrease in microbubble concentration. Among the examined microbubbles, 5:5 DSPC/PEG40St microbubble composition was found to be the most stable microbubble composition. 5:5 DSPC/PEG40 St microbubbles were observed to be even more durable than DSPC/DSPE-PEG2000 microbubbles although DSPE-PEG2000 as an emulsifier has double tail in the hydrophobic part, resulting in stronger van der Waals interactions. However, DSPC/DSPE-PEG2000 microbubbles were more stable than DSPC/DSPE-PEG1000 microbubbles at molar ratio of 5:5. Unexpected result observed with DSPC/DSPE-PEG2000 microbubbles was attributed to shape of the emulsifier. While DSPE-PEG2000 has cylindrical shape, PEG40 St is in conical shape, filling the spaces between cylindrical phospholipid molecules covering spherical microbubble surface. Due to shorter PEG Chain in DSPE-PEG1000 compared to DSPE-PEG2000, this effect was more pronounced in DSPC/DSPE-PEG1000 microbbubles, supporting our argument.

Since the intercations between microbubble shell components were secondary type of interactions, temperature is an important parameter. Our results showed that microbubbles are more prone to destruction with increasing temperature. We surmise that decreased van der Waals interactions between the shell components and thus less cohesive shell with increasing temperature resulted in instability of microbbubles.

Effect of gas core on microbubble stability was investigated by preparing PFC filled DSPC/PEG40St at molar ratio of 9:1, 7:3 and 5:5. In general, PFC-filled microbubbles were found to be smaller and more resistive to shear than air-filled microbubbles due to hydrophobic interaction between PFC gas and microbubble shell.

While concentration of air-filed microbubbles decreased with increasing shear stress, microbubble destruction was not affected by increasing shear stress for PFC filled microbbubles. PFC filled microbbubles showed a high rate of decrease in concentration at 0,028 Pa shear stress, but the further increase in shear stress did not accelerate the microbubble destruction. In general, in the PFC-filled microbubble formulations, larger microbubbles disappeared first when they were exposed to shear stress at all temperatures, exhibiting a size reduction in microbubble population. However, such a trend was not exist in air-filled microbubbles.

Effect of gas core on stability was observed more in 9:1 formulation since air-filled 9:1 microbubbles were very fragile even under low shear stresses. This proves that not only the gas core but also the shell structure plays important role in microbubble stability. This result also suggest us increasing PEG40 St content in microbubble formulation made the shell more cohesive, minimizing the effect of type of gas core. This result is also important from the economical point of view since PFC is an expensive gas.

One of the main parameters affecting microbubble stability in in-vivo applications is their protein propellant capability. In order to investigate effect of PEG40St molar ratio on protein (BSA) resistance of microbubble shell, LB and SPR techniques were used as comparative methods. To see effect of packing density and temperature, experiments were performed at surface pressures of 30mN/m and 40 mN/m and temperatures of 20 ^{o}C and 38 ^{o}C. In LB experiments, it was observed that while DSPC monolayer adsorbed BSA, PEG40St monolayer repel it. Both in LB and SPR experiments showed that protein adsorption to the monolayer decreases with increasing PEG40 St content and increasing packing density, but increases with temperature. Observation of less protein adsorption with increasing surface pressure (packing density) was attributed to conformational changes in the PEG Chains from mushroom to brush conformation. The opposite trend observed in protein adsorption with increasing temperature in SPR and LB can be explained by the nature of the systems. While protein adsorbed on PEG chains in LB experiments may decrease the molecular density at the air-water interface by “pulling down” of protein adsorbed PEG40 St molecules from the monolayer, all the molecules remain “sitting” on the SPR substrate even after protein adsorption. Our results in general showed that SPR and LB can be used as complemantary techniques for protein adsorption studies. LB provides some advantageous since creation of an environment close to physiological conditions

(air-water interface, pH, ionic strength, temperature, etc.) can be controlled much easily in LB, however quantitative analysis of proteins adsorption can be done by SPR method.

Analysis of the data obtained during protein studies using LB technique showed that composition of the shell membrane has a big influence on intermolecular interactions. The pi-A isotherms shifted to higher mean molecular area with increasing emulsifier content below the plateau region. However, the order was reverse after the plateau, shifting toward to lower mean molecular areas. Excess Gibbs free energy was negative at 20 ^{o}C for the compositions of DSPC/PEG40 St at molar ratio of 9:1, 7:3 and 5:5. The minimum of excess gibbs free energy was obtained with 7:3 mixture. These analyses showed us that LB technique can be used as a preliminary to investigate the shell cohesiveness of the microbubbles. In the remaining part of the study, we tested the effect of addition of a third component to DSPC/PEG40 St formulation. StGly, DSPS, $StNH_2$ and DSTAP were added as the third component and their intermolecular interactions were investigated using LB and phase behaviors of mixed monolayers at different compositions were visualized via BAM.

StGly is an amphiphilic molecule capable of making hydrogen bonding owing to the hydroxyl groups in its structure. In DSPC/PEG40St/StGly mixed films prepared at various molar ratios, increasing StGly molar fraction resulted in π-A isotherms shifted to smaller mean molecular areas. In all π-A isotherms, as observed with binary mixtures of DSPC/PEG40 St, the plateau region was observed at a surface pressure close to 35mN/m ± 2. Pure StGly molecule showed circular domains in BAM. In its mixtures with DSPC and PEG40St, at the earlier stages of compressions phase separations were observed. Increasing surface pressure generally resulted in thick films with bright domains. These domains were attributed to collapse of the monolayer at the air-water interface, which may be resulting from the hydrogen groups present in StGly. In cycle experiments performed with DSPC/PEG40St/StGly 0:5:5, in the first and second compression monolayer reached the 50 mN/m surface pressure at the same mean molecular area and this result showed that in plateau regions observed in π-A isotherms there was no material loss, however in PEG40St rich areas local collapses may occur. StGly may form condense film, however, since it has a single tail, it may not form stable microbubbles.

In LB experiments performed with ternary mixtures of DSPC/PEG40St/$StNH_2$, all mixed films exhibited negative mixing gibbs free energies due to strong electrostatic

interactions between head groups of zwitterionic DSPC and cationic $StNH_2$. Elasticity behaviors of mixed films were similar and generally liquid condensed phase was observed. BAM images of DSPC/PEG40St/$StNH_2$ mixed films were generally exhibited homogeneous phase behavior and generally liquid condense phases were observed. On the other hand, $StNH_2$ may not form stable microbubble due to its shape.

DSPC/PEG40St/DSPS ternary mixture π-A isotherms showed very similar behavior at different molar compositions. Thermodynamic analysis showed that ternary mixtures were miscible while binary mixture of PEG40St and DSPS was immiscible. Miscibility of ternary mixture may result from strong ionic interaction between head groups of DSPC and DSPS. Elasticity behavior of mixtures were close and they generally exhibited liquid expand phase despite the condense behavior of DSPS and DSPC. This may result from repulsive interactions between DSPS and PEG40St. In BAM images of mixtures generally homogeneous images were obtained. DSPC/PEG40St/DSPS 2:5:3 mixture may be recommended an anionic microbubble for drug delivery purpose.

In DSPC/PEG40St/DSTAP ternary mixtures, increasing DSTAP molar fraction more than 30% result in shift large mean molecular areas in π-A isotherm due to lateral ionic repulsive forces. Examined all compositions were miscible. Compressional modulus values of mixtures were similar an generally showed liquid condensed phase behavior. In BAM images of mixtures, coexistence of liquid expand and solid phases were observed due to ionic repulsion. DSPC/PEG40St/DSTAP can be recommended as cationic microbubble formulation by holding DSTAP molar fraction less than 30%. It can be a good candidate for DNA transport.

REFERENCES

Arwin, H. (1986). Optical properties of thin layers of bovine serum albumin, γ-globulin, and hemoglobin. *Applied spectroscopy, 40*(3), 313-318.

Barrack, Thomas, & Stride, Eleanor. (2009). Microbubble destruction during intravenous administration: a preliminary study. *Ultrasound in medicine & biology, 35*(3), 515-522.

Bekeredjian, Raffi, Grayburn, Paul A, & Shohet, Ralph V. (2005). Use of ultrasound contrast agents for gene or drug delivery in cardiovascular medicine. *Journal of the American College of Cardiology, 45*(3), 329-335.

Bloch, Susannah H, Wan, Mingxi, Dayton, Paul A, & Ferrara, Katherine W. (2004). Optical observation of lipid-and polymer-shelled ultrasound microbubble contrast agents. *Applied Physics Letters, 84*(4), 631-633.

Borden, M.A., & Longo, M.L. (2002). Dissolution behavior of lipid monolayer-coated, air-filled microbubbles: Effect of lipid hydrophobic chain length. *Langmuir, 18*(24), 9225-9233.

Borden, Mark. (2009). Nanostructural features on stable microbubbles. *Soft Matter, 5*(4), 716-720.

Borden, Mark A, Caskey, Charles F, Little, Erika, Gillies, Robert J, & Ferrara, Katherine W. (2007). DNA and polylysine adsorption and multilayer construction onto cationic lipid-coated microbubbles. *Langmuir, 23*(18), 9401-9408.

Borden, Mark A, Dayton, Paul, Zhao, Shukui, & Ferrara, Katherine W. (2004). *Physico-chemical properties of the microbubble lipid shell [ultrasound contrast agents]*. Paper presented at the Ultrasonics Symposium, 2004 IEEE.

Borden, Mark A, Martinez, Gary V, Ricker, Josette, Tsvetkova, Nelly, Longo, Marjorie, Gillies, Robert J, . . . Ferrara, Katherine W. (2006). Lateral phase separation in lipid-coated microbubbles. *Langmuir, 22*(9), 4291-4297.

Borden, Mark A, Pu, Gang, Runner, Gabriel J, & Longo, Marjorie L. (2004). Surface phase behavior and microstructure of lipid/PEG-emulsifier monolayer-coated microbubbles. *Colloids and Surfaces B: Biointerfaces, 35*(3), 209-223.

Burns, Peter N, & Wilson, Stephanie R. (2006). Microbubble contrast for radiological imaging: 1. Principles. *Ultrasound quarterly, 22*(1), 5-13.

Chou, T.H., & Chu, I. (2003). Thermodynamic characteristics of DSPC/DSPE-PEG2000 mixed monolayers on the water subphase at different temperatures. *Colloids and Surfaces B: Biointerfaces, 27*(4), 333-344.

Coatney, Robert W. (2001). Ultrasound imaging: principles and applications in rodent research. *Ilar Journal, 42*(3), 233-247.

Cui, Wenjin, Bei, Jianzhong, Wang, Shenguo, Zhi, Guang, Zhao, Yuying, Zhou, Xiaoshu, . . . Xu, Yong. (2005). Preparation and evaluation of poly (L-lactide-co-glycolide)(PLGA) microbubbles as a contrast agent for myocardial contrast echocardiography. *Journal of Biomedical Materials Research Part B: Applied Biomaterials, 73*(1), 171-178.

Dayton, Paul A, Morgan, KE, Klibanov, AL, Brandenburger, GH, & Ferrara, KW. (1999). Optical and acoustical observations of the effects of ultrasound on contrast agents. *Ultrasonics, Ferroelectrics and Frequency Control, IEEE Transactions on, 46*(1), 220-232.

Dey, T., Anam, K., Afrin, F., & Ali, N. (2000). Antileishmanial activities of stearylamine-bearing liposomes. *Antimicrobial Agents and Chemotherapy, 44*(6), 1739-1742.

Dicker, S, Mleczko, M, Schmitz, G, & Wrenn, SP. (2010). Determination of microbubble cavitation threshold pressure as function of shell chemistry. *Bubble Science, Engineering & Technology, 2*(2), 55-64.

Dijkmans, PA, Juffermans, LJM, Musters, RJP, Van Wamel, A., Ten Cate, FJ, Van Gilst, W., . . . Kamp, O. (2004). Microbubbles and ultrasound: from diagnosis to therapy. *European Journal of Echocardiography, 5*(4), 245-246.

Dressaire, Emilie, Bee, Rodney, Bell, David C, Lips, Alex, & Stone, Howard A. (2008). Interfacial polygonal nanopatterning of stable microbubbles. *Science, 320*(5880), 1198-1201.

Efremova, Nadezhda V, Bondurant, Bruce, O'Brie, David F, & Leckband, Deborah E. (2000). Measurements of interbilayer forces and protein adsorption on uncharged lipid bilayers displaying poly (ethylene glycol) chains. *Biochemistry, 39*(12), 3441-3451.

Efremova, NV, Sheth, SR, & Leckband, DE. (2001). Protein-induced changes in poly (ethylene glycol) brushes: molecular weight and temperature dependence. *Langmuir, 17*(24), 7628-7636.

El-Khouri, Rita J, Frey, Shelli L, Szmodis, Alan W, Hall, Emily, Kauffman, Karlina J, Patten, Timothy E, . . . Parikh, Atul N. (2011). A Stripe-to-Droplet Transition Driven by Conformational Transitions in a Binary Lipid− Lipopolymer Mixture at the Air− Water Interface. *Langmuir, 27*(5), 1900-1906.

El-Sherif, Dalia M, & Wheatley, Margaret A. (2003). Development of a novel method for synthesis of a polymeric ultrasound contrast agent. *Journal of Biomedical Materials Research Part A, 66*(2), 347-355.

Ferrara, Katherine W, Borden, Mark A, & Zhang, Hua. (2009). Lipid-shelled vehicles: engineering for ultrasound molecular imaging and drug delivery. *Accounts of chemical research, 42*(7), 881-892.

Forsberg, F, Shi, WT, & Goldberg, BB. (2000). Subharmonic imaging of contrast agents. *Ultrasonics, 38*(1), 93-98.

Fuller, Gerald G. (2003). Rheology of mobile interfaces. *Rheology Reviews*, 77-124.

Gaines, George L. (1966). *Insoluble monolayers at liquid-gas interfaces*: Interscience New York.

Geers, Bart, Lentacker, Ine, Sanders, Niek N, Demeester, Joseph, Meairs, Stephen, & De Smedt, Stefaan C. (2011). Self-assembled liposome-loaded microbubbles: The missing link for safe and efficient ultrasound triggered drug-delivery. *Journal of Controlled Release, 152*(2), 249-256.

Greenough, K.P., & Blanchard, GJ. (2009). Lipid headgroups mediate organization and dynamics in bilayers. *Spectrochimica Acta Part A: Molecular and Biomolecular Spectroscopy, 71*(5), 2050-2056.

Harder, P, Grunze, M, Dahint, R, Whitesides, GM, & Laibinis, PE. (1998). Molecular conformation in oligo (ethylene glycol)-terminated self-assembled monolayers on gold and silver surfaces determines their ability to resist protein adsorption. *The Journal of Physical Chemistry B, 102*(2), 426-436.

Harris, J. Milton. (1992). *Poly (ethylene glycol) chemistry: biotechnical and biomedical applications*: Plenum Publishing Corporation.

Hell, S, Reiner, G, Cremer, C, & Stelzer, Ernst HK. (1993). Aberrations in confocal fluorescence microscopy induced by mismatches in refractive index. *Journal of microscopy, 169*(3), 391-405.

Hernot, Sophie, & Klibanov, Alexander L. (2008). Microbubbles in ultrasound-triggered drug and gene delivery. *Advanced drug delivery reviews, 60*(10), 1153-1166.

Heuberger, M, Drobek, T, & Spencer, ND. (2005). Interaction forces and morphology of a protein-resistant poly (ethylene glycol) layer. *Biophysical journal, 88*(1), 495-504.

Hoenig, Dirk, & Moebius, Dietmar. (1991). Direct visualization of monolayers at the air-water interface by Brewster angle microscopy. *The Journal of Physical Chemistry, 95*(12), 4590-4592.

Hucknall, Angus, Rangarajan, Srinath, & Chilkoti, Ashutosh. (2009). In pursuit of zero: polymer brushes that resist the adsorption of proteins. *Advanced Materials, 21*(23), 2441-2446.

Jung, Linda S, Campbell, Charles T, Chinowsky, Timothy M, Mar, Mimi N, & Yee, Sinclair S. (1998). Quantitative interpretation of the response of surface plasmon resonance sensors to adsorbed films. *Langmuir, 14*(19), 5636-5648.

Kaya, Mehmet, Gregory V, Thomas S, & Dayton, Paul A. (2009). Changes in lipid-encapsulated microbubble population during continuous infusion and methods to maintain consistency. *Ultrasound in medicine & biology, 35*(10), 1748-1755.

Korpanty, Grzegorz, Grayburn, Paul A, Shohet, Ralph V, & Brekken, Rolf A. (2005). Targeting vascular endothelium with avidin microbubbles. *Ultrasound in medicine & biology, 31*(9), 1279-1283.

Kotyńska, J., & Figaszewski, Z.A. (2007). Adsorption equilibria at interface separating electrolyte solution and phosphatidylcholine–stearylamine liposome membrane. *Biophysical chemistry, 127*(1), 84-90.

Kwan, J.J., & Borden, M.A. (2010). Microbubble dissolution in a multigas environment. *Langmuir, 26*(9), 6542-6548.

Kwan, J.J., & Borden, M.A. (2012a). Lipid monolayer collapse and microbubble stability. *Advances in Colloid and Interface Science*.

Kwan, J.J., & Borden, M.A. (2012b). Lipid monolayer dilatational mechanics during microbubble gas exchange. *Soft Matter, 8*(17), 4756-4766.

Lasic, Danilo D. (1994). Sterically stabilized vesicles. *Angewandte Chemie International Edition in English, 33*(17), 1685-1698.

Lasic, DD. (1997). Recent developments in medical applications of liposomes: sterically stabilized liposomes in cancer therapy and gene delivery in vivo. *Journal of controlled release, 48*(2), 203-222.

Levin, Carly S, Bishnoi, Sandra Whaley, Grady, Nathaniel K, & Halas, Naomi J. (2006). Determining the conformation of thiolated poly (ethylene glycol) on Au nanoshells by surface-enhanced Raman scattering spectroscopic assay. *Analytical chemistry, 78*(10), 3277-3281.

Liang, HD, & Blomley, MJK. (2003). The role of ultrasound in molecular imaging. *British Journal of Radiology, 76*(suppl 2), S140-S150.

Lozano, M.M., & Longo, M.L. (2009). Microbubbles coated with disaturated lipids and DSPE-PEG2000: phase behavior, collapse transitions, and permeability. *Langmuir, 25*(6), 3705-3712.

Luna, Carlos, Stroka, Kimberly M, Bermudez, Harry, & Aranda-Espinoza, Helim. (2011). Thermodynamics of monolayers formed by mixtures of phosphatidylcholine/phosphatidylserine. *Colloids and Surfaces B: Biointerfaces, 85*(2), 293-300.

Markey, F. (1999). What is SPR anyway. *BIA journal, 6*, 14-17.

Mayer, Susan, & Grayburn, Paul A. (2001). Myocardial contrast agents: recent advances and future directions. *Progress in cardiovascular diseases, 44*(1), 33-44.

Moghaddam, Behfar, Ali, M Habib, Wilkhu, Jitinder, Kirby, Daniel J, Mohammed, Afzal R, Zheng, Qinguo, & Perrie, Yvonne. (2011). The application of

monolayer studies in the understanding of liposomal formulations. *International journal of pharmaceutics, 417*(1), 235-244.

Moghaddam, Behfar, McNeil, Sarah E, Zheng, Qinguo, Mohammed, Afzal R, & Perrie, Yvonne. (2011). Exploring the Correlation Between Lipid Packaging in Lipoplexes and Their Transfection Efficacy. *Pharmaceutics, 3*(4), 848-864.

NEUROBLASTOMA, METABOLISM IN. (2003). TRIFLUOPERAZINE: EFFECTS ON POLYPHOSPHOINOSITIDE.

Pattnaik, Priyabrata. (2005). Surface plasmon resonance. *Applied biochemistry and biotechnology, 126*(2), 79-92.

Plant, Anne L, Brighamburke, Michael, Petrella, Eugene C, & Oshannessy, Daniel J. (1995). Phospholipid/alkanethiol bilayers for cell-surface receptor studies by surface plasmon resonance. *Analytical biochemistry, 226*(2), 342-348.

Quaia, Emilio. (2005). Classification and safety of microbubble-based contrast agents *Contrast Media in Ultrasonography* (pp. 3-14): Springer.

Roberts, Gareth Gwyn. (1990). *Langmuir-blodgett films* (Vol. 1): Plenum press New York.

Ross, Michaela, Steinem, Claudia, Galla, Hans-Joachim, & Janshoff, Andreas. (2001). Visualization of chemical and physical properties of calcium-induced domains in DPPC/DPPS Langmuir-Blodgett layers. *Langmuir, 17*(8), 2437-2445.

Ruiz Domínguez, Manuela, Narváez, Isabel González, & Rodríguez Patino, Juan M. (1998). Aqueous subphase pH influence on nonionizable material monolayers. Structural and rheological characteristics. *Industrial & engineering chemistry research, 37*(3), 936-943.

Singhal, S, Moser, CC, & Wheatley, MA. (1993). Surfactant-stabilized microbubbles as ultrasound contrast agents: stability study of Span 60 and Tween 80 mixtures using a Langmuir trough. *Langmuir, 9*(9), 2426-2429.

Sukhishvili, Svetlana A, Chen, Yan, Müller, Joachim D, Gratton, Enrico, Schweizer, Kenneth S, & Granick, Steve. (2000). Materials science: Diffusion of a polymer 'pancake'. *Nature, 406*(6792), 146-146.

Szíjjártó, Csongor, Rossi, Simona, Waton, Gilles, & Krafft, Marie Pierre. (2012). Effects of Perfluorocarbon Gases on the Size and Stability Characteristics of Phospholipid-Coated Microbubbles: Osmotic Effect versus Interfacial Film Stabilization. *Langmuir, 28*(2), 1182-1189.

Talu, Esra, Lozano, Monica M, Powell, Robert L, Dayton, Paul A, & Longo, Marjorie L. (2006). Long-term stability by lipid coating monodisperse microbubbles formed by a flow-focusing device. *Langmuir, 22*(23), 9487-9490.

Talu, Esra, Powell, Robert L, Longo, Marjorie L, & Dayton, Paul A. (2008). Needle size and injection rate impact microbubble contrast agent population. *Ultrasound in medicine & biology, 34*(7), 1182-1185.

Teixeira, H., Dubernet, C., Rosilio, V., Benita, S., Lepault, J., Erk, I., & Couvreur, P. (2000). New bicompartmental structures are observed when stearylamine is mixed with triglyceride emulsions. *Pharmaceutical research, 17*(10), 1329-1332.

Tirosh, Oren, Barenholz, Yechezkel, Katzhendler, Jehoshua, & Priev, Aba. (1998). Hydration of polyethylene glycol-grafted liposomes. *Biophysical journal, 74*(3), 1371-1379.

Uchida, Katsumi, Otsuka, Hidenori, Kaneko, Mitsuhiro, Kataoka, Kazunori, & Nagasaki, Yukio. (2005). A reactive poly (ethylene glycol) layer to achieve specific surface plasmon resonance sensing with a high S/N ratio: the substantial role of a short underbrushed PEG layer in minimizing nonspecific adsorption. *Analytical chemistry, 77*(4), 1075-1080.

Ulman, Abraham. (1995). Langmuir-Blodgett Films. *The Handbook of Surface Imaging and Visualization*, 277.

Unger, Evan C, Porter, Thomas, Culp, William, Labell, Rachel, Matsunaga, Terry, & Zutshi, Reena. (2004). Therapeutic applications of lipid-coated microbubbles. *Advanced drug delivery reviews, 56*(9), 1291-1314.

Wan, K., Chovelon, JM, & Jaffrezic-Renault, N. (2000). Enzyme–octadecylamine Langmuir–Blodgett membranes for ENFET biosensors. *Talanta, 52*(4), 663-670.

Wang, Wenhua, Moser, Chris C, & Wheatley, Margaret A. (1996). Langmuir trough study of surfactant mixtures used in the production of a new ultrasound contrast agent consisting of stabilized microbubbles. *The Journal of Physical Chemistry, 100*(32), 13815-13821.

Wheatley, Margaret A, Schrope, Beth, & Shen, Peng. (1990). Contrast agents for diagnostic ultrasound: development and evaluation of polymer-coated microbubbles. *Biomaterials, 11*(9), 713-717.

Wiese, G., Barthel, S.R., & Dimitroff, C.J. (2009). Analysis of physiologic E-selectin-mediated leukocyte rolling on microvascular endothelium. *Journal of visualized experiments: JoVE*(24).

Williams, Ross, Hudson, John M, Lloyd, Brendan A, Sureshkumar, Ahthavan R, Lueck, Gordon, Milot, Laurent, . . . Burns, Peter N. (2011). Dynamic microbubble contrast-enhanced US to measure tumor response to targeted therapy: a proposed clinical protocol with results from renal cell carcinoma patients receiving antiangiogenic therapy. *Radiology, 260*(2), 581-590.

Wydro, P., & Witkowska, K. (2009). The interactions between phosphatidylglycerol and phosphatidylethanolamines in model bacterial membranes:: The effect of the

acyl chain length and saturation. *Colloids and Surfaces B: Biointerfaces, 72*(1), 32-39.

Xing, Z., Ke, H., Wang, J., Zhao, B., Yue, X., Dai, Z., & Liu, J. (2010). Novel ultrasound contrast agent based on microbubbles generated from surfactant mixtures of Span 60 and polyoxyethylene 40 stearate *Acta Biomaterialia* (Vol. 6, pp. 3542-3549).

Xu, Zhong, Holland, Nolan B, & Marchant, Roger E. (2001). Conformations of short-chain poly (ethylene oxide) lipopolymers at the air-water interface: a combined film balance and surface tension study. *Langmuir, 17*(2), 377-383.

Zhao, Bin, & Brittain, William J. (2000). Polymer brushes: surface-immobilized macromolecules. *Progress in Polymer Science, 25*(5), 677-710.